UNIVERSITÀ DEGLI STUDI DI PADOVA

DIPARTIMENTO DI INGEGNERIA INDUSTRIALE

TESI DI LAUREA MAGISTRALE IN INGEGNERIA ENERGETICA

OPTIMIZED CONFIGURATIONS OF ORC SYSTEMS FOR UTILIZATION OF LOW TEMPERATURE HEAT SOURCES

Relatore: Prof. Andrea Lazzaretto
Correlatore: Ing. Giovanni Manente

Laureando: Eleonora Bonamico
Matricola:1077452

ANNO ACCADEMICO 2015 – 2016

Ad Arianna

INDEX

FIGURES TABLE

1. ABSTRACT

Organic Rankine Cycles (ORCs) are a well-known technology for power generation from low-to-moderate temperature heat sources such as geothermal energy, solar thermal energy, waste heat, biomass and ocean thermal energy.

The majority of the existing plants are single pressure ORCs that have been extensively analyzed in the literature. Instead, the potential of dual pressure systems has not been fully explored up till now. In the first part of this work subcritical single and dual pressure ORCs are systematically compared, using a wide set of working fluids (including hydrofluoroolefins) and heat sources in the range 100÷200˚C at 25°C intervals. Optimum cycle parameters maximizing the net power output are identified for both configurations and a criterion is introduced to decide about single and dual pressure configuration. Results show that the dual pressure ORC does not give any advantage when the optimization indicates that the single pressure configuration reaches the maximum allowed pressure, that is when both thermal and cycle efficiency are simultaneously maximized.

In the second part, the performance of both ORC configurations are analyzed using the pinch analysis technique when the heat source is not anymore made of a unique flow, but it is the composition of three different heat capacities. In this case, results show that the dual pressure ORC is always advantageous.

2. NOMENCLATURE

A	heat transfer area, m^2
ACC	Air Cooled Condenser
AR	Area ratio (=A_{tot}/W_{net}), m^2/kW
C	Cost, $
$\dot{C}$	heat capacity, kW/K
CCC	Cold Composite Curve
c_p	specific heat, kJ/(kg K)
D	capacity or size parameterfor the equipment
F	factor
GCC	Grand Composite Curve
GWP	Global Warming Potential
H	Enthalpy, kJ
h	specific enthalpy, kJ/kg
HCC	Hot Composite Curve
HP	High Pressure
LP	Low Pressure
$\dot{m}$	mass flow rate, kg/s
MCT	Module Costing Technique
o.f.	objective function
ODP	Ozone Depletion Potential
ORC	Organic Rankine Cycle
p	pressure
Q	heat flow, kW
q	specific heat, kJ/kg
r	vaporization enthalpy, kJ/kg
r_{ex}	expansion ratio
S	shifted temperature, °C
s	specific entropy, kJ/(kg K)
SIC	specific investment cost, $/kW
T	temperature, °C
T_r	reduce temperature (=T/T_{cr})
U	overall heat transfer coefficient, $W/(m^2 K)$
$\dot{V}$	volumetric flow rate, m^3/s
W	power, kW
w	specific work, kJ/kg
x	vapour quality

Greek symbols

η efficiency

φ heat recovery factor

ΔT_{SH} Superheating degree, °C

ΔT_{PP} Pinch Point temperature difference, °C

ΔT_{ml} Logarithmic mean temperature difference, °C

Subscripts and superscripts

AP Approach Point

atm atmospheric

av available

BM bare module

cond condensation

cr critical

DS Desuperheating

EV Evaporator

geo Geothermal brine

GR grassroutes

HS Heat Source

in Inlet

M material

max cycle maximum

min minimum

net net

out Outlet

p Pump

P Purchase

PH Preheater

pp Pinch Point

sat saturation

SH Superheater

SR Subcooling

sys System

t Turbine

th Thermal

TM Total Module

tot Total

wf working fluid

0 base condition

3. INTRODUCTION

With the 2015 United Nations conference on climate change (Cop21), 195 countries committed to keeping the increase in global average temperature to well below 2°C above pre-industrial levels [1]. To do this CO_2 emissions have to decrease significantly and renewable energies play an important role on the gradual replacement of fossil fuels, which are mostly responsible for global warming. According to this perspective it is necessary not to waste energy and exploit low and medium temperature heat sources.
Organic Rankine cycles are a technology suitable to use efficiently low and medium temperature heat sources to produce electricity. It consists of the same components of a traditional steam Rankine cycle, yet the working fluid is an organic compound characterized by a lower boiling temperature than water, thus it allows power generation from low heat source temperatures.

The advantages in using an organic fluid over water are [2]:

- Less heat is required during the evaporation process.
- The evaporation process takes place at lower pressure and temperature; high pressures usually lead to higher investment costs and increased complexity.
- Organic fluids usually have a positive or isentropic slope of the saturated vapor in the temperature-entropy diagram, thus the expansion process ends in the vapor region and hence the superheating is not required and the risk of blades erosion is avoided. Water is instead a "wet" fluid with a negative saturated vapor slope and needs superheating to prevent condensation during expansion.
- The smaller temperature difference between evaporation and condensation also means that the pressure drop/ratio will be much smaller and thus simple single stage turbines can be used.

Furthermore, ORC has the characteristics of simple structure, high reliability and easy maintenance [3].
The choice of the appropriate organic fluid is very important because it influences the thermodynamic performance of the cycle; some authors identified some guidelines for the selection of the suitable working fluid [2,4,5]:

- High thermodynamic performance (high energetic/exergetic efficiency);
- Vapor saturation curve with zero or positive slope. As mentioned before a negative saturation vapor curve leads to droplets formation during expansion;
- High density. A low density leads to a higher volume flow rate: the sizes of the heat exchangers must be increased to limit the pressure drops. This has a non-negligible impact on the cost of the system;
- The melting point should be lower than the lowest ambient temperature through the year to avoid freezing of the working fluid;
- Acceptable condensing and evaporating pressures, the first should be higher than the atmospheric pressure in order to avoid air infiltration into the cycle and the second should not be too high in order to limit the costs;
- Good heat transfer properties (low viscosity, high thermal conductivity);
- Good thermal and chemical stability (stable at high temperature);
- Good compatibility with materials (non-corrosive);
- Good safety characteristics (non-toxic and non-flammable);
- Low environmental impacts (low ODP, low GWP);

- Low cost and good availability.

Moreover, in the search for the optimum working fluid, some criteria have been suggested in the literature which correlate the system efficiency of single stage ORC systems with the working fluid critical temperature. According to Vetter et al. [6] the maximum net power is obtained when the ratio between working fluid critical temperature and heat source inlet temperature ($T_{cr}/T_{HS,in}$) is between 0.8 and 0.9. A similar result was also obtained by Astolfi et al. [7], who found the optimal ratio $T_{cr}/T_{HS,in}$=0,88÷0,92 for the maximum power output. While Li et al. [8] found the optimal point in the range of $T_{HS,in}$-T_{cr}=25÷35°C. Finally, Vivian et al. [9] suggested, for subcritical cycles, an optimal value of $T_{HS,in}$-T_{cr} around 35°C. Fluids with an higher difference (>55°C) have a low cycle efficiency, whereas fluids with a critical temperature close or higher than the brine inlet temperature show a low heat recovery factor.

Dual pressure ORC systems have been recently proposed in the literature to improve the performance of single pressure systems. For example, Guzovic et al. [10] analyzed the replacement of a basic ORC with a dual pressure ORC in the Velika Ciglena geothermal power plant located in the Republic of Croatia. They found that the dual pressure ORC has a slightly lower thermal efficiency but considerably higher exergy efficiency and net power. Also Li et al. [11] obtained an improvement in the net power output and a decrease of the total irreversible loss using a dual stage ORC. In addition, they compared two different configurations of dual pressure ORC: the series and the parallel one discovering that the first one is more performing especially at increasing heat source inlet temperatures.

Di Genova at al. [12] handled the problem of multiple low temperature waste heat streams, trying to find the ORC configuration which could create the best matching between a complex hot composite curve (HCC) and the cold composite curve (CCC) using the pinch analysis technique. The best resulting configuration was made of four reheat stages, two pressure levels and balanced recuperators, achieving 28,5% conversion efficiency against 20,9% of the basic ORC.
Also Desai et al. [13] investigated the integration of ORC systems with a background process using pinch analysis. They demonstrated it is possible to improve the work production by incorporating different cycle modifications, in particular simultaneous regeneration and turbine bleeding improves, on an average by 16.5% the thermal efficiency of the ORC based on the 16 dry fluids. They then highlighted how an appropriate choice of working fluid is important to optimize the performance of the ORC and the integrated system.

Traditionally HFC-R134a and HFC-R245fa have been largely used, but environmental issues ask for new fluids with lower GWP. Besides HFC and hydrocarbons, the new class of hydrofluoroolefins refrigerants are considered here.

The aim of this work is to find the optimal layout of Organic Rankine Cycle systems. In the first part, for utilization of geothermal fluids in the range between 100°C and 200°C employing seven different organic working fluids: isopentane, isobutane, R245fa, which are dry fluids with a positive slope of the saturation vapor curve (Figure 1), R1234ze(Z), R1234ze(E), R1234yf, which are isentropic fluids with infinitely large slope (Figure 2), and R134a, which has a slightly negative slope (Figure 3).
In the second part to fit a composite heat source with a complex Temperature-Enthalpy profile using isobutane, R1234ze(Z), R245fa and isopentane.

4. HEAT SOURCE AT CONSTANT HEAT CAPACITY

In this Section, single and dual pressure ORC configurations are considered for the exploitation of a geothermal heat source made of a unique flow at constant heat capacity. The analysis is carried out varying the brine inlet temperature in the range 100÷200°C at 25°C intervals.
Subcritical single pressure and dual pressure Organic Rankine Cycles (ORCs) are considered in combination with seven working fluids (Table 1) having critical temperatures between 95°C and 187°C and different Global Warming Potential (GWP) values [14,15].

Table 1. Working fluid properties.

Working fluid	T_{cr}	p_{cr}	GWP
R1234yf	94,7°C	33,82 bar	4
R134a	101°C	40,59 bar	1430
R1234ze(E)	109,4°C	36,32 bar	7
Isobutane	134,7°C	36,4 bar	3
R1234ze(Z)	150,1°C	35,33 bar	7
R245fa	154°C	36,51 bar	1030
Isopentane	187,2°C	33,7 bar	11

According to the selection criteria suggested in the literature (see Section 3) the following working fluids are chosen for the single stage ORC depending on the inlet temperature of the heat source: R1234yf and R134a for 100-125°C, R1234ze(E) for 100-150°C, isobutane, R1234ze(Z) and R245fa for 150-175°C and finally isopentane for 150°C, 175°C and 200°C.
For the dual stage ORC all fluids are used for 100-125°C heat source inlet temperature, R1234ze(E), isobutane, R1234ze(Z), R245fa and isopentane for 150°C, isobutane, R1234ze(Z), R245fa and isopentane for 175°C and finally only isopentane for 200°C.
Figure 1 to 3 show the T-s diagrams for a dry, an isentropic and a wet fluid respectively.

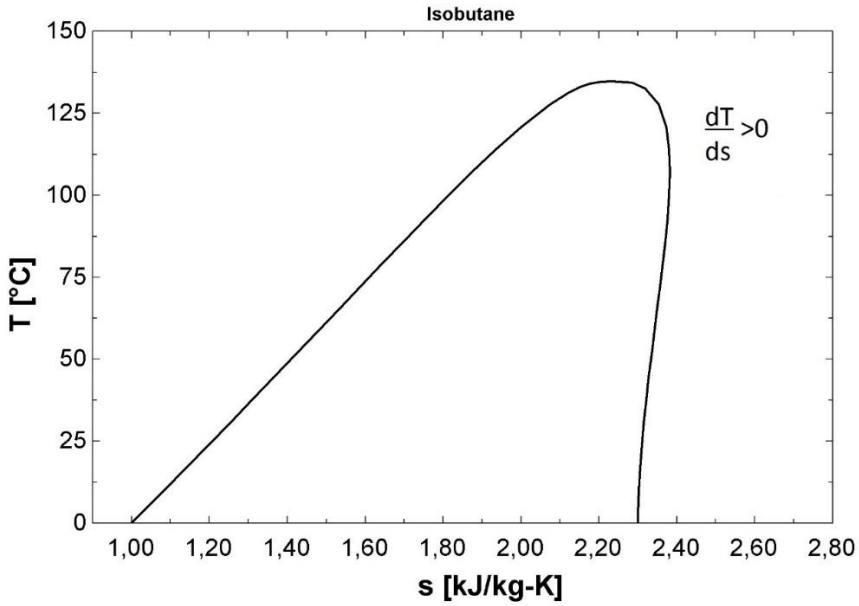

Figure 1. T-s diagram for a dry fluid (isobutane).

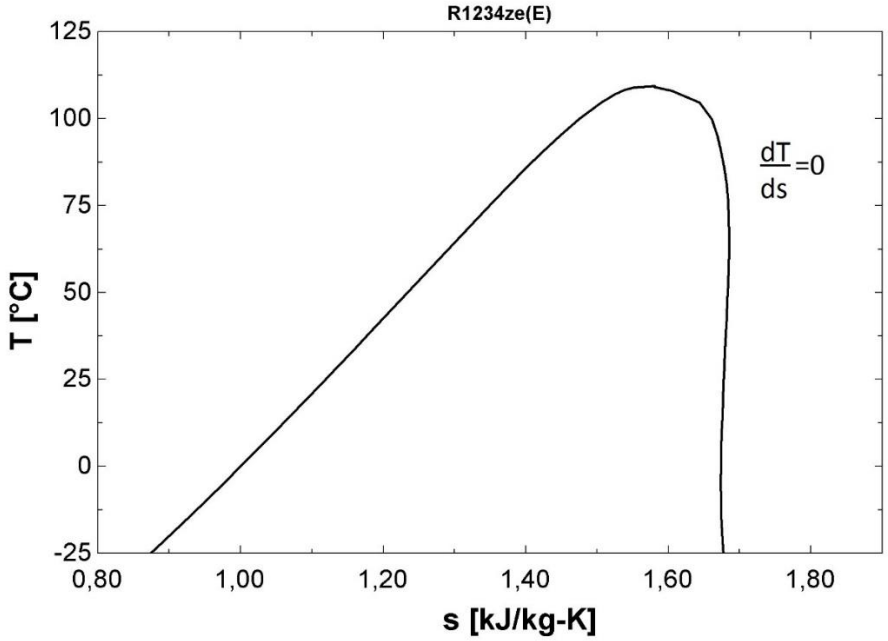

Figure 2. T-s diagram for an isentropic fluid (R1234ze(E)).

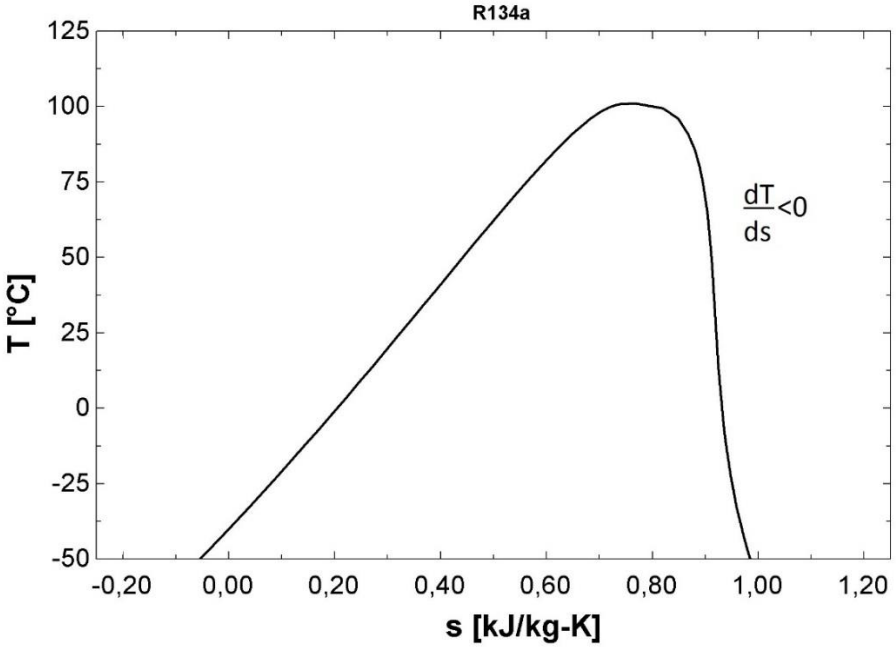

Figure 3. T-s diagram for a wet fluid (R134a).

4.1 SYSTEM CONFIGURATION

In the next paragraphs the ORC system layout is presented, firstly for the single pressure and secondly for the dual pressure configuration.

4.1.1 Single Pressure ORC

The system layout of a subcritical single pressure ORC is shown in Figure 4. The basic components consist of a preheater, an evaporator, a turbine, a condenser and a working fluid pump. In this work an air cooled condenser is considered.

The working fluid is subjected to the following processes as shown in the *T-s* diagram (Figure 5):

- working fluid compression in the feed pump, from the condensation pressure p_{cond} to the maximum cycle pressure p_{max} (1-2),
- preheating till the saturation temperature at p_{max} (2-3_{ph}),
- evaporation with an eventual superheating till the maximum cycle temperature T_{max} (3_{ph}-3),
- expansion in the turbine from p_{max} to p_{cond},
- desuperheating and condensation (4-1).

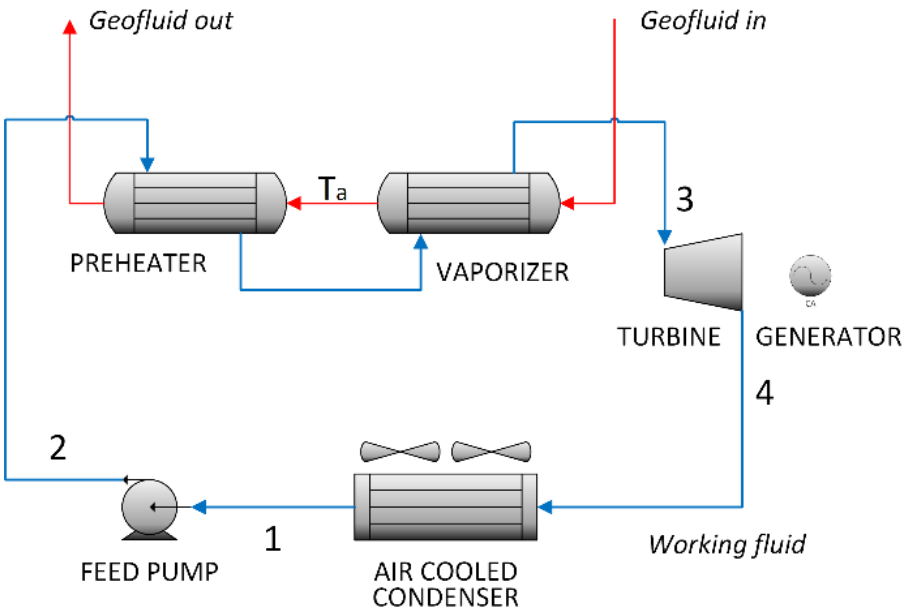

Figure 4. Single pressure configuration layout.

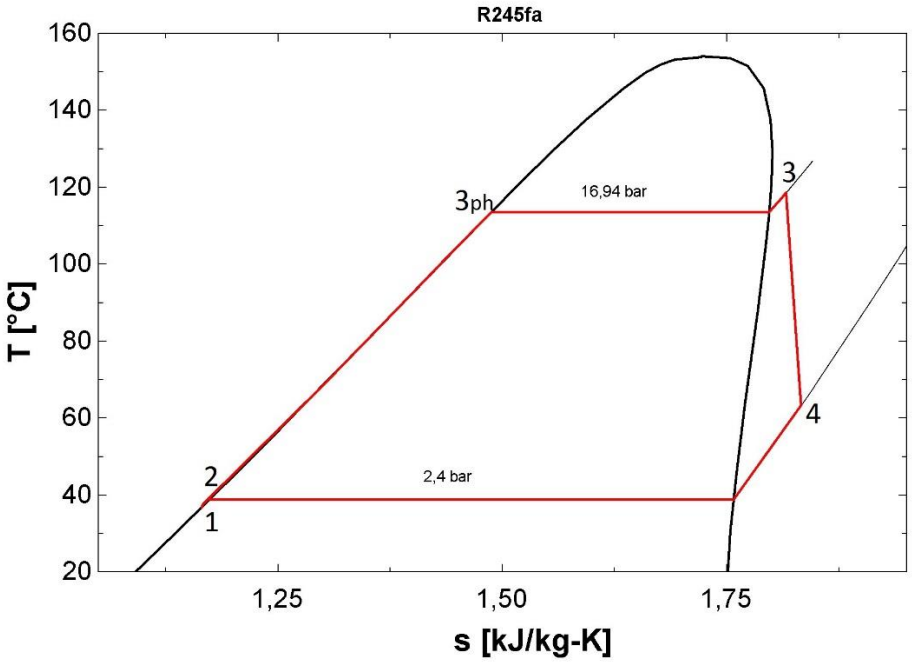

Figure 5. T-s diagram for a single pressure ORC using R245fa.

From the enthalpy differences between the individual state points, the specific energy contribution of each component can be calculated:

- Work supplied in the feed pump: $w_p = h_2 - h_1$ (4.1.1)
- Heat supplied in the heat exchangers: $q_{in} = h_3 - h_2$ (4.1.2)
- Specific work of the turbine: $w_t = h_3 - h_4$ (4.1.3)
- Heat removed in the condenser: $q_{cond} = h_4 - h_1$ (4.1.4)

4.1.2 Dual Pressure ORC

In the dual pressure ORC basic components and processes are the same as in the single pressure, but there are two turbines, two pumps and the heat exchangers are doubled. Thus, the investment costs are higher and they have to be compensated by an increase in power production.

Here the working fluid is split into two different pressure levels. In the "series configuration" of a dual pressure ORC system (Figure 6 and 7) this separation occurs after the first preheating, so the entire mass flow passes through the low-pressure (LP) preheater (2-3), then the LP flow is evaporated (3-9) and the high-pressure (HP) one is further compressed and heated up until the maximum cycle temperature (4-6). The working fluid is then expanded in the HP turbine (6-7) and, after a mixing at the inlet of the LP turbine (point 8), undergoes a second expansion (8-10). In the "parallel configuration", the mass flow rate is split at the condenser outlet, so also the preheating process is split into two streams which are then rejoined before LP expansion.

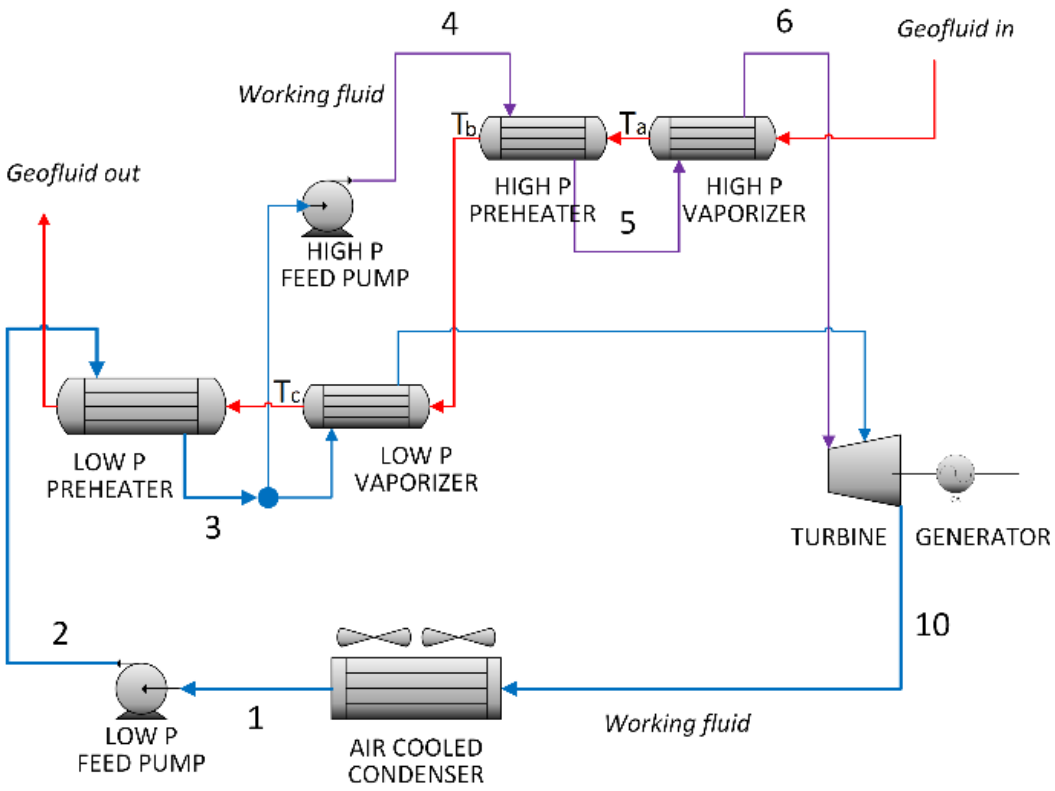

Figure 6. Dual pressure series configuration layout.

From the enthalpy differences between the individual state points, the specific energy contribution of each component can be calculated:

- Work supplied in the LP feed pump: $w_{p,LP} = h_2 - h_1$ (4.1.5)
- Work supplied in the HP feed pump: $w_{p,HP} = h_4 - h_3$ (4.1.6)
- Heat supplied in the LP preheater: $q_{PH,LP} = h_3 - h_2$ (4.1.7)
- Heat supplied in the LP evaporator: $q_{EV,LP} = h_9 - h_3$ (4.1.8)
- Heat supplied in the HP preheater: $q_{PH,HP} = h_5 - h_4$ (4.1.9)
- Heat supplied in the HP evaporator: $q_{EV,HP} = h_6 - h_5$ (4.1.10)
- Specific work of the LP turbine: $w_{t,LP} = h_8 - h_{10}$ (4.1.11)
- Specific work of the HP turbine: $w_t = h_6 - h_7$ (4.1.12)
- Heat removed in the condenser: $q_{cond} = h_{10} - h_1$ (4.1.13)

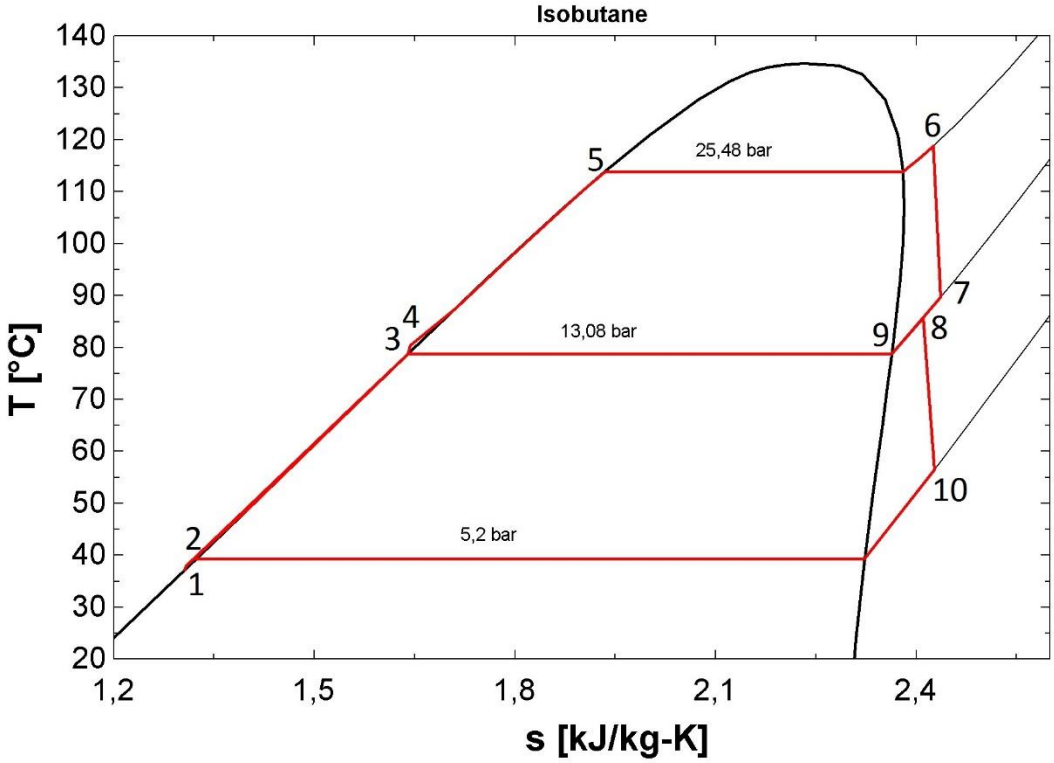

Figure 7. T-s diagram for a dual pressure ORC using isobutane.

Only the series arrangement of the dual pressure configuration is taken into account in the following because it provides more net power [16] compared to the parallel ORC because of the improved matching between thermal profiles of heat source and working fluid. In fact, as appear from Figure 8, the series configuration allows generating a higher mass flow at low temperature and higher evaporation pressures, which in turn result in higher evaporation temperatures.

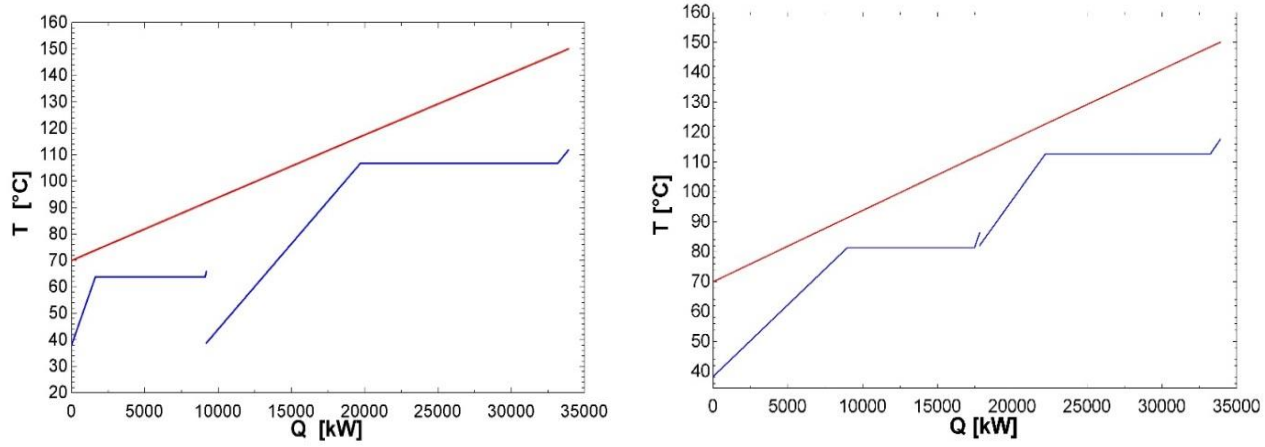

a) *b)*

Figure 8. T-Q diagram using R245fa of: a) parallel dual stage ORC; b) series dual stage ORC.

Moreover Li et al. [16] demonstrated that the parallel ORC deteriorates the matching between geothermal water and the working fluid in the high stage evaporator. The extent of deterioration is

proportional to the $T_{in,HS}$, and this is the reason why the parallel could not have better performance with the increase of the $T_{in,HS}$. On the contrary, the series arrangement pumps a portion of the saturated liquid in the low stage evaporator to the high stage evaporator, which could make it achieve better performance. The series absorbs a portion of heat from the lower temperature range to preheat the working fluid in the HP evaporator, whereas the working fluid in the HP evaporator for the parallel absorbs heat totally from the high temperature range. This is the main reason for their different performance.
Simulations carried out during the work validated this conclusion.
For example, using R245fa, the parallel arrangement gives -8,1%, -7,6%, -9,2% and -9,7% net power output at $T_{in,HS}$=100°C, 125°C, 150°C and 175°C respectively.

4.2 METHODOLOGY

The purpose of this section is to explain the followed procedure to build the optimization models. The analysis is limited to subcritical plant configurations at their design conditions. Each configuration is modelled in the Engineering Equation Solver (EES) environment, which is used to solve the set of equations and to evaluate the performance for a given set of independent variables. In a further step, the design variables, that mostly influence the performances, are left free to vary within specified limits and optimized in order to find the optimal values of two objective functions, which are:

a) Net power maximization $max(W_{net})$;
b) Ratio between total heat transfer area and net power output minimization $min(A_{tot}/W_{net})$.

These two objective functions are defined with the aim of evaluating the differences in the performances between single and dual pressure ORCs at homogenous conditions. $max(W_{net})$ is consider to take into account the potential of the ORC system for the energy production and $min(A_{tot}/W_{net})$ to give an indication about the heat transfer performance and reduce the investment costs due to the heat exchanger. Both objective functions will be examined in Section 4.4.
The performance metrics in the analysis of the thermodynamic performance are the "heat recovery factor" which accounts for a good utilization of the energy of the heat source and the "thermal efficiency" which accounts for the conversion into power. An increase in evaporation temperature corresponds to an increase in cycle efficiency, but, on the other hand, to a decrease in the amount of heat transferred to the cycle [14,15]. The optimum cycle parameters are therefore a compromise between a high thermal efficiency and an effective cooling of the heat source.
The heat recovery factor is

$$\varphi = \frac{Q_{in}}{Q_{av}} \tag{4.2.1}$$

where Q_{in} is the heat absorbed by the working fluid from the heat source and Q_{av} is the heat made available by the heat source.
Cycle efficiency expresses the ratio between power output and heat input:

$$\eta_{th} = \frac{W_{net}}{Q_{in}} \tag{4.2.2}$$

The product between η_{th} and φ gives the "total heat-recovery efficiency":

$$\eta_{sys} = \varphi \cdot \eta_{th} = \frac{W_{net}}{Q_{av}} \tag{4.2.3}$$

A simulation model is built in the EES environment for both single and dual pressure cycles, using the internal library for the evaluation of the real fluids properties.
The models are based on mass and energy balances, fluids thermodynamic properties and characteristic equations of components.
Furthermore, in order to build the cycle, independent and decision variables are to be set.

- Input variables are:
  - Inlet geothermal source temperature T_{in} (the outlet is left free to vary);
  - Geothermal water mass flow rate $\dot{m}_{geo}$=100 kg/s;
  - Environmental temperature and pressure T_{atm}=20°C e p_{atm}=1 atm;
- Independent variables fixed as parameters are:
  - Pinch point temperature difference (ΔT_{PP}=10°C);
  - Condensation pressure which guarantees a condensation temperature equal to 39°C (some slight deviations are possible due to rounding in the corresponding saturation pressure);
  - Maximum cycle pressure 1.3 bar below the critical pressure to avoid unstable operation close to the critical point;
  - Minimum degree of superheating at turbine equal to 5°C to avoid turbine erosion by residual liquid droplets. In the dual pressure ORC, there is no need of superheating in the LP stage because of the mixing with the superheated vapor leaving the HP turbine;
  - Minimum vapor quality at the outlet of the HP turbine equal to 0,99 to avoid droplets at the inlet of the LP turbine also when the saturation curve is slightly negative;
  - Minimum vapor quality at the end of the expansion at the condensation pressure equal to 0,9;
  - Pinch point temperature difference at the condenser (5°C);
  - Subcooling degree (2°C) at the condenser outlet to guarantee the complete condensation of the working fluid;
  - Turbine and pump efficiencies η_T=0,85, η_P=0,7.

  Pressure losses in the pipes, heat exchangers and condenser are neglected.
- Decision variables are:
  - The evaporation pressures, p_{max} in the single pressure model, p_{HP} and p_{LP} in the dual pressure one;
  - The superheating degree: ΔT_{SH} in the single pressure ORC, $\Delta T_{SH,HP}$ and $\Delta T_{SH,LP}$ in the dual pressure ORC at both HP and LP stages.

The choice of the evaporating pressures and ΔT_{SH} as decision variables was taken because these two parameters mostly effect the performance metrics.
As regards the condenser, typical cooling options include air coolers and recirculation towers. Two simplified approaches were proposed in the literature to evaluate the power required by the condenser W_{cond}: one assumes a specific consumption of 0.15 kW/kg_{air} [17], the other one considers that an air cooling process requires a power input in the range of 0.5–1.25 kW to remove 100 kW [18,19]. The two approaches resulted to be almost equivalent in all simulations when a 1kW input power is considered in the latter, which was used in all calculations.
Overall heat transfer coefficients (U) in Table 2 were considered [20] to evaluate the total heat transfer area A_{tot}.

Table 2. Overall heat transfer coefficients.

U superheater	[W/(m^{2}K)]	600
U evaporator	[W/(m^{2}K)]	1000
U preheater	[W/(m^{2}K)]	750
U desuperheater	[W/(m^{2}K)]	100
U condenser	[W/(m^{2}K)]	850
U subcooler	[W/(m^{2}K)]	850

4.3 MODELLING

In this section the main mass and energy balances and characteristic equations of components are described, in order to outline both single and dual pressure model.
The complete EES programs written for this work are fully reported in Appendix A and B for single and dual stage ORC respectively.
The model construction starts at the end of the condensation (point 1 in Figure 9) as condensation pressure and temperature are known.
Considering the single pressure configuration (Figure 9a), after the condensation, the working fluid is compressed in the feed pump, as the process is not ideal, point 2 is determined through the pump efficiency:

$$\eta_P = \frac{h_{2,id} - h_1}{h_2 - h_1} \tag{4.3.1}$$

Where $h_{2,id}$ is the ideal enthalpy calculated at the same entropy as in point 1.
After the preheating (point 3_{ph}), the evaporation and the eventual superheating (point 3), the working fluid is then expanded in the turbine. As the process is irreversible, point 4 is defined through turbine efficiency:

$$\eta_T = \frac{h_3 - h_4}{h_3 - h_{4,id}} \tag{4.3.2}$$

Where $h_{4,id}$ is the ideal enthalpy calculated at the same entropy as in point 3.
After the condensation the cycle begins again
Considering now the dual pressure ORC in the "series configuration", point 2 is determined according to Eq. 4.3.1. Then the entire mass flow rate ($\dot{m}_{wf}$) is preheated till point 3, in this point occurs the partition of $\dot{m}_{wf}$ in $\dot{m}_{HP}$, which is further compressed (point 4) and heated up (point 5 and 6), and in $\dot{m}_{LP}$, which is vaporized and eventually superheated till point 9. The definition of the LP turbine inlet (point 8) requires an energy balance:

$$\dot{m}_{LP} h_9 + \dot{m}_{HP} h_7 = \dot{m}_{wf} h_8 \tag{4.3.3}$$

The two turbine expansions follow a relation similar to Eq. 4.3.2.

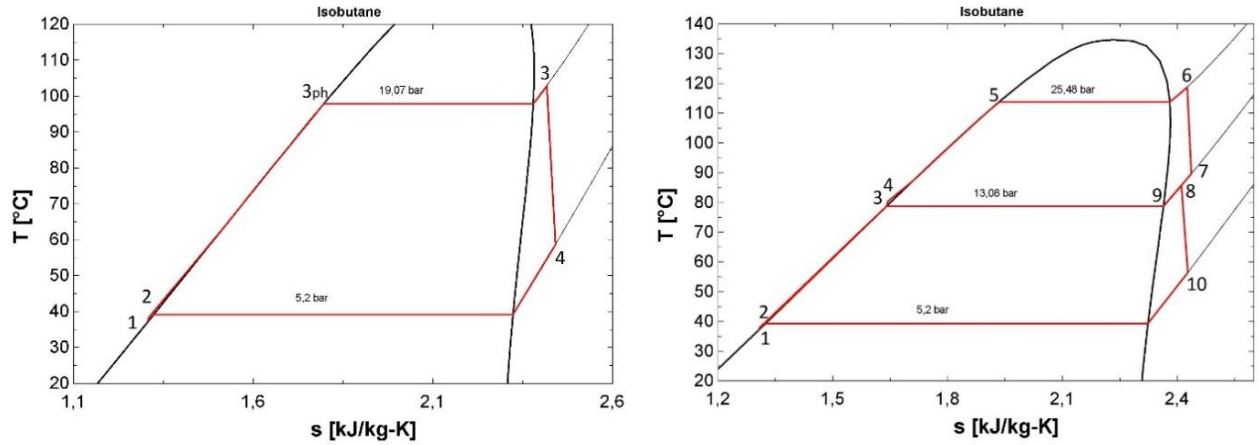

a) *b)*

Figure 9. T-s diagram using isobutane for a) single pressure ORC and b) dual pressure ORC.

In Figure 10 the T-Q diagram for the single pressure ORC is shown. The red line represents the brine, which is cooled down from the inlet temperature T_{in} to the reinjection temperature $T_{out,real}$; the blue line represents instead the working fluid during the heating processes.

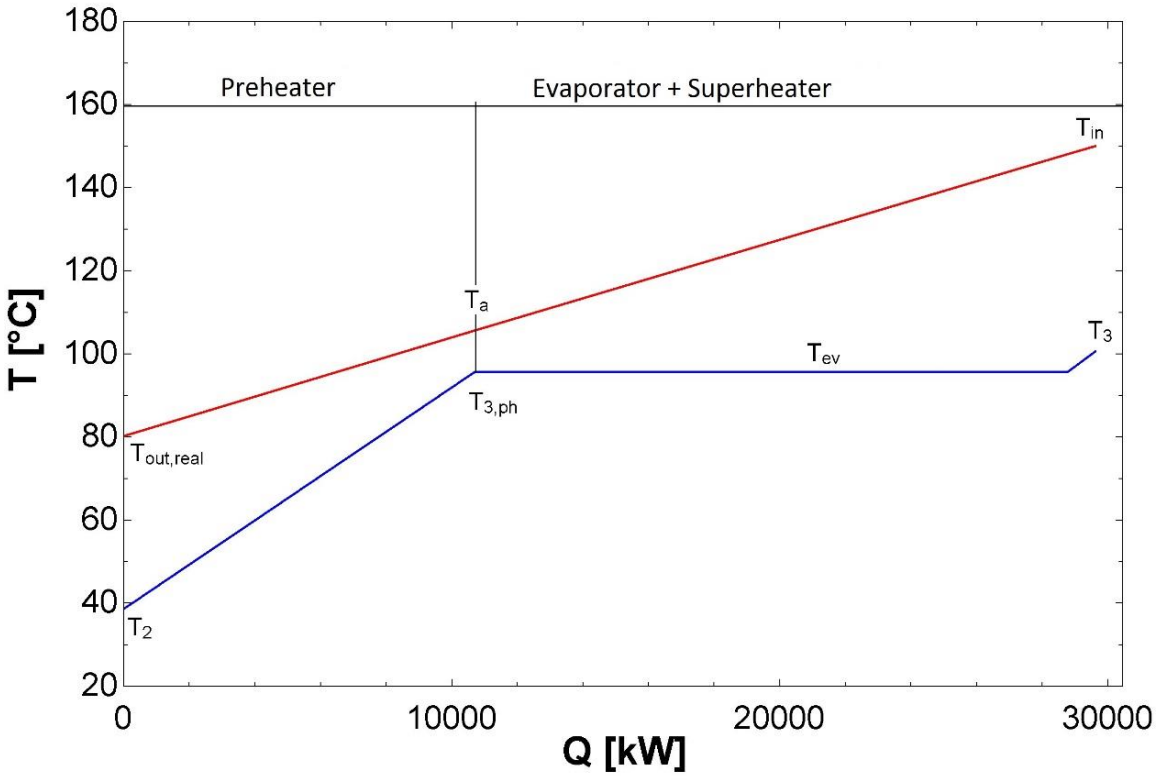

Figure 10. T-Q diagram for single pressure ORC using R245fa.

To be noticed is the pinch point location, that is the point where the heating and the cooling curves are closest, which is at beginning of the evaporation. In this point the working fluid temperature is $T_{3,ph}$ and the brine correspondent temperature is T_a.

It is however possible that the pinch point moves at the beginning of the preheating, for this reason a temperature control was set between T_2 and $T_{out,real}$, whose difference has to be greater than ΔT_{PP}.

The following Eqs. 4.3.4 and 4.3.5 show the energy balances in the heat exchangers of the single stage configuration, in which the unknowns are respectively $\dot{m}_{wf}$ and $T_{out,real}$.
At the evaporator+superheater:

$$\dot{m}_{geo} \cdot c_{p,geo} \cdot (T_{in} - T_a) = \dot{m}_{wf} \cdot (h_3 - h_{3,ph}) \tag{4.3.4}$$

At the preheater:

$$\dot{m}_{geo} \cdot c_{p,geo} \cdot (T_a - T_{out,real}) = \dot{m}_{wf} \cdot (h_{3,ph} - h_2) \tag{4.3.5}$$

Figure 11 shows the T-Q diagram for the dual pressure ORC, the colors have the same meaning as in Figure 10. The brine temperatures T_a and T_c are fixed as parameters because they corresponds to the pinch points. As mentioned before, the pinch point can be located also at the preheating beginning, so that T_b-T_4 and T_{out}-T_2 are constrained to be greater than ΔT_{PP}. Furthermore, when the LP ΔT_{SH} is increased the pinch point can be also at the LP preheater outlet, for this reason T_b-T_9 is subject to the same constraint.

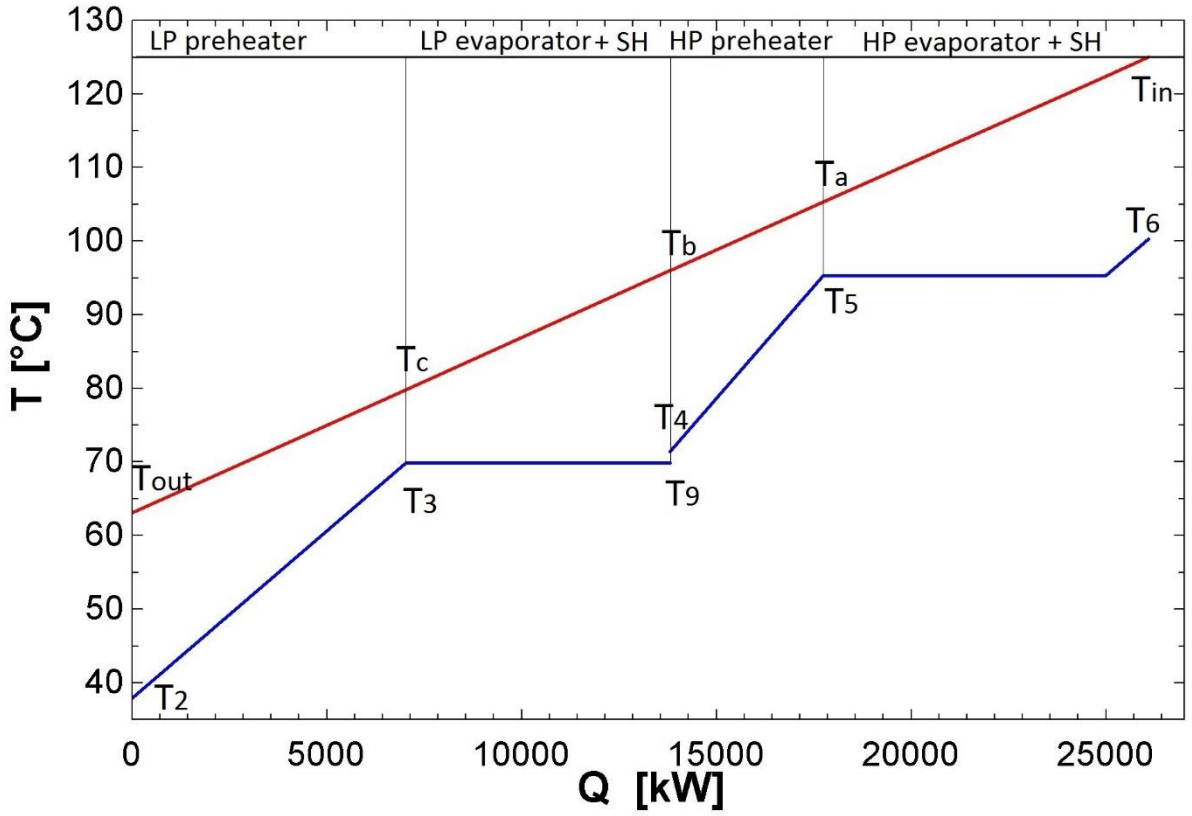

Figure 11. T-Q diagram for the dual pressure ORC using R1234ze(E).

The following Eqs. 4.3.6 and 4.3.10 show the energy and mass balances in the heat exchangers of the dual stage configuration, in which the unknowns are respectively $\dot{m}_{HP}, T_b, \dot{m}_{LP}, \dot{m}_{wf}$ and T_{out}, being the other variables known from the independent variables fixed as parameters.
Energy balance at the HP evaporator+superheater:

$$\dot{m}_{geo} \cdot c_{p,geo} \cdot (T_{in} - T_a) = \dot{m}_{HP} \cdot (h_6 - h_5) \tag{4.3.6}$$

Energy balance at the HP preheater:

$$\dot{m}_{geo} \cdot c_{p,geo} \cdot (T_a - T_b) = \dot{m}_{HP} \cdot (h_5 - h_4) \quad (4.3.7)$$

Energy balance at the LP evaporator:

$$\dot{m}_{geo} \cdot c_{p,geo} \cdot (T_b - T_c) = \dot{m}_{LP} \cdot (h_8 - h_3) \quad (4.3.8)$$

Mass balance:

$$\dot{m}_{wf} = \dot{m}_{HP} + \dot{m}_{LP} \quad (4.3.9)$$

Energy balance at the LP preheater:

$$\dot{m}_{geo} \cdot c_{p,geo} \cdot (T_c - T_{out}) = \dot{m}_{wf} \cdot (h_3 - h_2) \quad (4.3.10)$$

Another energy balance is necessary to determine the air mass flow ($\dot{m}_{air}$) at the condenser. The air outlet temperature is an independent variable fixed at 5°C below the condensation temperature and the air specific heat ($c_{p,air}$) is evaluated at the mean temperature between T_{amb} and $T_{air,out}$.

$$\dot{m}_{air} \cdot \left(T_{air,out} - T_{amb}\right) = \dot{m}_{wf} \cdot (h_4 - h_1) \quad (4.3.11)$$

The working fluid specific enthalpy at the condenser inlet is h_4 in case of the single pressure ORC and h_{10} in case of a dual pressure one.

The T-Q diagram for the condenser is shown in Figure 12, the red line represents the working fluid, which is cooled down by the air (blue line).

Having calculated the mass flows rates, the specific works (Eqs. 4.1.1 to 4.1.13) and the heating loads (Eqs. 4.3.4 to 4.3.11) is easy now to determine the turbines, pumps and condenser power (W_t, W_p, W_{cond}), the heat absorbed by the working fluid (Q_{in}), the heat available from the heat source (Q_{av}), evaluated between T_{in} and T_{amb}, and the performance metrics (η_{th}, φ, η_{sys}).

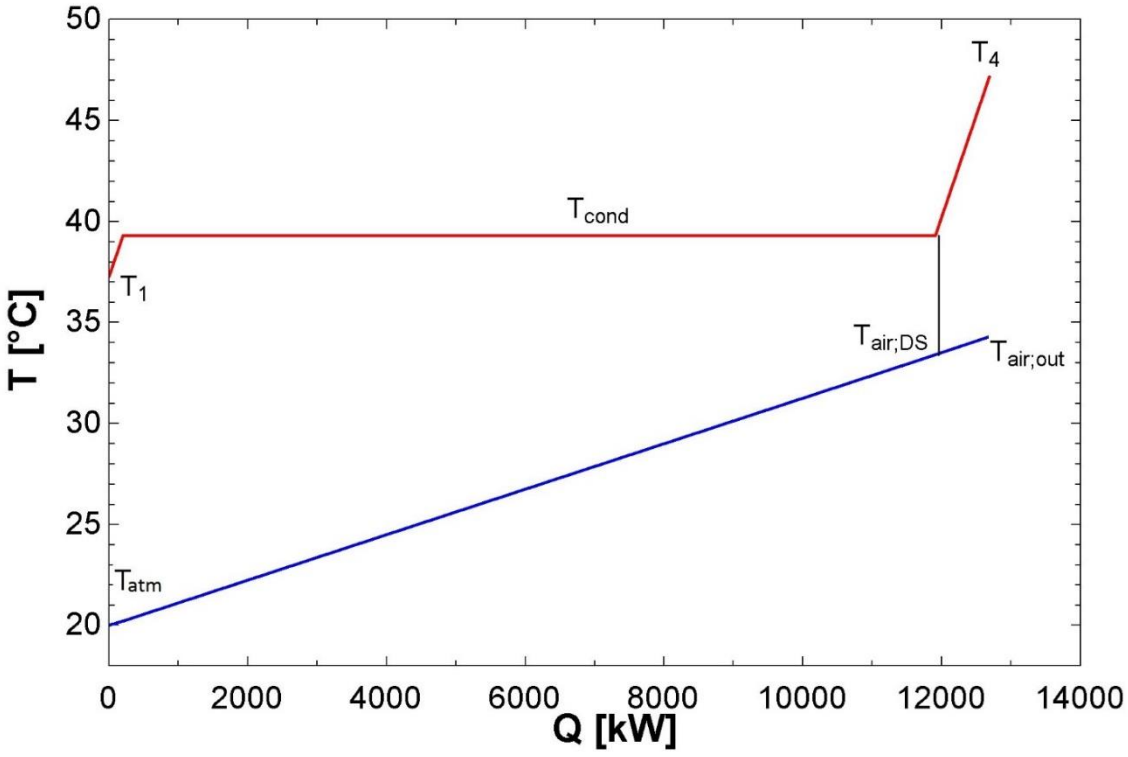

Figure 12. T-Q diagram at the condenser.

For the evaluation of the heat transfer area, the logarithmic mean temperature difference method is applied.

As example, it is here presented the calculation for the evaporator area. The total heat transfer area (A_{TOT}) is the sum of all heat exchangers area.

$$T_{geo,2} = \frac{T_{geo,1}+T_a}{2} \quad (4.3.12)$$

$$c_{p,geo\_EV} = c_p(Water; T = T_{geo,2};\ p = p_{geo}) \quad (4.3.13)$$

$$\Delta T_{ml\_EV} = \frac{((T_{geo,1}-T_{sat})-(T_a-T_{sat})}{ln\frac{(T_{geo,1}-T_{sat})}{(T_a-T_{sat})}} \quad (4.3.14)$$

$$Q_{ev} = \dot{m}_{geo} \cdot c_{p,geo_{EV}} \cdot (T_{geo,1} - T_a) \quad (4.3.15)$$

$$A_{EV} = \frac{Q_{EV}}{U_{EV} \cdot \Delta T_{ml\_EV}} \quad (4.3.16)$$

Where $T_{geo,1}$ is the brine temperature at the superheater outlet, T_{sat} is the saturation temperature at the evaporation pressure and U_{EV} is set according to Table 2.

4.4 OPTIMIZATION

The design optimization procedure consists in searching for the minimum/maximum value of an objective function (o.f.) subject to equality and inequality constraints imposed by the equations of the ORC system model

Min/Max o.f.

Subject to g(x)=0
h(x)≥0

Two objectives functions are considered here: the net power output and the area ratio. The former is to be maximized to get the maximum profit from the ORC system operation, the latter is to be minimized to reduce investment costs.

Net power output (W_{net}) is

$$W_{net} = W_t - W_p - W_{cond} \quad (4.4.1)$$

where W_t is the turbine power output, W_p is the power required by the pump and W_{cond} is the power required by the air cooled condenser.

The area ratio (AR) is the ratio between total heat transfer area (A_{TOT}) and net power output:

$$AR = A_{tot}/W_{net} \quad (4.4.2)$$

A_{tot} is given by Eq (4.4.3) for the single pressure ORC and by Eq (4.4.5) for the dual pressure one:

$$A_{tot} = A_{SH} + A_{EV} + A_{PH} + A_{DS} + A_{cond} + A_{SR} \quad (4.4.3)$$

Where A_{SH} is the heat transfer area at the superheater, A_{EV} the evaporator area, A_{PH} the preheater area, A_{DS} the desuperheater area, A_{cond} the condenser area and A_{SR} the subcooler area. Similarly, in Eq. (4.4.4), where there are two superheaters, two evaporators and two preheater indicated with the subscripts HP (high-pressure) and LP (low-pressure):

$$A_{tot} = A_{SH,HP} + A_{EV,HP} + A_{PH,HP} + A_{SH,LP} + A_{EV,LP} + A_{PH,LP} + A_{DS} + A_{cond} + A_{SR} \quad (4.4.4)$$

In the search for the optimum W_{net} and AR the evaporation pressure and the superheating degrees are chosen as free variables because of their strong influence on the performance parameters φ and η_{th},

and in turn on η_{sys}. Note that the maximization of the net power output corresponds to the maximization of the total heat recovery efficiency. This is because the total heat recovery efficiency is defined as the net power output divided by the available heat which is constant in all cases.

- In the single pressure ORC the evaporation pressure is optimized at different superheating degrees (varied at steps of 2,5°C).
- Similarly, in the dual pressure ORC both low and high evaporation pressures are optimized at discrete values of the superheating degree (which is varied at 5°C steps from 5° to 20°C at the high evaporation pressure and from 0,01 to 20°C at the low evaporation pressure).

Optimization runs are performed using the EES optimization tool, which uses two different descendent methods that need an initial guess value of all variables included in the model: if there is one degree of freedom, EES minimize/maximize the selected variable using either a Golden Section search or a Quadratic Approximations method, multidimensional optimization are instead carried out using the Conjugate directions method or the Variable metric method.
Both methods were applied in the optimization runs in search of the optimum. When the solution was unstable, some of the guess variables are changed.

The main difficulty was found in the convergence of the dual stage model, where the optimization variables were four: $p_{HP}, p_{LP}, \Delta T_{SH,HP}, \Delta T_{SH,LP}$. For this reason, the superheating degree was varied at discrete steps, in this way the search of the optimum occurred with only two decision variables at time. The best solution was then taken among the different optimization runs.

4.5 ECONOMIC MODEL

The economic model is based on the module costing technique (MCT).
This technique was developed for chemical processes, but it can be used for preliminary costs estimation for energy plants too, as Toffolo et al. did in [17].
The methodology, which is followed here, is explained in detail by Turton et al. in [28].
The procedure consists in the calculation of capital costs associated with the construction of the ORC systems with the basic relationships for scaling costs with equipment size.
The capital cost considers direct costs such as:

- Purchased costs of the equipment, C_P;
- Materials required for installation, including piping, insulation and fireproofing, foundations and structural supports, instrumentation and electrical;
- Labor to install equipment and material.

And indirect costs such as:

- Transportation costs for shipping equipment and materials to the plant site:
- Insurance and taxes;
- Salaries for the engineering and project management personnel in the project;
- Costs for temporary buildings and salaries for the supervisory personnel.

The MCT is generally accepted as the best for making preliminary costs estimates [28]. It relates all costs to the purchased cost of equipment evaluated for the "base conditions", indicated with C_P^0 (the superscript zero "0" stands for basic conditions).
"Base conditions" means equipment made of the most common material, usually carbon steel, and operating at near ambient pressure.
Deviations from these base conditions are handled by using multiplying factors that depend on the specific equipment type, the specific system pressure and the specific materials of construction.
The costs equations are expressed by:

$$log_{10}C_P^0 = K_1 + K_2 log_{10}(D) + K_3 (log_{10}(D))^2 \quad (4.5.1)$$

where D is the capacity or size parameter for the equipment and the constants K_1, K_2 and K_3 are peculiar to each component and type. The values for K_1, K_2 and K_3 for each equipment piece are indicated in [28] along with their validity range.
The MCT defines also the bare module equipment cost, which represents the sum of direct and indirect cost and it is given by:

$$C_{BM} = C_P^0 F_{BM} \quad (4.5.2)$$

where C_{BM} stands for bare module equipment cost, C_P^0 is above defined and F_{BM} is the aggregate multiplication factor that accounts for all direct and indirect costs.
The bare module cost factor at base conditions is given by [28] for many different types of process equipment.
When a component does not operate at base conditions, the expression of the bare module cost factor for heat exchangers and pumps becomes:

$$F_{BM} = B_1 + B_2 F_M F_p \quad (4.5.3)$$

where B_1 and B_2 depend on the type of heat exchanger or pump and F_p and F_M account for the effects of the operating pressure and construction material costs respectively.
For the other components (expanders, fans, etc.) the coefficient F_{BM} is directly given as a multiplier which incorporates all affecting parameters: type, operation pressure and material.

The components of the ORC system, which are analyzed are:

- Centrifugal carbon steel feed pumps;
- Carbon steel shell and tube heat exchanger with fixed tubes;
- Single radial steam turbines;
- Carbon steel air cooled condenser (ACC);
- Fiberglass axial vane ACC fans.

For them the pressure factor F_p is given by:

$$log_{10}F_p = C_1 + C_2 log_{10}(p) + C_3 (log_{10}(p))^2 \quad (4.5.4)$$

with p expressed in bar gauge or barg (1 bar=0,0 barg).

From the combination of material and pressure factors, the actual purchased cost is obtained:

$$C_P = C_P^0 F_p F_M \quad (4.5.5)$$

All heat exchangers of the system that work in the range $5<p<140$ barg have $C_i \neq 0$, under 5 barg $C_i=0$. The ACCs considered in this work operate at $p<10$ barg and hence have $C_i=0$. For the fans the hypothesis of pressure loss less than 1 kPa is kept and hence $C_i=0$.
All employed coefficients are summarized in Table 3.

Further hypotheses regard the F_M estimation for turbine and fans and the number of pumps and fans. Similarly as it was done by Toffolo et al. [17], the number of pumps is calculated so that $W_{max} \leq 300$ kW to remain in the validity range given by Turner [28] and the number of funs is calculating assuming a volumetric flow rate for each fan equal to 65 m^3/s. F_M for turbine and fans are taken equal to those in [17], which were obtained from the comparison with real cost data.
Moreover, the cost equation for the expanders is used beyond its maximum value (1500 kW).
The heat transfer area is calculated following the procedure presented in Section 4.3.

Table 3. Cost coefficients.

Component	D	B_1, B_2	C_1, C_2, C_3	F_{BM}	F_M	K_1, K_2, K_3
Feed pump	W [kW]	1,89 1,35	-0,3935 0,03957 -0,00226		1,5	3,3892 0,0536 0,1538
Turbine	W [kW]		0 0 0	11,6	4,77	2,2476 1,4965 -0,1618
Shell and tube heat exchanger	A [m^2]	1,63 1,66	0,03881 -0,11272 0,08183		1	4,3247 -0,3030 0,1634
AAC fans	$\dot{V}$ [m^3/s]		0 0 0	5	2,5	3,1761 -0,1373 0,3414
ACC heat exchanger	A [m^2]	0,96 1,21	0 0 0		1	4,0336 0,2341 0,0497

After having defined all cost coefficient, the last step is determining the total module cost and the grassroots cost.
The total module cost can be evaluated considering that contingency and fee costs are respectively 15% and 3% of the bare module cost. Adding these costs to the bare module cost provides the total module cost:

$$C_{TM} = 1{,}18 \sum_{i=1}^{n} C_{BM,i} \quad (4.5.6)$$

where *n* represents the total number of pieces of equipment.
The term grass roots refers to completely new plant built on essentially undeveloped land, a grass field, where the ORC system is supposed to be installed.
The grassroots costs, which include the total module cost and costs for site development and auxiliary facilities, are assumed to be 50% of the bare module cost for the base conditions:

$$C_{GR} = C_{TM} + 0{,}50 \sum_{i=1}^{n} C_{BM,i}^{0} = 1{,}18 \sum_{i=1}^{n} C_{BM,i} + 0{,}50 \sum_{i=1}^{n} C_{BM,i}^{0} \quad (4.5.7)$$

Using the MCT is possible to estimate the capital cost for the single and dual pressure ORC and see if the heat transfer area reduction leads really to a consistent reduction of the investment cost or if its impact in the total purchased cost is not that relevant. Furthermore, the comparison of these costs can give another hint in the decision about the configuration.
Results, given in US dollars $, are showed in Section 6.2.2.
It is to notice, tough, that the economic model is simplified and does not take into account the working fluid cost, the electric equipment.

5. HEAT SOURCE AT DIFFERENT HEAT CAPACITIES

Often, in the conversion of waste heat into electricity, there is more than one low temperature stream available. In this chapter, a complex heat source composed of three different flows is analyzed. The first is pressurized water employed as heat carrier in solar collectors, the second is the brine of a geothermal source, whose temperature is constrained due to silica precipitation issues, and the third is again water coming from an industrial waste heat recovery process.
The heat source input data are shown in Table 4 and in the T-H diagram of Figure 13.

Table 4. Heat source input data.

Mass flow rate [kg/s]	T_{in} [°C]	T_{out} [°C]
$\dot{m}_1$=50	150	110
$\dot{m}_2$=30	130	90
$\dot{m}_3$=20	130	100

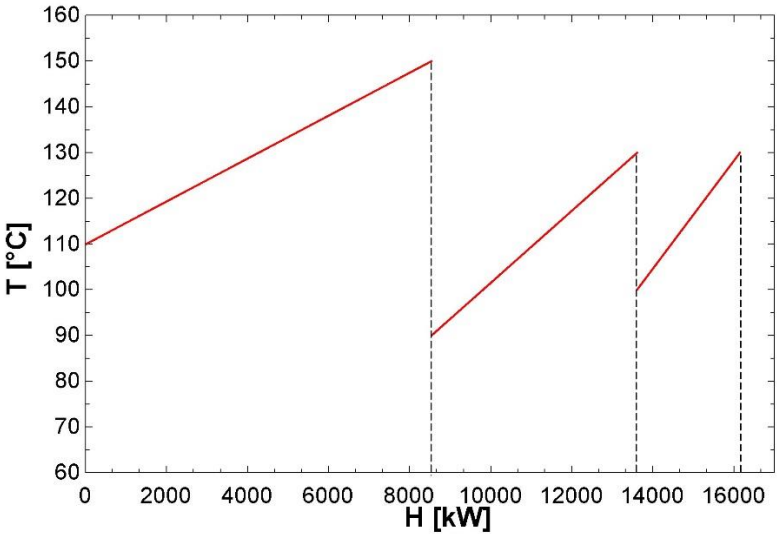

Figure 13. T-H diagram of the hot streams

In the literature there are several examples of ORC systems used to exploit this kind of heat sources and match composite temperature-enthalpy profiles using the pinch analysis technique. Di Genova et al. [12] proposed a set of ORC design concepts to recover heat from a Fischer Tropsch synthesis plant; Desai and Bandyopadhyay [13] searched for the optimal integration with a ‘‘background process’’ and Soffiato et al. [21] presented the design optimization to recover heat from the jacket water, lubricating oil and charge air cooling of the engines of a ship.
From these works it results that a basic ORC configuration is not as effective as a more complex one, but economic issues can still lead to the simple ORC.
A similar result is obtained in the present work.

5.1 PINCH TECHNOLOGY

Pinch technology was firstly used to solve design problem in chemical processes, later the technique was extended to energy targeting and network integration with the aim of improving the integration of the processes and simplify the heat recovery networks.

As Kemp well explains in his work [22], the analysis starts with the identification of the cold and hot streams, any flow which need to be heated up is a cold stream and conversely any flow which must be cooled down is a hot stream.

Theoretically, it is possible to satisfy the heating and cooling loads with external utilities, but this clearly implies an energy waste. To reduce energy consumption, it is then better to recover from the hot streams and use it to heat the cold streams in a heat exchanger.

In this study, hot streams are represented by the three flows of Table 3 and the cold streams are the working fluid heating processes in the ORC systems.

To understand how much heat can be actually recovered, the hot and the cold streams are plotted in the Temperature-Enthalpy (*T-H*) diagram, where *H* represents the heat content of a stream measured in kW.

For a feasible heat exchange, the hot curve must be at all points hotter than the cold stream. Moreover, the temperature difference between the streams cannot be zero, otherwise an infinitely heat transfer area would be required. The minimum admissible temperature difference is called ΔT_{min}.

To handle multiple streams, the heat capacities and the heat loads of all streams, existing over any given temperature range, are added together. In this way, a single composite curve of all hot streams and a single composite curve of all cold streams can be produced in the *T-H* diagram.

In this case, there are three hot streams and each of them could be plotted separately knowing their supply and target temperatures and calculating their heat capacity. Thus, a series of temperature intervals can be defined.

For example, referring to Table 3, between 150° and 130°C only the first stream is involved, between 130° and 110°C all three are present, between 110° and 100°C exist the second and the third and from 100° to 90°C only the second. So that, in the interval 130°-110°C, the heat available is given by:

$$\Delta H = (\dot{C}_1 + \dot{C}_2 + \dot{C}_3) \cdot (130 - 110) \quad (5.1.1)$$

where $\dot{C}_i$ are the heat capacities of the different streams.

In this way, a series of values of ΔH can be obtained for each interval.

The resulting *T-H* plot (Figure 13) is a single curve representing all the hot streams, which is called hot composite curve (HCC).

A similar procedure gives the cold composite curve (CCC).

The overlap between the composite curves establishes the maximum amount of heat recovery possible within the process.

ΔT_{min} can occur anywhere in the interchange region in correspondence to the closest distance between the HCC and the CCC, i.e. at the pinch point.

Another instrument used in the pinch analysis is the Problem Table.

The Problem Table is an algorithm for setting the energy targets algebraically. It considers the temperature intervals of cold and hot streams together and for each interval the enthalpy balance is calculated.

It is also necessary to ensure that, within any interval, hot and cold streams are at least ΔT_{min} apart. This is done by shifting the temperatures of $\Delta T_{min}/2$ below hot streams and $\Delta T_{min}/2$ above cold streams.

It is however possible to shift only the HCC or the CCC of ΔT_{min}. In the present work only the HCC is shifted, to avoid errors in the enthalpies calculation near the evaporation zones.
Setting up the intervals in this way guarantees that full heat interchange within any interval is possible. Hence, each interval has either a net surplus (positive ΔH) or a net deficit (negative ΔH) of heat as dictated by enthalpy balance but never both.
Enthalpy balances are calculated as:

$$\Delta H = (S_i - S_{i+1}) \cdot (\sum(\dot{C})_H - \sum(\dot{C})_C)_i \quad (5.2.2)$$

For any interval i, with S shifted temperature.
All "surplus" intervals reject heat to cold utility and all "deficit" intervals take heat from hot utility.
The total heat recovered by the heat exchange is found by adding the heat loads for all the hot streams and all the cold streams (cumulative heat load Q). As negative heat flows between intervals are thermodynamically unfeasible, the cumulative heat load hat each interval (Q_i) has always to be positive or at least null.
Where the cumulative heat load is zero finds the pinch point.
Finally, from the problem table, it is possible to plot a diagram of net heat flow against shifted temperature. The result is the grand composite curve (GCC), which represents the difference between the heat available from the hot streams and the heat required by the cold streams at a given shifted temperature.
The GCC shows how much net heating and cooling is required and shows the pinch point position, which is located at the point where the net heat flow has zero value and the GCC touches the axis.

5.2 METHODOLOGY AND OPTIMIZATION PROCEDURE

For the study of the best integration between single or dual pressure ORC, pinch analysis techniques are employed, following the procedure suggested in [22].
The single and dual pressure system configuration and the independent variables are the same presented in Sections 4.1 and 4.2. The decision variables, in addition to the evaporation pressures and the superheating degrees, are the working fluid mass flow rate ($\dot{m}_{wf}$) in the simple ORC and the ratio between HP mass flow rate and the entire working fluid mass flow rate ($\dot{m}_{HP}/\dot{m}_{wf}$) in the dual stage one.
The method employed to get the maximum power output from a composite heat source is based on the following steps:

1. Choice of the minimum temperature difference (ΔT_{min}) between the HCC and the CCC. This value is set at 10°C like ΔT_{PP}.
2. Building of the HCC. From the heat source input data is possible to obtain the mass flow rate $\dot{m}$, the heat capacity $\dot{C}$, the heat load H and the cumulative heat load Q for every temperature interval of the hot streams as showed in Table 5, which are sufficient to get the HCC showed in Figure 14.
3. Calculation of thermodynamic intensive variables of the working fluid in all states of the cycle according to the models presented is Section 4.3. The implemented programs in EES are fully reported in Appendix C and D for the single and dual pressure ORC respectively.

Table 5. Temperature intervals of the HCC.

$\dot{m}$ [kg/s]	T_{in} [°C]	T_{out} [°C]	$\dot{C}$ [kW/K]	H [kW]	Q [kW]
50	150	130	214,3	4287	16153
100	130	110	424,7	8493	11867
50	110	100	211,1	2111	3374
30	100	90	126,3	1263	1263

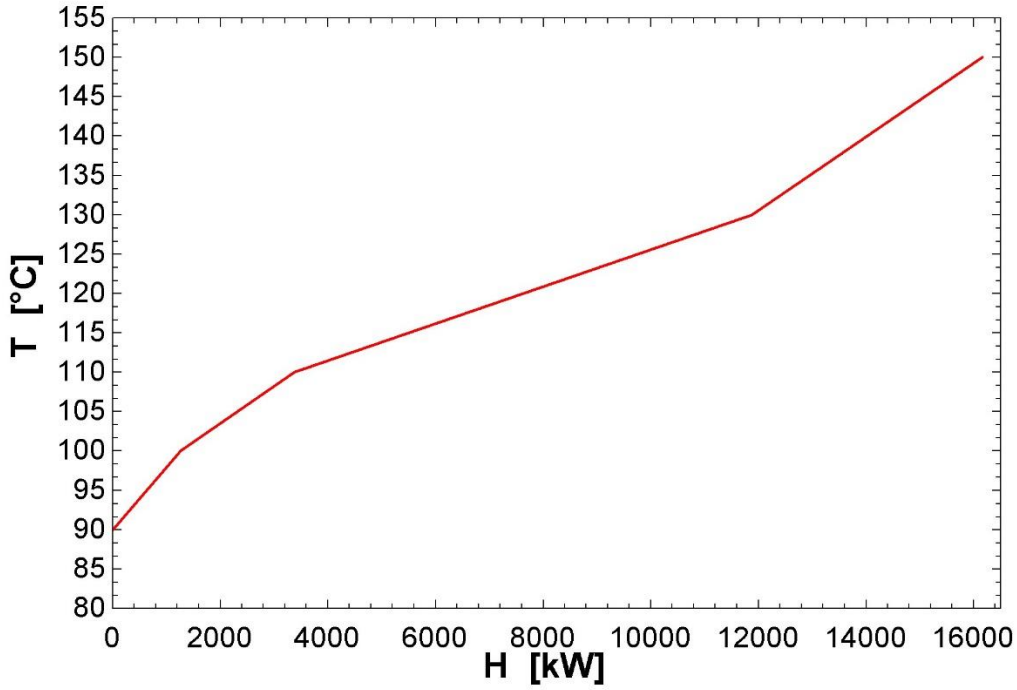

Figure 14. Hot composite curve.

4. Definition of the decision variables and their limits. The evaporation pressure can vary from the condensation pressure to $p_{cr} - 1{,}3$ bar, the superheating degree from 5°C to 20°C (HP stage and single pressure ORC) or from 0,01°C to 20°C (LP stage).
   With the single pressure ORC a limit is imposed to the working fluid mass flow rate, which has to respect the following constraint:
   $$\dot{m}_{wf} \leq \frac{Q_{av}}{h_5 - h_2} \quad (5.2.1)$$
   Where $h_5 - h_2$ is the specific enthalpy difference from the pump outlet to the turbine inlet.
   With the dual pressure ORC a limit is imposed to the heat absorbed by the working fluid, which must be less or at least equal to the heat available from the heat source:
   $$Q_{in} \leq Q_{av} \quad (5.2.2)$$
   Moreover, it was necessary to suppose the HP pinch point position in order to write the energy balance at HP-evaporator and hence obtain an expression for $\dot{m}_{HP}$. After the first optimization, the pinch point location was checked and eventually changed.
   In this way, it was possible to define also $\dot{m}_{wf}$ and $\dot{m}_{LP}$ as follows:
   $$\dot{m}_{HP} = \frac{\dot{m}_{geo,1} \cdot (h_{w1} - h_{w2}) + \dot{m}_{geo,2} \cdot (h_{w2} - h_{w3})}{h_7 - h_5} \quad (5.2.3)$$

Where $\dot{m}_{geo,1}$ and $\dot{m}_{geo,2}$ are the heat source mass flow rate of the first two intervals of the HCC and the other points refer to Figure 15, with *w3* in correspondence to the supposed pinch point position.

Defining then the optimization variable:

$$ratio = \frac{\dot{m}_{HP}}{\dot{m}_{wf}} \quad (5.2.4)$$

The total working fluid and the LP mass flow rates are given by:

$$\dot{m}_{HP} = \dot{m}_{HP} \cdot ratio \quad (5.2.5)$$

$$\dot{m}_{LP} = \dot{m}_{wf} - \dot{m}_{HP} \quad (5.2.6)$$

5. Building of the CCC. From the thermodynamic intensive variables of the ORC cycle and knowing the working fluid mass flow rates it is possible to build the CCC, considering the heating process from feed pump outlet to the expander inlet for the simple ORC and from LP pump outlet to HP turbine inlet for the dual pressure configuration.
6. First optimization. The aim of this first optimization is to locate the temperatures of the cold streams even if ΔT_{min} is not respected at the pinch points, in order to find the temperature intervals for the Problem Table.

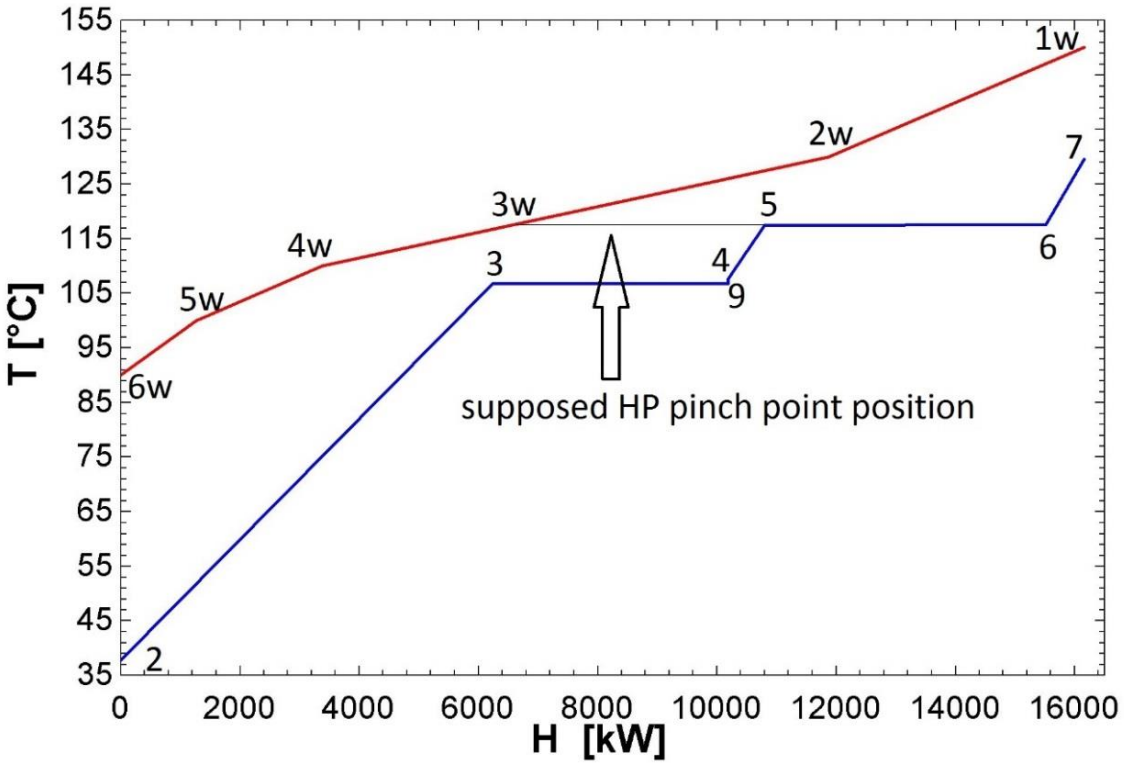

Figure15. Supposition of the HP pinch point position.

7. Building of the Problem Table. The HCC curve is shifted by ΔT_{min} while the CCC keeps its real temperatures. The enthalpy balances are obtained with the shifted temperatures and the cumulative heat load is calculated at every temperature interval.
8. The heat transfer feasibility is checked by assigning at every temperature interval in the problem table a positive or at least null value of the cumulative heat load.

9. Iteration of the optimization to find the correct distance between the HCC and the CCC. The net power output is now correctly calculated.

Following the procedure summarized in Figure 16, it was possible to obtain the optimum for both single and dual pressure configuration using isobutane, R1234ze(Z), R245fa and isopentane.

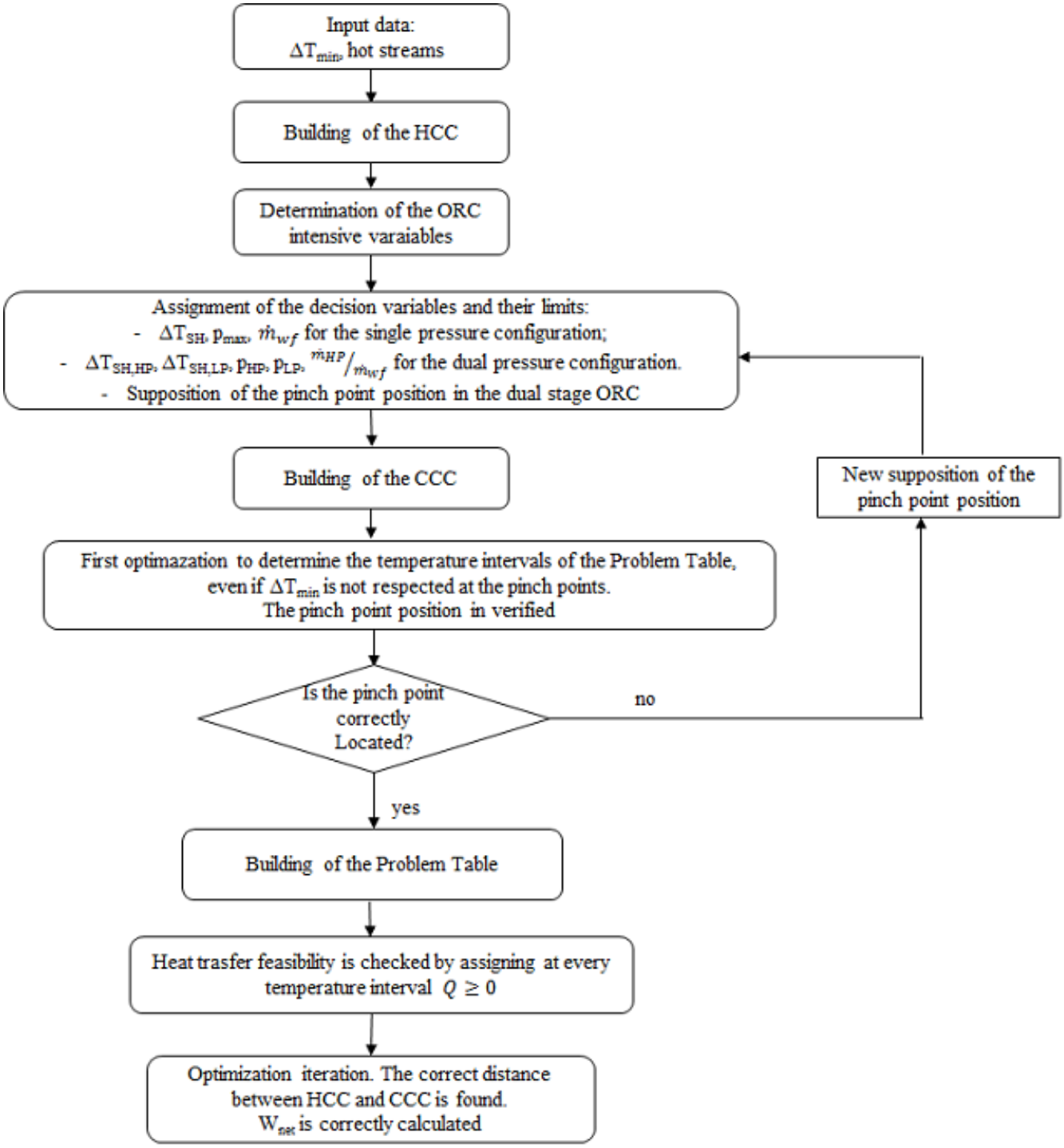

Figure16. Optimization procedure.

Some difficulties where found in the construction of the Problem Table. The order of the temperature intervals depends on the CCC, being the HCC fixed. To collocate the temperatures in the right order an internal procedure was written in EES for the introduction of a "if cycle". This procedure worked for the single pressure ORC, but not for the dual pressure one. In this case, a solution could not be found, because of convergence issues.
To solve the problem, the HP-pinch point position was supposed and, by setting the limit $Q_{in} \leq Q_{av}$, it was possible to find the order of the temperature intervals. After the first optimization, the pinch point position was verified. If it was correct so was also the order of the temperature intervals, because having set that constraint on the absorbed heat made the heat transfer theoretically feasible, the only problem could be found at the pinch points, where ΔT_{min} could not be respected. It was then necessary to move the CCC curve to the right to keep the right distance to the HCC, this was done by setting a positive or at least null cumulative heat at every temperature interval.

6. RESULTS

In this chapter, the optimization results are presented.
First, the single pressure configuration coupled with the heat source at constant heat capacity is analyzed, followed by the dual pressure configuration at the same conditions. The working fluid selection criterion for basic ORC is validated and a criterion is introduced to select the fluid for the dual pressure ORC. With the net power maximization (Section 6.1), the aim is to identify the thermodynamic conditions in which the dual stage configuration can be advantageous respect to the simple one.
In Section 6.2 some economic consideration based on *AR* optimization and costs calculation are presented.
In the last section, both ORC configurations are coupled with heat sources at different heat capacities and analyzed following pinch analysis procedure explained in the previous chapter.

6.1 NET POWER MAXIMIZATION

The results about the maximization of the net power output W_{net} are here presented, in the first subsection for the single pressure ORC and in the second subsection for the dual pressure one.
The best fluid for the dual stage ORC resulted to be the same of the single pressure ORC.
Regarding pinch point position, it has been found that at the minimal superheating degree, for both single and dual pressure configuration is at the beginning of the evaporation, but in the dual stage ORC, when the superheating increases, the pinch point can be located at the end of the low-pressure superheater or, when the maximal pressure is near the permitted limit, at the beginning of the HP evaporation.

6.1.1 Single Stage ORC

Analyzing the single stage ORC, it is found that superheating (ΔT_{SH}) is never advantageous.
The employed fluids for each heat source inlet temperature ($T_{in,HS}$) are shown in Table 6.

Table 6. Employed working fluids for each brine inlet temperature.

$T_{in,HS}$ [°C]	Fluids
100	R1234yf, R134a, R1234ze(E)
125	R1234yf, R134a, R1234ze(E)
150	R1234ze(E), isobutane, R1234ze(Z), R245fa, isopentane
175	Isobutane, R1234ze(Z), R245fa, isopentane
200	Isopentane

At the lowest brine inlet temperatures, the excluded fluids have $T_{cr}>T_{HS,in}$ which translates in a low heat recovery factor φ; whereas at the higher $T_{in,HS}$, the excluded fluids have a temperature difference $T_{HS,in}-T_{cr}>50°C$ and hence a low thermal efficiency η_{th}.
For each $T_{HS,in}$ the optimal points, obtained with the different working fluids, are reported in tables.

- $T_{in,HS}$=100°C

When the heat source inlet temperature is 100°C the fluids R1234yf, R134a and R1234ze(E) are used. In Table 7 the results are shown when the net power is maximized.

Table 7. Optimum working point with $T_{in,HS}$=100°C

Fluid	**R1234yf**	R134a	R1234ze(E)
p_{max} [bar]	19,3	20,12	15,22
ΔT_{SH} [°C]	5	5	5
W_{net} [kW]	**694,7**	627,8	631,4
AR [m^2/kW]	4,206	3,854	4,222
T_{cond} [°C]	39,28	39,37	39,16
p_{cond} [bar]	10	10	7,5
m_{wf} [kg/s]	87,28	69,21	70,79
T_{max} [°C]	72,32	72,72	72,52
$T_{out,real}$ [°C]	67,81	70,01	69,91
φ	0,4033	0,3758	0,3770
η_{th}	0,0514	0,0499	0,0500
η_{sys}	**0,0207**	0,0187	0,0188

R1234yf is the most performing fluid, giving around 9,5% more power than R134a and R1234ze(E). This is in accord to the working fluids selection criteria [6-9], being R1234yf the only with $T_{cr} < T_{in,HS}$. In Figure 17 and 18 the comparison among the fluids in the *T-s* and *T-Q* diagrams is shown. R1234yf is the one that allows the best exploitation of the available heat, having the highest heat recovery factor φ. Consequently, as it is visible from Figure 16, the brine outlet temperature ($T_{out,real}$ in the tables) is the lowest.

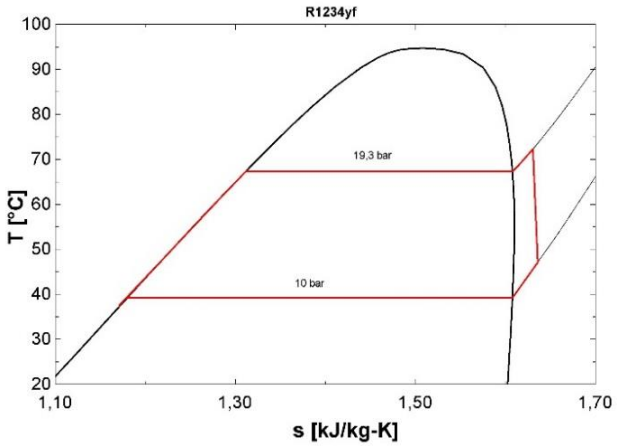

a) R1234yf

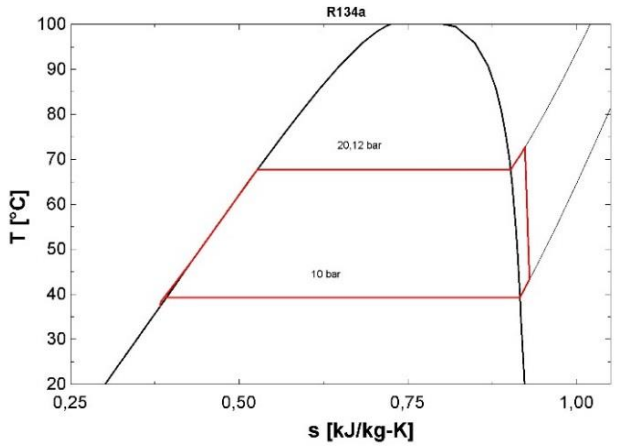

b) R134a

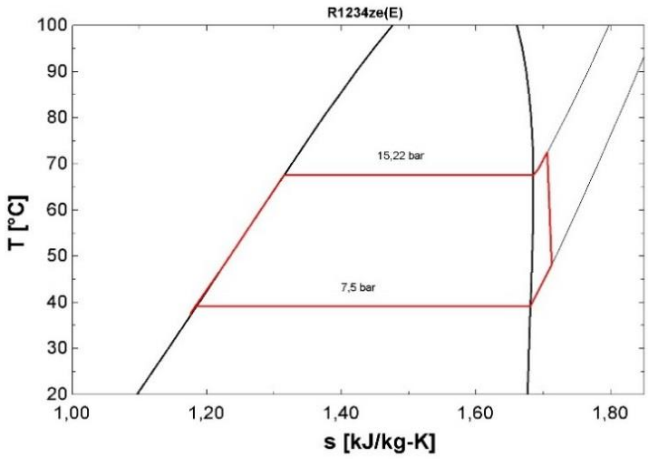

c) 1234ze(E)

Figure 17. T-s diagrams with $T_{in,HS}$=100°C for single pressure ORC.

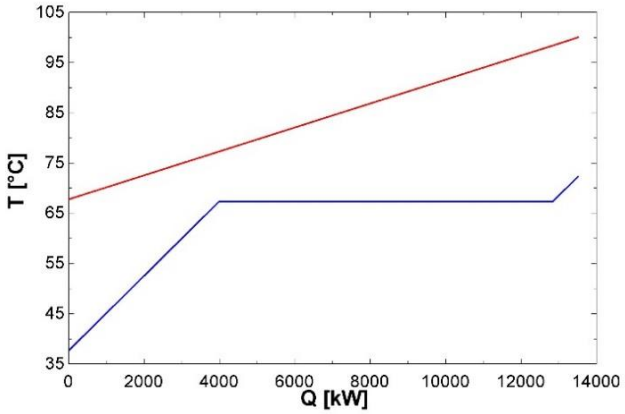

a) R1234yf

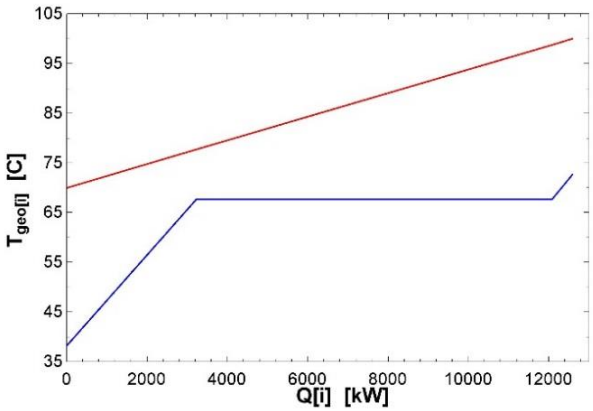

b) R134a

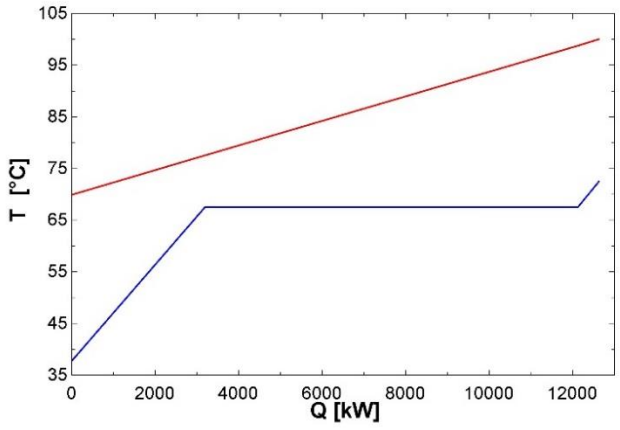

c) 1234ze(E)

Figure 18. T-Q diagrams with $T_{in,HS}$=100°C for single pressure ORC.

An analysis around the optimum is also carried out. The decision variables, i.e. the evaporation pressure (p_{max}) and the superheating degree (ΔT_{SH}), are varied to study their influence on W_{net}.
The results of this sensitivity analysis are shown in Figure 19, where W_{net} trend is plotted in the diagram p_{max} versus ΔT_{SH}.
Using R1234yf (Figure 19a), W_{net} is influenced by both p_{max} and ΔT_{SH}, R134a and R1234ze(E) exhibit a similar behavior (Figure 19b and c), in which the effect of ΔT_{SH} on W_{net} is almost negligible, being the lines nearly vertical.

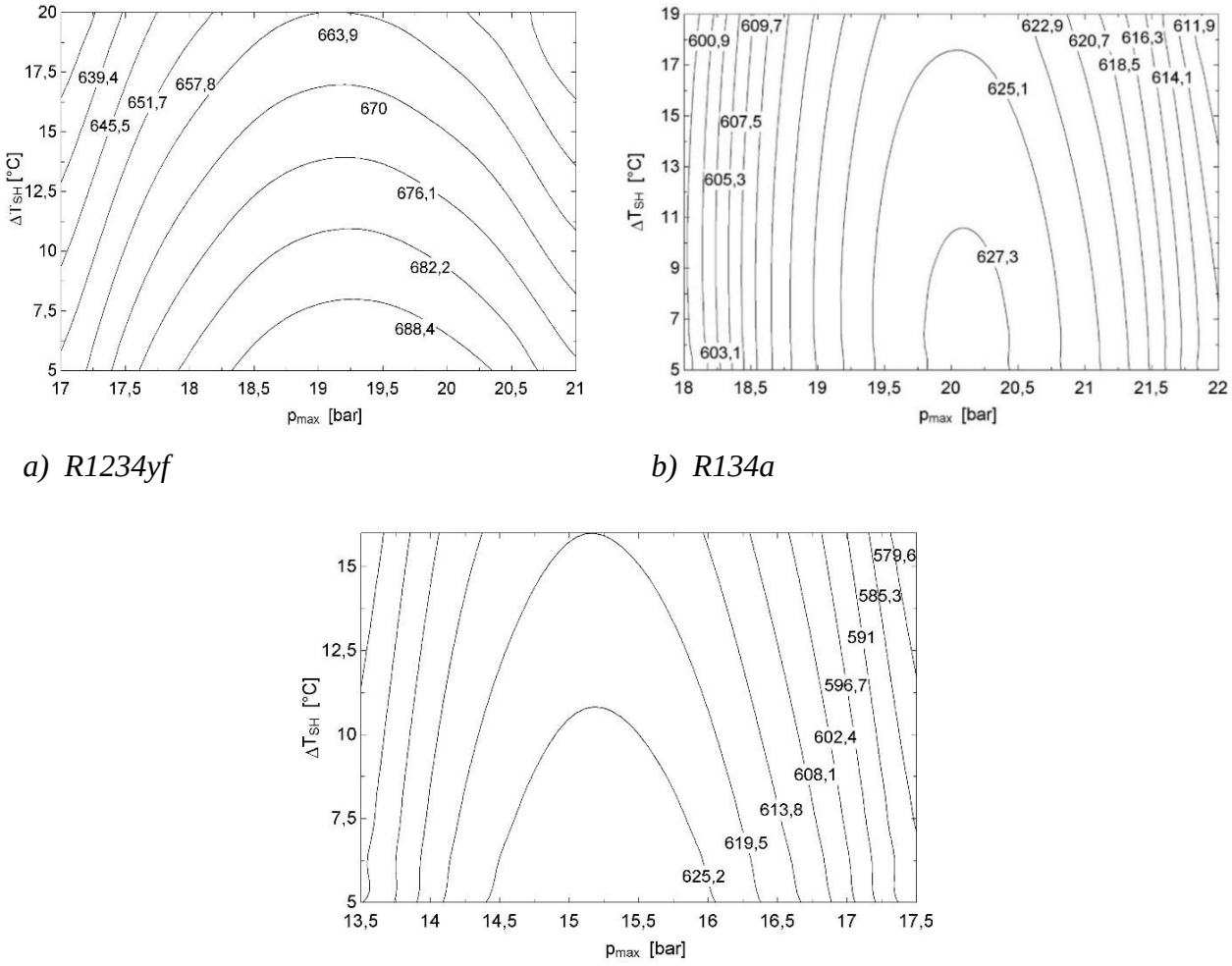

a) R1234yf *b) R134a*

c) 1234ze(E)

Figure 19. Variation of W_{net} with maximum cycle pressure and superheating at T_{in_HS}=100°C.

- $T_{in,HS}$=125°C

With 125°C brine inlet temperature, the same fluids as in the previous case are employed and again R1234yf is the most performing fluid, giving around 21% more net power respect to R134a and R1234ze(E).
At this $T_{in,HS}$, for all fluids results that $T_{cr} < T_{in,HS}$.
Analyzing the ratio $T_{cr}/T_{in,HS}$ and the difference $T_{in,HS}$-T_{cr}, it is found that the working fluid selection criteria proposed by Li [8] and Vivian [9] are more precise than those suggested by Vetter [6] and Astolfi [7], having R1234yf $T_{in,HS}$-T_{cr}=30,3°C, in the range recommended in [8,9], but

$T_{cr}/T_{in,HS}$=0,758 which is below the range recommended in [6,7]. According to this last criterion the ideal $T_{cr}/T_{in,HS}$ ratio is between 0,8 and 0,9 [6] or between 0,88 and 0,92 [7], hence the most suitable fluid should have been R1234ze(E) with $T_{cr}/T_{in,HS}$=0,875.

Table 8. Optimum working point with $T_{in,HS}$=125°C.

Fluid	**R1234yf**	R134a	R1234ze(E)
p_{max} [bar]	32,5	29,84	21,6
ΔT_{SH} [°C]	5	5	5
W_{net} [kW]	**2038**	1620	1592
AR [m^2/kW]	2,695	2,253	2,804
T_{cond} [°C]	39,28	39,37	39,16
p_{cond} [bar]	10	10	7,5
m_{wf} [kg/s]	162,5	118,4	118,1
$T_{\_max}$ [°C]	72,32	72,72	72,52
$T_{out,real}$ [°C]	97,7	90,91	88,44
φ	0,5736	0,4917	0,4928
η_{th}	0,0802	0,0747	0,0733
η_{sys}	**0,0462**	0,0367	0,0361

R1234yf reaches the maximum allowed pressure, being its critical pressure 33,82 bar. That is visible also from Figure 20, which represents the *T-s* diagram of the different fluids, where for R1234yf p_{max} almost "touches" the top of the bell (Figure 20a).
From Figure 21 it is clear why R1234yf has the highest heat recovery factor φ (57% against 49% of R134a and R1234ze(E)): in Figure 21a the heating and the cooling curves are closer than in Figure 21b-c, being almost parallel during the preheating. Moreover, working in the upper part of the bell means a shorter evaporation zone allowing a better match of these curves.

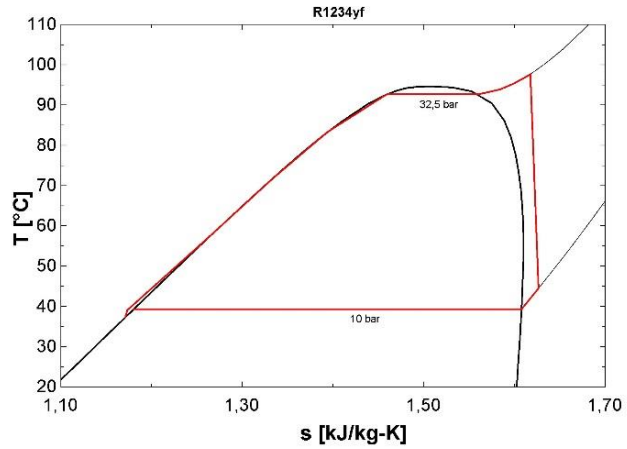

a) R1234yf

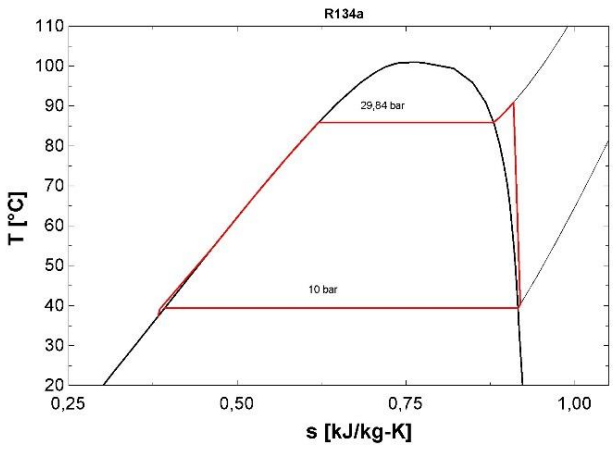

b) R134a

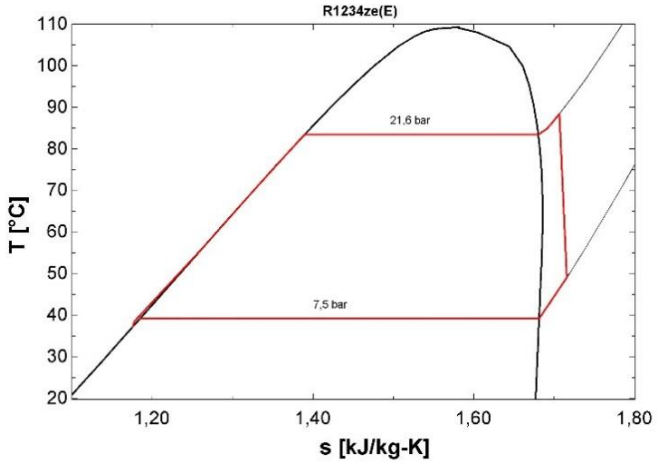

c) 1234ze(E)

Figure 20. T-s diagrams with $T_{in,HS}$=125°C for single pressure ORC.

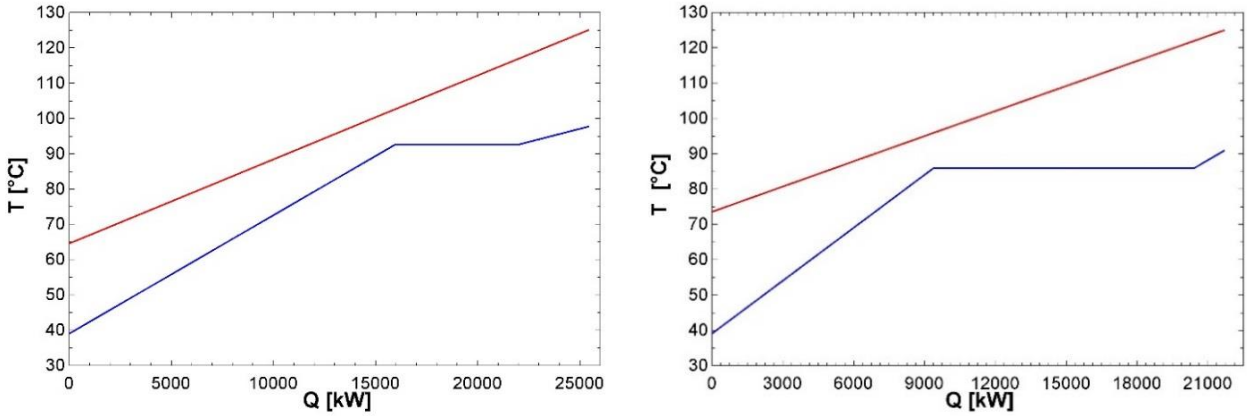

a) R1234yf *b) R134a*

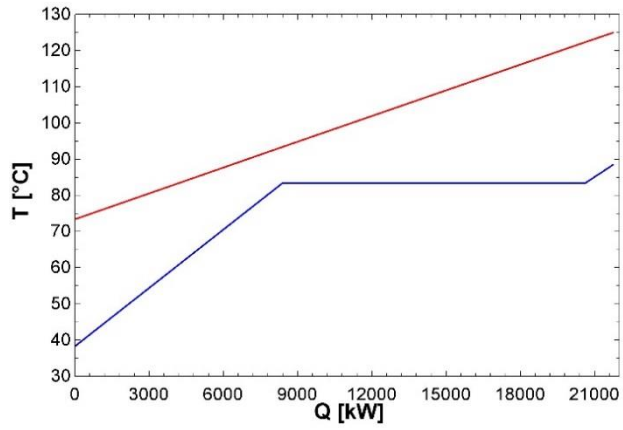

c) 1234ze(E)

Figure 21. T-Q diagrams with $T_{in,HS}$=125°C for single pressure ORC.

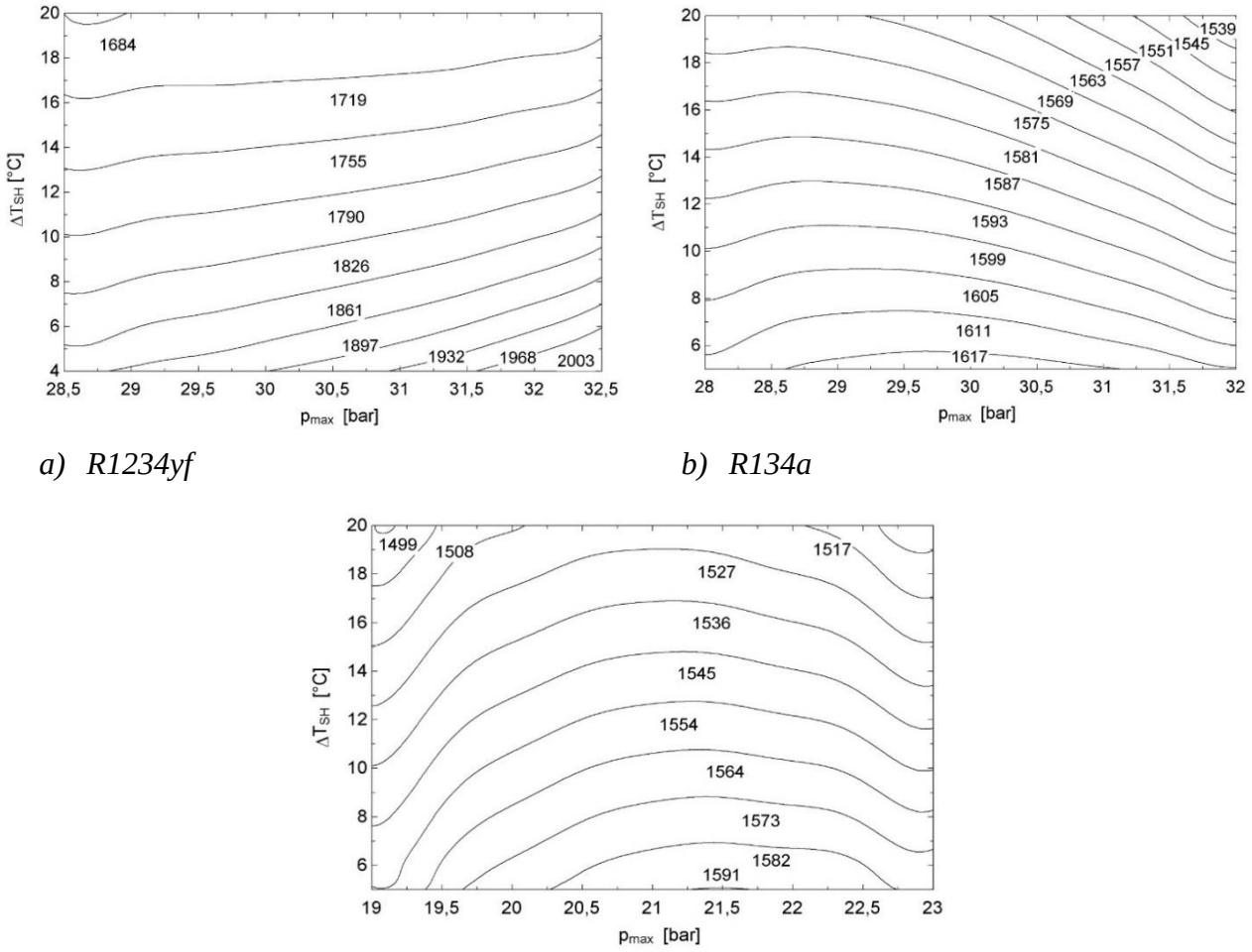

a) R1234yf *b) R134a*

c) 1234ze(E)

Figure 22. Variation of W_{net} with maximum cycle pressure and superheating at $T_{in,HS}$=125°C.

Finally, the analysis around the optimum (Figure 22) shows that for R1234yf and R134a (Figure 22a-b) W_{net} in general is strongly influenced by ΔT_{SH} but not by p_{max}, but near the optimum point of R1234yf the lines are closer, meaning that, when the maximum allowed pressure is reached, the operation is more unstable.
Using R1234ze(E) W_{net} is influenced by both decision variables.

- $T_{in,HS}$=150°C

At this brine inlet temperature, R1234ze(E), isobutane, R1234ze(Z), R245fa and isopentane are used. R1234ze(E) is the fluid which gives the maximum net power (on average 29% more than the others). This fluid has $T_{cr}/T_{in,HS}$=0,729 and $T_{in,HS}$-T_{cr}=40,6°C, whereas isobutane has $T_{cr}/T_{in,HS}$=0,898 and $T_{in,HS}$-T_{cr}=15,3°C, this is another confirm of the criterion presented by Vivian et al. [9], for which the most suitable fluids for single pressure ORC have $T_{in,HS}$-T_{cr} around 35°C.
R1234ze(Z), R245fa and isopentane, having T_{cr}>$T_{in,HS}$, are penalized because of the lower φ.
Optimum working points are showed in Table 9.
R1234ze(E) results the best choice especially for the decisively high heat recovery factor, which is more than 25% higher than the other fluids.

Table 9. Optimum working point with $T_{in,HS}$=150°C.

Fluid	**R1234ze(E)**	Isobutane	R1234ze(Z)	R245fa	Isopentane
ΔT_{SH} [°C]	5	5	5	5	5
P_{max} [bar]	35	19,07	11,99	11,35	6,315
W_{net} [kW]	**4002**	2923	2815	2886	2710
AR [m^2/kW]	2,515	2,122	1,733	2,012	2,043
T_{cond} [°C]	39,16	39,21	38,84	38,82	39,73
p_{cond} [bar]	7,5	5,2	2,8	2,4	1,5
m_{wf} [kg/s]	226,9	78,05	124,3	131,5	67,23
T_{max} [°C]	112,5	102,9	99,57	100,1	98,94
$T_{out,real}$ [°C]	50,98	77,03	82,57	79,16	81,58
φ	0,7629	0,5646	0,5222	0,5483	0,5298
η_{th}	0,0957	0,0945	0,0984	0,0960	0,0934
η_{sys}	**0,0730**	0,0533	0,0514	0,0527	0,0495

From Figure 23 it can be seen that R1234ze(E) reaches the maximum allowed pressure (35 bar), whereas all other fluids operate at a considerable lower pressure.

This picture shows also why the superheating is not advantageous: with higher ΔT_{SH} the expansion would end in a more superheated steam zone increasing the cooling load at the condenser.

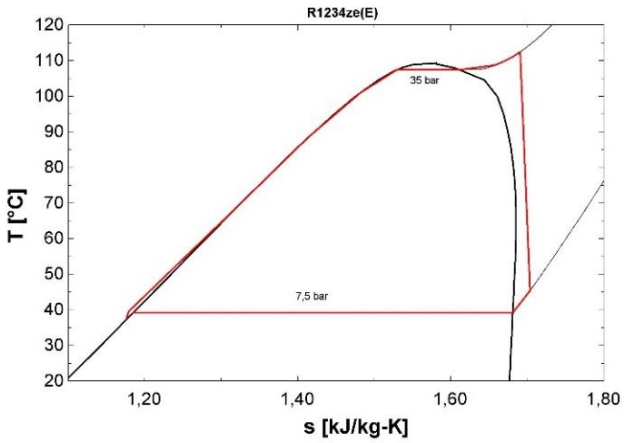

a) R1234ze(E)

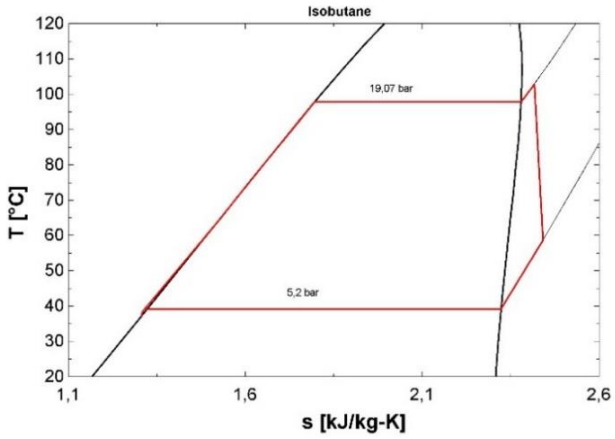

b) Isobutane

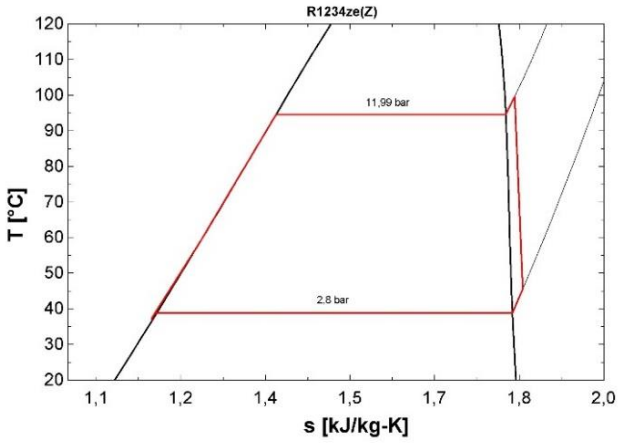

c) R1234ze(Z)

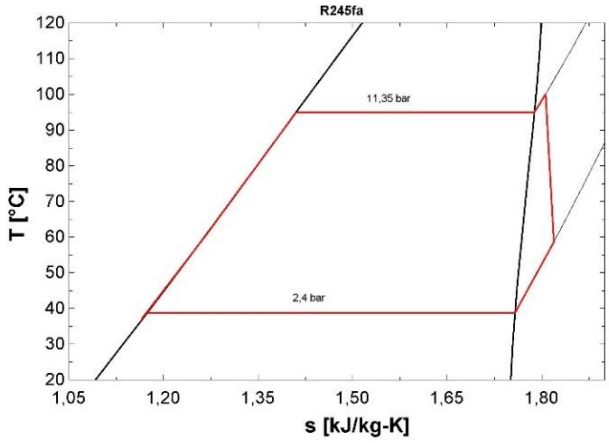

d) R245fa

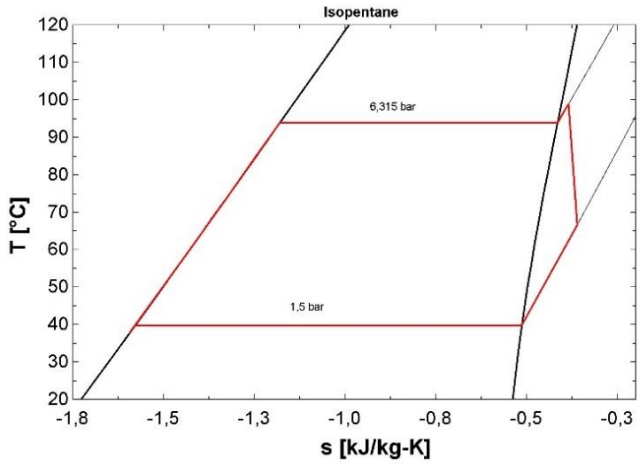

e) Isopentane

Figure 23. T-s diagrams with $T_{in,HS}$=150°C for single pressure ORC.

From Figure 24a the perfect match is visible, during preheating, between the heating and the cooling curves of R1234ze(E), which lose their approach in the evaporation zone, which is however short.

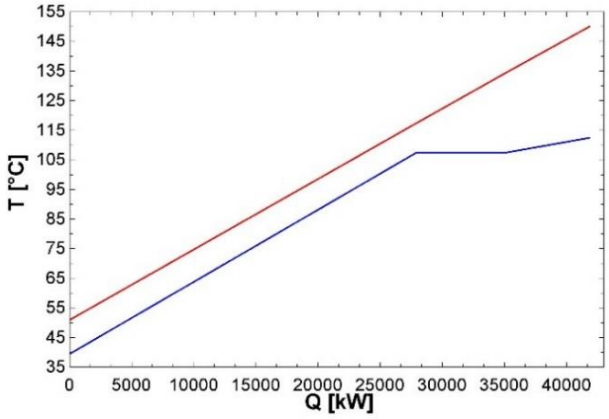

a) R1234ze(E)

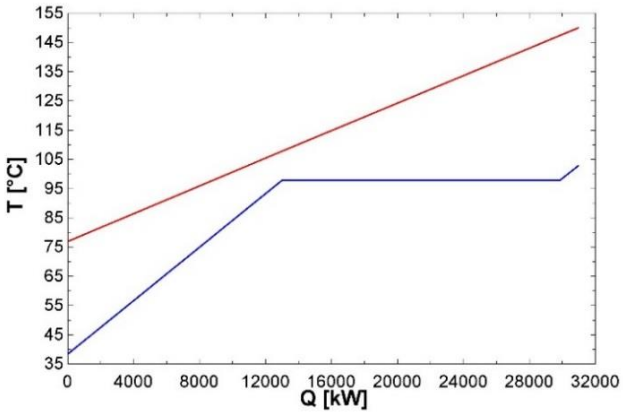

b) Isobutane

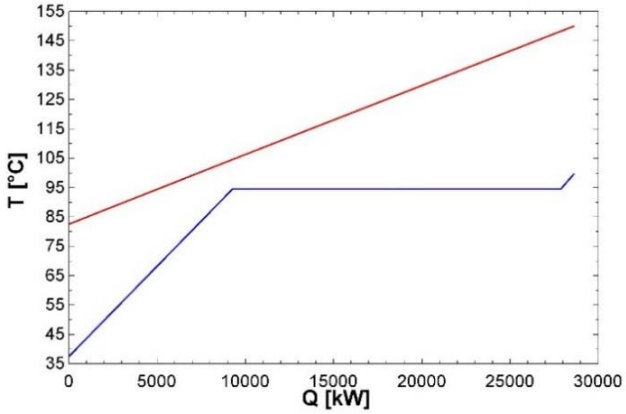

c) R1234ze(Z)

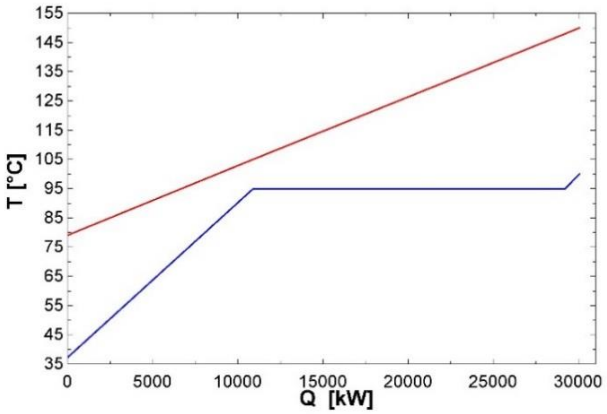

d) R245fa

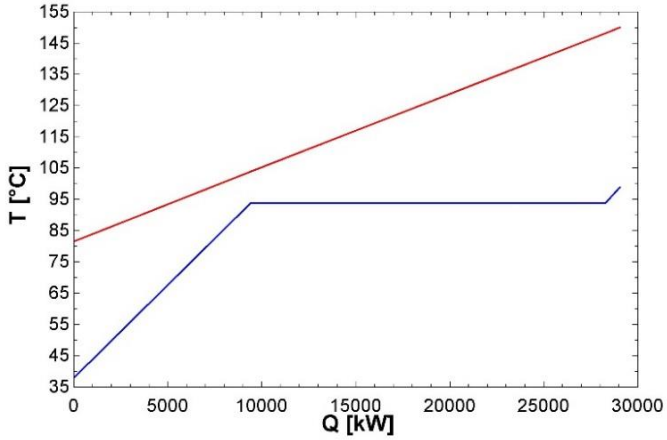

e) Isopentane

Figure 24. T-Q diagrams with $T_{in,HS}$=150°C for single pressure ORC.

Figure 24c-e confirm that fluids with $T_{cr}>T_{in,HS}$ lead to a low φ because of the bad matching of the temperature profiles in the evaporator.

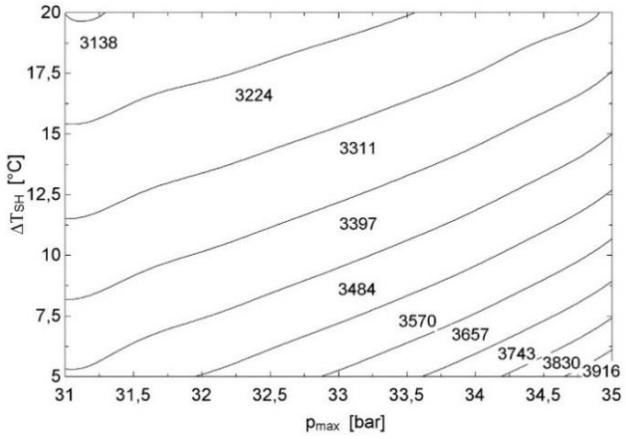

a) R1234ze(E)

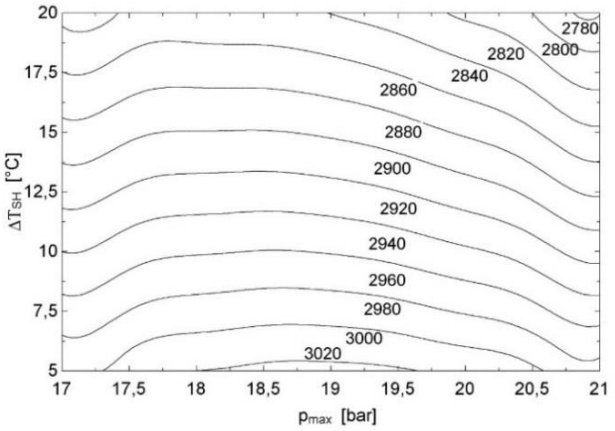

b) Isobutane

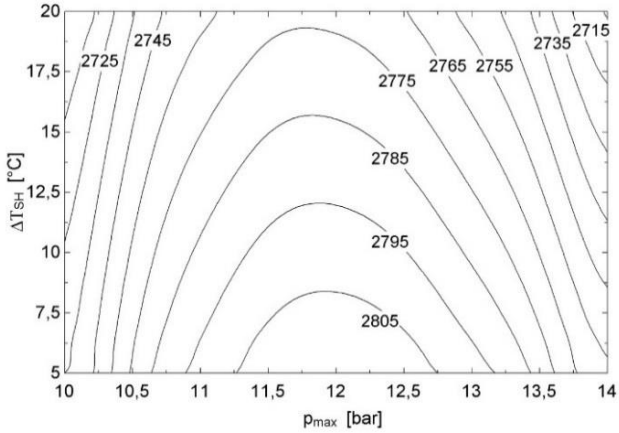

c) R1234ze(Z)

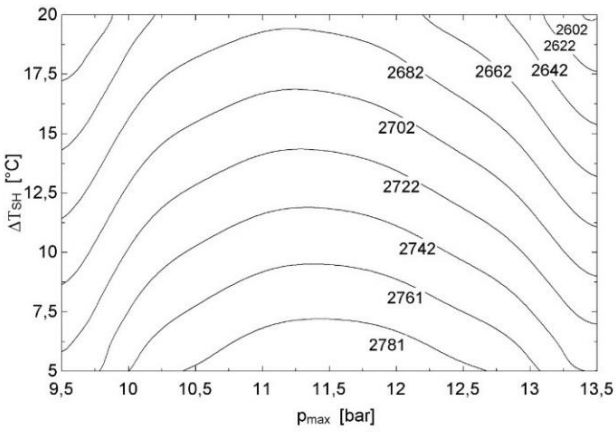

d) R245fa

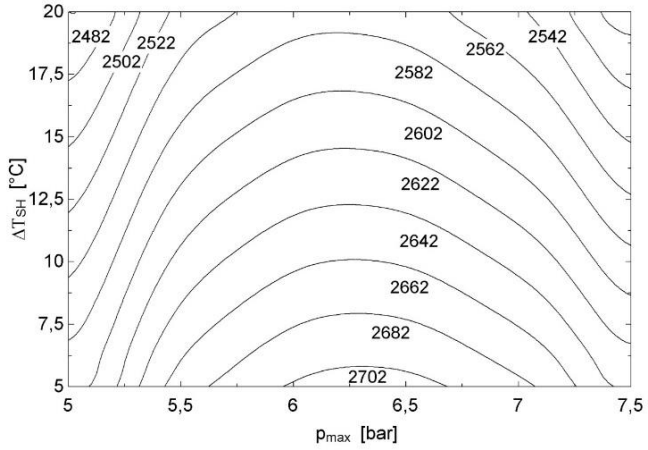

e) Isopentane

Figure 25. Variation of W_{net} with maximum cycle pressure and superheating at $T_{in,HS}$=150°C.

Figure 25 shows the analysis around the optimum of the various fluids.
R1234ze(E), having reached the maximum allowed pressure, presents a high variability of W_{net} close to the optimal point (Figure 25a), moving from this point, the isopower lines are more stretched out and the influence of both p_{max} and ΔT_{SH} is relevant.
Using isobutane, W_{net} results more affected by ΔT_{SH} than by p_{max} being the isopower lines almost horizontal.
R1234ze(Z), R245fa and isopentane show instead a similar trend: both p_{max} and ΔT_{SH} influence W_{net}.

- $T_{in,HS}$=175°C

Isobutane, R1234ze(Z), R245fa and isopentane are employed when $T_{in,HS}$=175°C.
The optimum working points are presented in Table 10.
Considering the selection criteria, the results validate again that the best fluid has $T_{in,HS}$-T_{cr} around 35°C. In fact, isobutane gives the highest W_{net} (on average 26% more than the others) with a difference $T_{in,HS}$-T_{cr}=40,3°C. R1234ze(Z) and R245fa have a value of 24,9°C and 21°C respectively. Looking at the ratio $T_{cr}/T_{in,HS}$, isobutane has a value of 0,77, R1234ze(Z) of 0,86 and R245fa of 0,88. Hence, the criterion of keeping the difference between heat source inlet temperature and critical temperature about 35°C seems the most accurate.

Table 10. Optimum working point with $T_{in,HS}$=175°C.

Fluid	**Isobutane**	R1234ze(Z)	R245fa	Isopentane
ΔT_{SH} [°C]	5	5	5	5
p_{max} [bar]	35	17,72	16,94	8.743
W_{net} [kW]	**6349**	4709	4853	4454
AR [m^2/kW]	2,01	1,382	1,656	1,678
T_{cond} [°C]	39,21	38,84	38,82	39,73
p_{cond} [bar]	5,2	2,8	2,4	1,5
$m_{\_wf}$ [kg/s]	125,6	166,6	174,4	87,71
T_{max} [°C]	137,4	118,1	118,5	114,2
$T_{out,real}$ [°C]	52,84	83,27	77,27	81,41

φ	0,7898	0,5966	0,6348	0,6084
η_{th}	0,1225	0,1202	0,1165	0,1115
η_{sys}	**0,09671**	0,07173	0,07393	0,06784

Figure 26 shows the *T-s* diagrams of all the employed fluids. With isobutane (Figure 26a) the maximum allowed pressure of 35 bar is reached, having p_{cr}=36,4 bar.

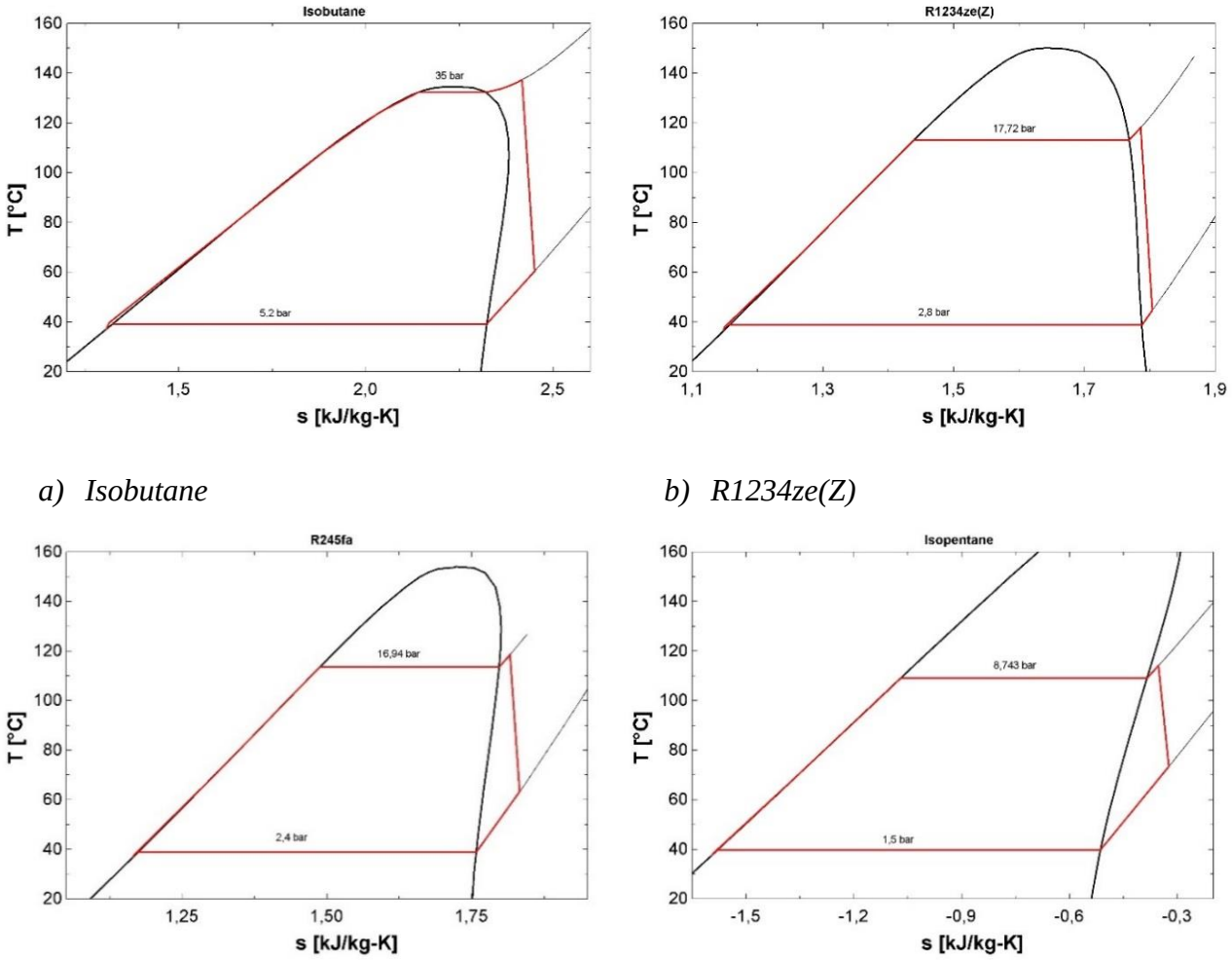

a) Isobutane

b) R1234ze(Z)

c) R245fa

d) Isopentane

Figure 26. T-s diagrams with $T_{in,HS}$=175°C for single pressure ORC.

In Figure 27 the match of the temperature profiles is shown.
Isobutane (Figure 27a) realizes a rally good match between the heating and the cooling curves, leading to a 20% to 25% higher *φ* respect to the other fluids.

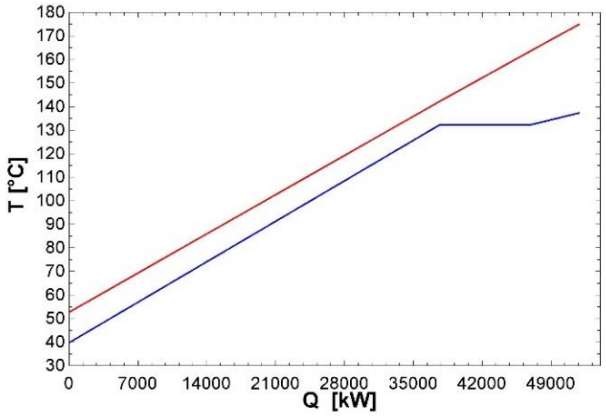

a) Isobutane

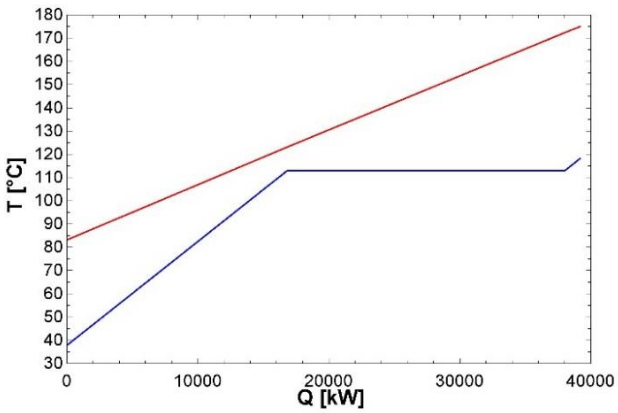

b) R1234ze(Z)

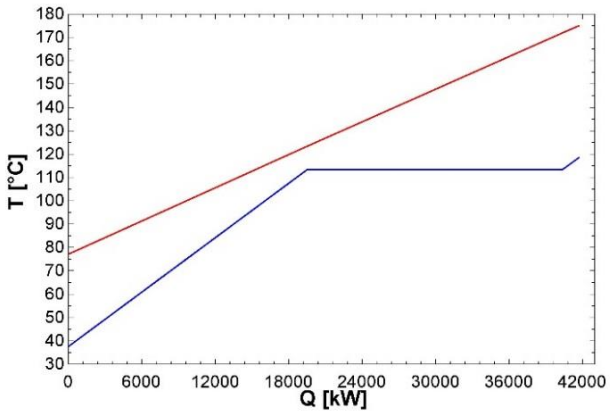

c) R245fa

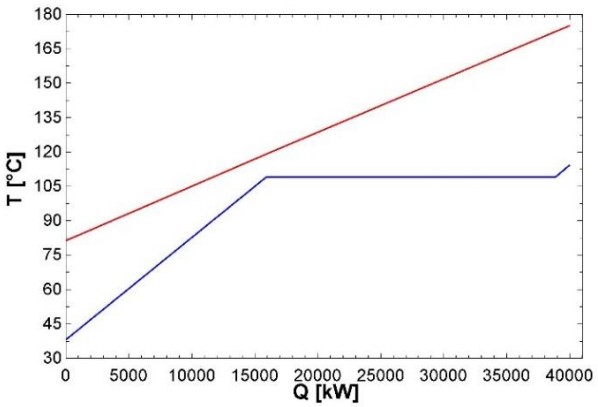

d) Isopentane

Figure 27. T-Q diagrams with $T_{in,HS}$=175°C for single pressure ORC.

Analyzing the behavior around the optimum (Figure 28), it is found that W_{net} with isobutane, R1234ze(Z) and R245fa varies a lot with ΔT_{SH} but it is more constant at the changing of p_{max}. Only approaching to the maximum allowed pressure the operation with isobutane becomes more unstable, being the isopower lines very close to each other. With isopentane both decision variables affect W_{net}.

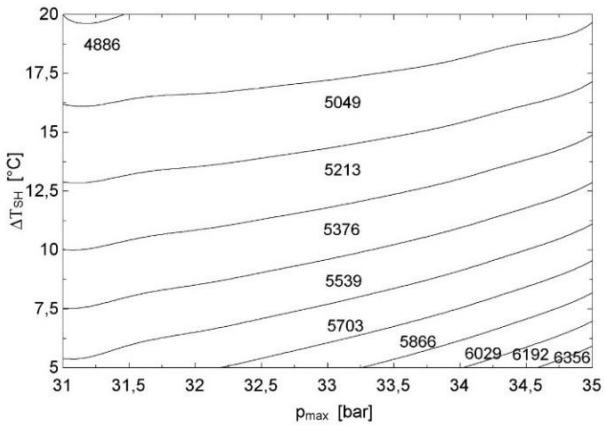

a) Isobutane

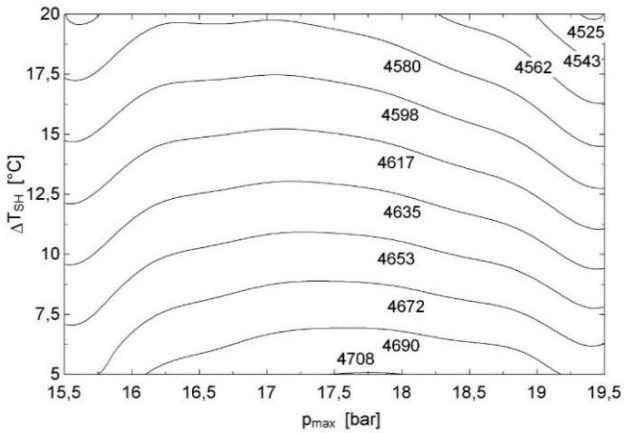

b) R1234ze(Z)

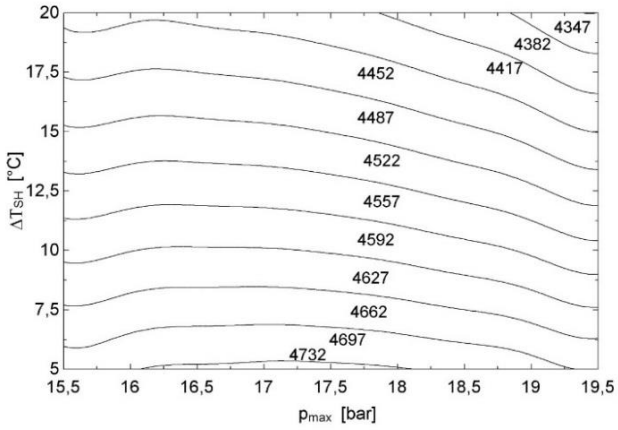

c) R245fa

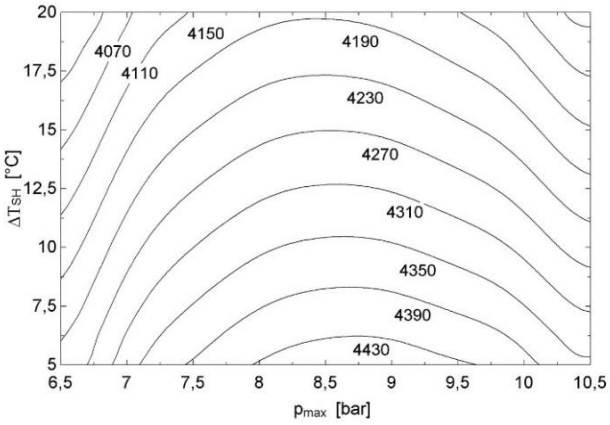

d) Isopentane

Figure 28. Variation of W_{net} with maximum cycle pressure and superheating at $T_{in,HS}$=175°C.

- $T_{in,HS}$=200°C

At this brine inlet temperature only isopentane is used. The optimum working point is presented in Table 11.

Table 11. Optimum working point for isopentane with $T_{in,HS}$=200°C.

ΔT_{SH}	p_{max}	W_{net}	AR	m_{wf}	T_{max}	$T_{out,real}$	φ	η_{th}	η_{sys}
[°C]	[bar]	[kW]	[m^2/kW]	[kg/s]	[°C]	[°C]			
5	12,49	6828	1,444	109,6	132,4	76,73	0,69	0,129	0,08902

The difference $T_{in,HS}$-T_{cr} is only 12,8°C and the ratio is 0,936. Probably, following the indication of the selection criteria, a working fluid with a critical temperature between that of R245fa and isopentane would produce more net power.

In Figure 29 the principal diagrams are plotted. Isopentane realizes a good temperature profile match in the preheating zone (Figure 29b), which results in a 12% higher φ than the previous case. With increasing brine temperature this match can improve given a higher total system efficiency.

Looking at Figure 29c, it can be seen that ΔT_{SH} influences the power output more than p_{max} and it can be concluded that the superheating is not advantageous because it leads to a decrease of W_{net}.

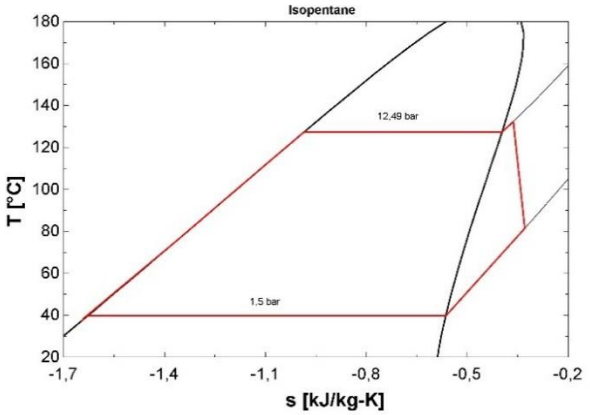

a) T-s diagram

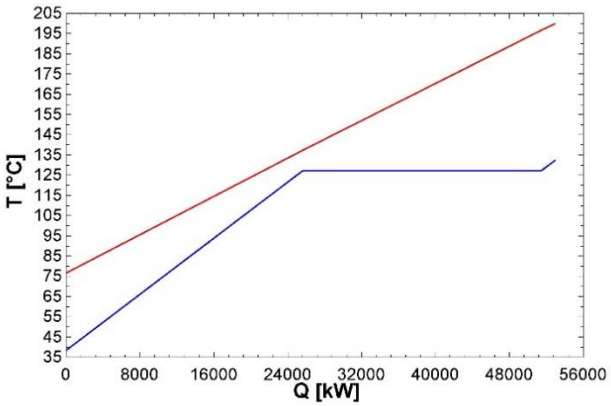

b) T-Q diagram

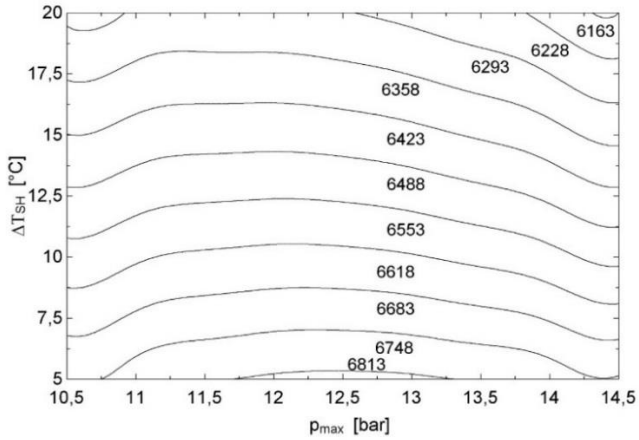

c) ΔT_{SH} - p_{max} diagram

Figure 29. Isopentane diagrams with $T_{in,SH}$=200°C.

6.1.1.1 Comparison with the literaure

To validate the results reported in the previous Section, they were compared with those available in the literature.

For example, Toffolo et al. [23] indicated isobutane and R134a as the best fluids for utilization of geothermal resources between 130°C and 180°C. Considering isobutane as working fluid, a heat source inlet temperature of 170°C and a brine mass flow rate of 100 kg/s, which are similar input data to the present work, the findings are comparable: evaporation pressure equal to 35,24 bar, thermal efficiency around 12% and 6,6 MW generated power, which is 250 kW higher than in this study with $T_{in,HS}$=175°C due to the lower condensation temperature (33°C).

Also Heberle and Brüggemann [24] found that isobutane is the most suitable fluid among the selected working fluids for $T_{in,HS}$=170°C.

Liu et al [25] investigated the potential of hydrofluoroolefins as working fluids in ORC systems, comparing their performance with those of R134a, R245fa and isopentane at different $T_{in,HS}$.

They set 30 bar as maximum cycle pressure and they considered geothermal resources at 120°C. 150°C and 180°C with 100 kg/s brine mass flow rate, fixing the pinch point temperature difference at 10°C.

With $T_{in,HS}$=120°C R1234yf was the most performing fluid reaching the maximum pressure and with a total system efficiency η_{sys}=4,7%, a similar result is here obtained at $T_{in,HS}$=125°C when R1234yf has η_{sys}=4,6%.

Also at $T_{in,HS}$=150°C the solutions found for R1234ze(E), R245fa, R1234ze(Z) and isopentane are similar to those here presented. In [25] η_{sys} is slightly higher because they opted for a higher pump efficiency (0,9).

The same can be notice comparing their results at $T_{in,HS}$=180°C with the ones at $T_{in,HS}$=175°C reported above.

6.1.2 Dual Stage ORC

With the dual pressure ORC the criterion for which the most suitable working fluid has $T_{in,HS}$-T_{cr} around 35°C is not more valid. In this section, the results are analyzed to find a correlation for the selection of the ideal working fluid for the dual stage ORC; with this purpose, expansion ratio (r_{ex}) and vaporization enthalpy (r) are taken into account.
Moreover, considering the low operation temperatures, the aim is trying to understand if there are conditions in which the addition of a second expansion brings to some advantages respect to single stage one.
Condensation pressure and temperature are the same of Section 6.1.1.
The optimum point in the dual pressure ORC is obtained with the minimum ΔT_{SH} for all temperature levels but 100°C.
Table 12 shows the employed fluids at each brine inlet temperature.

Table 12. Employed working fluids for each brine inlet temperature.

$T_{in,HS}$ [°C]	Fluids
100	R1234yf, R134a, R1234ze(E), isobutane, R1234ze(Z), R245fa, isopentane
125	R1234yf, R134a, R1234ze(E)
150	R1234ze(E), isobutane, R1234ze(Z), R245fa, isopentane
175	Isobutane, R1234ze(Z), R245fa, isopentane
200	Isopentane

- $T_{in,HS}$=100°C

At this brine inlet temperature, all fluids are selected. R1234yf gives the highest net power (W_{net}) as with the single pressure configuration, in this case however W_{net} is 21,7% higher. Moreover also R134a and R1234ze(E) show an improvement of more than 26%.
R1234yf is the fluid with the highest heat recovery factor φ, but it has the lowest thermal efficiency η_{th}, this confirms the necessity of a good compromise between these two performance parameters to guarantee a high total system efficiency η_{sys} and hence a high W_{net}.
It is to notice that R134a and R1234ze(Z) have their optimum when they are slightly superheated, whereas for the others ΔT_{SH} is at its minimum.
In Table 13 the optimum working point for each fluid is showed. R1234ze(Z) and R245fa perform well in spite of their high critical temperature. For this reason, considering only T_{cr} is not sufficient to select the suitable fluids for the dual pressure ORCs.
In Table 13 the expansion ration (r_{ex}) between HP and LP stage is also reported, because it could be another important parameter to consider in the fluid selection. It is defined as:

$$r_{ex} = \frac{p_{HP}}{p_{LP}} \tag{6.1.2.1}$$

At this ΔT_{SH} the optimal r_{ex} seems to be between 1,3 and 1,5.

Table 13. Optimum working point with T_{inHS}=100°C for the dual stage ORC.

Fluid	**R1234yf**	R134a	R1234ze(E)	Isobutane	R1234ze(Z)	R245fa	Isopentane
ΔT_{SH_HP} [°C]	5	13,5	5	5	6	5	5
$\Delta T_{SH\ LP}$ [°C]	0,01	11	0,01	0,01	14	0,01	0,01
p_{HP} [bar]	20,45	23,76	18,11	12,06	7,5	6.892	4,02
p_{LP} [bar]	15,42	16,6	12,6	8,513	4,966	4,456	2,669
W_{net} [kW]	**845,7**	794,1	799,7	794,1	813,9	820,7	776,6
AR [m^2/kW]	4,454	4,467	4,251	4,174	3,794	3,945	4,073
m_{HP} [kg/s]	79,69	45,71	49,93	23,32	37,2	39,75	20,51
m_{LP} [kg/s]	32,4	35,19	39,62	19,59	30,16	34,14	18,13
r_{ex}	1,326	1,431	1,437	1,417	1,51	1,547	1,506
T_{max} [°C]	75,01	88,7	80,26	79,87	80,46	79,63	79,8
T_{out} [°C]	59,31	63	62,48	63,34	64,19	63,45	64,49
φ	0,5095	0,4634	0,4699	0,4591	0,4485	0,4578	0,4448
η_{th}	0,0495	0,0511	0,0508	0,0516	0,0542	0,0535	0,0521
η_{sys}	**0,0252**	0,0237	0,0239	0,0237	0,0243	0,0245	0,0232

Figure 30 shows the optimum *T-s* diagrams for all employed working fluids.

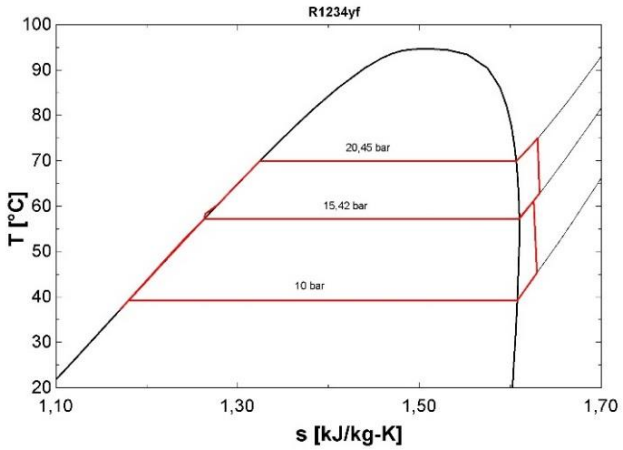

a) R1234yf

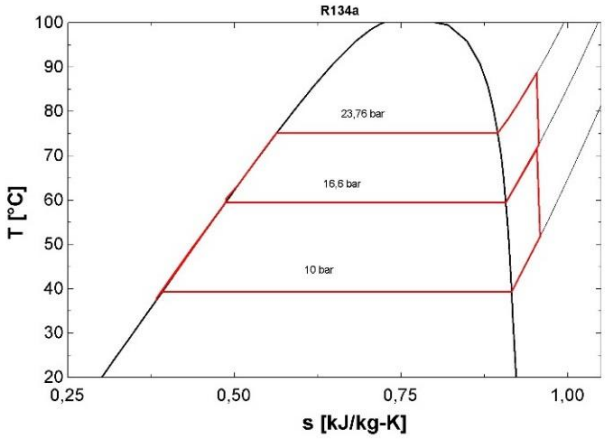

b) R134a

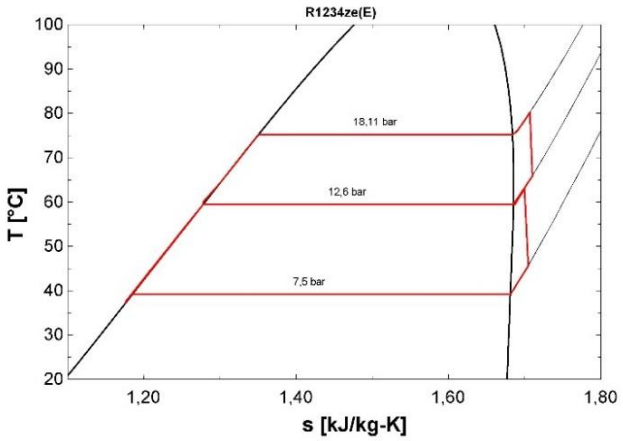

c) R1234ze(E)

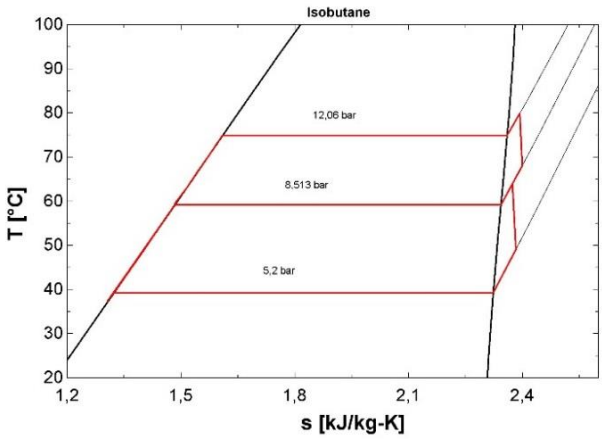

d) Isobutane

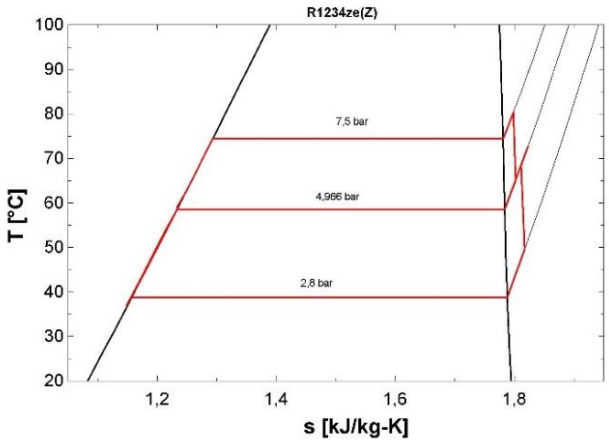

e) R1234ze(Z)

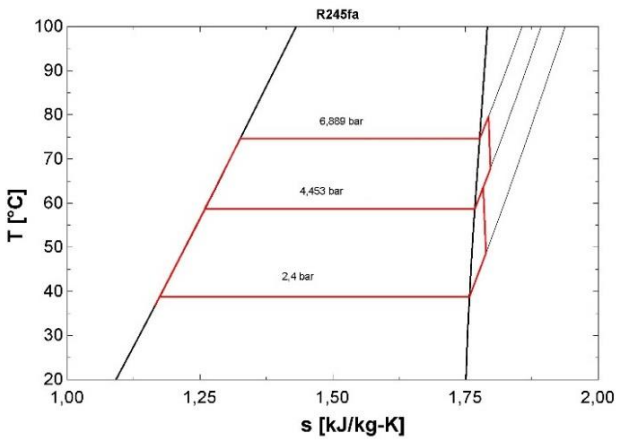

f) R245fa

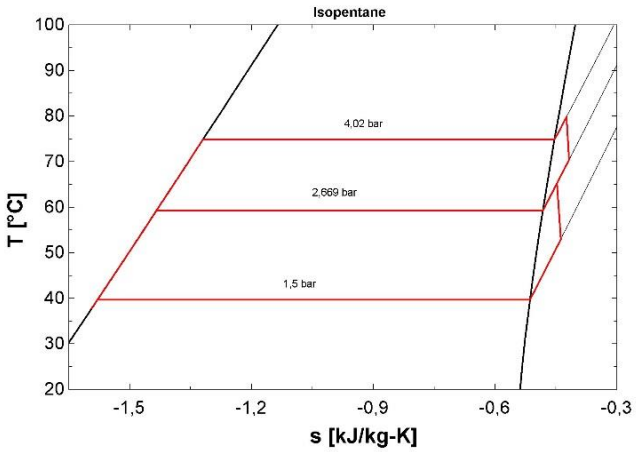

g) Isopentane

Figure 30. T-s diagrams with $T_{in,HS}$=100°C for dual pressure ORC.

From Figure 31, which shows the temperature profile of each fluid, it is possible to see the good match between the heating and cooling curves realized with R1234yf (Figure 31a), which gives also the lowest brine outlet temperature T_{out}.

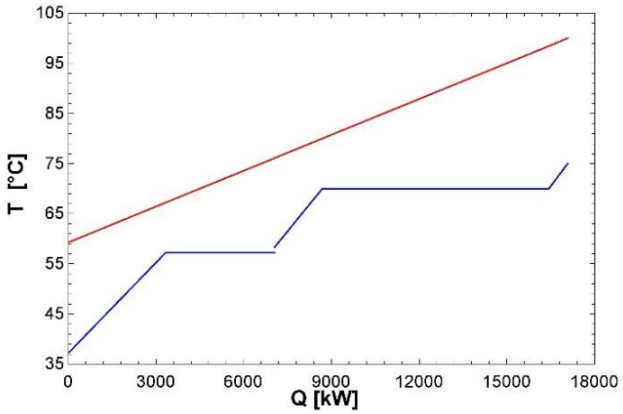

a) R1234yf

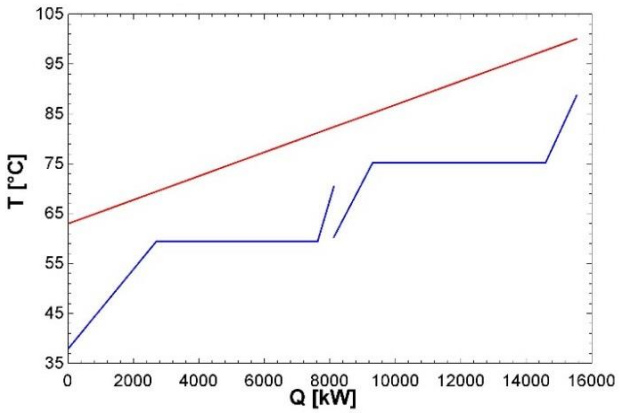

b) R134a

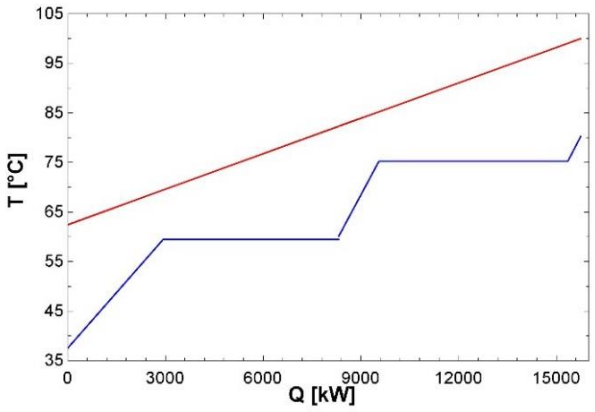

c) R1234ze(E)

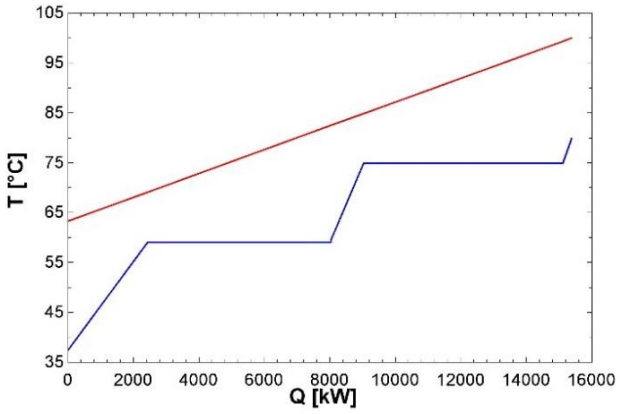

d) Isobutane

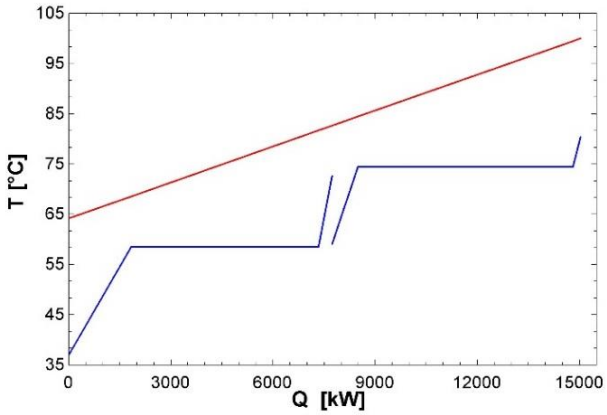

e) R1234ze(Z)

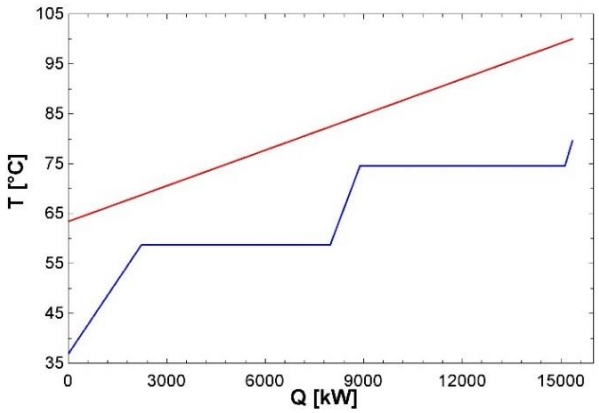

f) R245fa

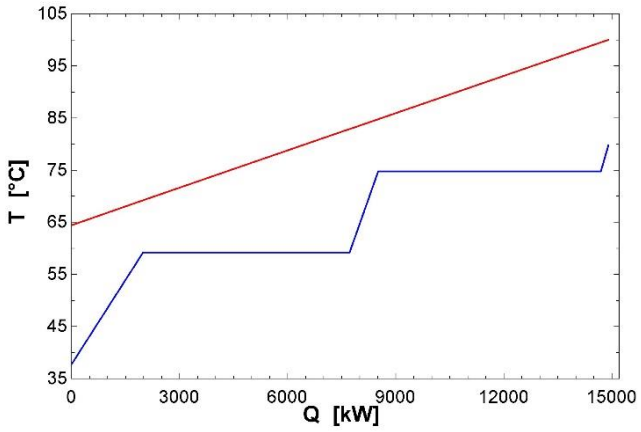

g) Isopentane

Figure 31. T-Q diagrams with $T_{in,HS}$=100°C for dual pressure ORC.

The diagrams plotted in Figure 32 show the trend of W_{net} with p_{HP} and p_{LP} keeping ΔT_{SH_HP} and ΔT_{SH_LP} at the optimum value. With all fluids, the operation around the optimum working point is quite stable. p_{LP} has a stronger influence on W_{net}, but moving far from the optimum also p_{HP} effect is relevant.

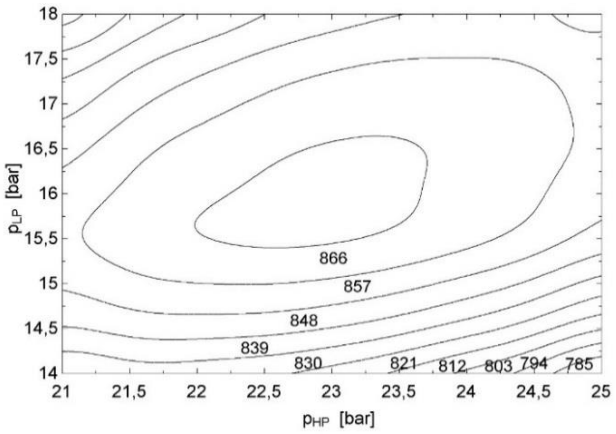

a) R1234yf

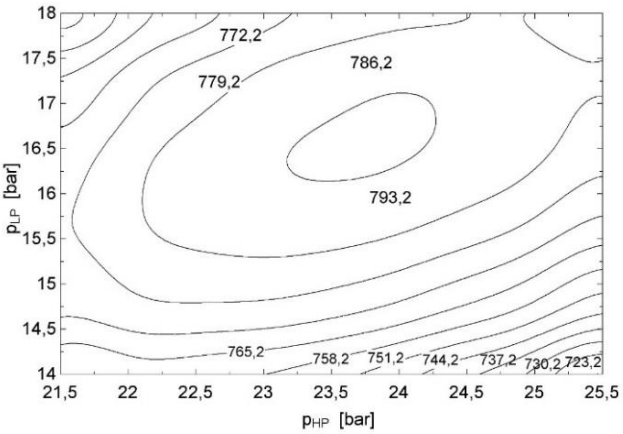

b) R134a

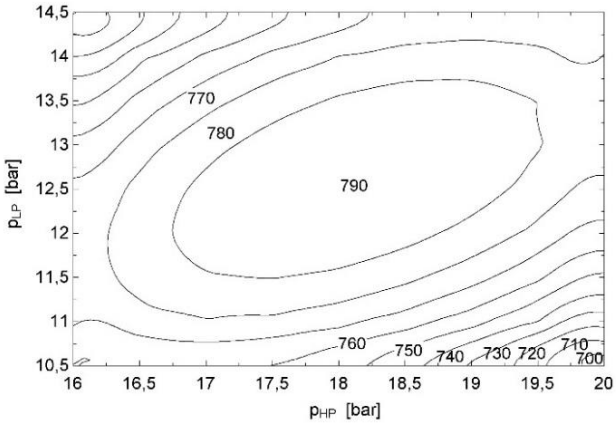

c) R1234ze(E)

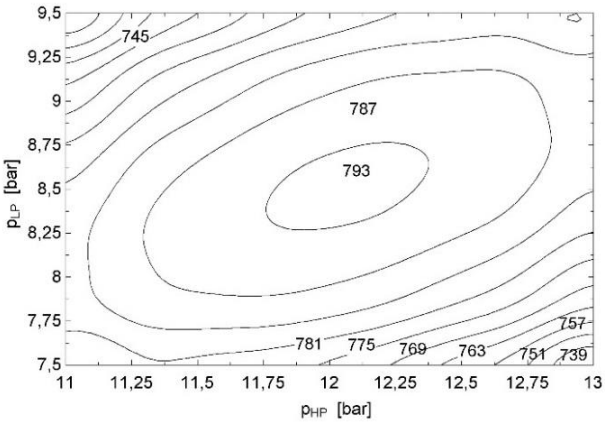

d) Isobutane

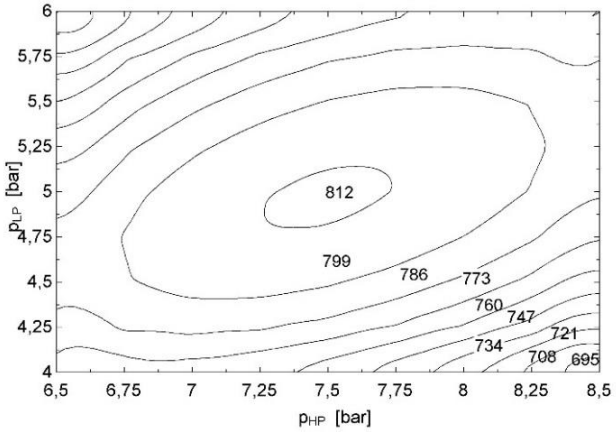

e) R1234ze(Z)

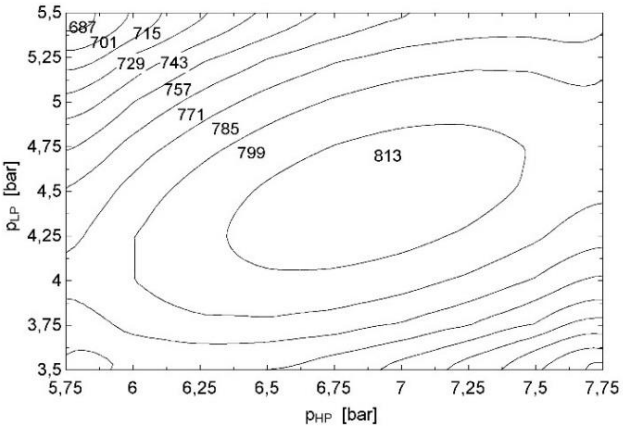

f) R245fa

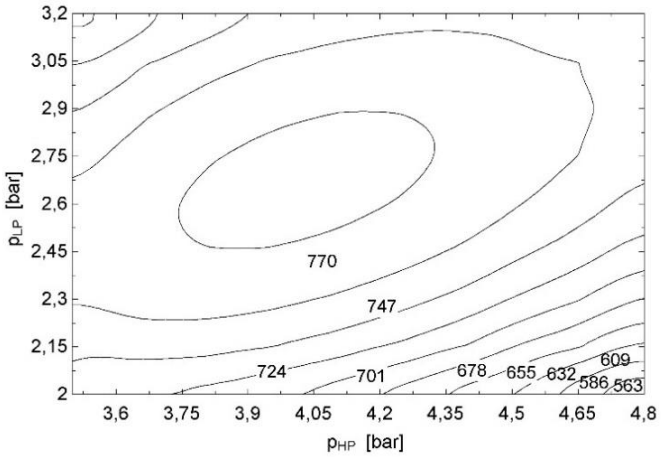

g) Isopentane

Figure 32. Variation of net power output with maximum cycle pressure and minimum cycle pressure at $T_{in,HS}$=100°C.

- $T_{in,HS}$=125°C

As in the previous case, also with $T_{in,HS}$=125°C all selected fluids are used. The optimum points, all obtained with the minimum ΔT_{SH} are presented in Table 14.

Again R1234yf is the best fluid having the highest φ and a good η_{th}. R1234ze(Z) gives the highest η_{th}=7,82%, but, having a low φ, it is not situated among the best performing fluids.

R12345yf produces 7,3% more W_{net} than in the single stage ORC. It is to notice that the low-stage mass flow rate ($\dot{m}_{LP}$) is low. The reduced performance improvement is due to the maximum pressure constraint. As the maximum allowed pressure was already reached with the single stage configuration, the HP level can't go above this limit and consequently enhance the cycle mean temperature, so η_{th} results even reduced than with the single pressure ORC (7,38% vs 8,02%) and the only advantages brought by the HP stage is the improved match between brine and working fluid temperature profiles. It is therefore important to notice that η_{sys} is higher thanks to the higher φ in spite of the lower η_{th}.

Considering that R134a and R1234ze(E) show instead an improvement of more than 20%, the optimal r_{ex} at this temperature is located between 1,7 and 1,8.

Table 14. Optimum working point with $T_{in,HS}$=125°C for the dual stage ORC.

Fluid	**R1234yf**	R134a	R1234ze(E)	Isobutane	R1234ze(Z)	R245fa	Isopentane
ΔT_{SH_HP} [°C]	5	5	5	5	5	5	5
$\Delta T_{SH\ LP}$ [°C]	0,01	0,01	0,01	0,01	0,01	0,01	0,01
p_{HP} [bar]	32,5	38	27,56	17,33	11,26	10,62	6,05
p_{LP} [bar]	16,63	20,53	16,04	10,47	6,275	5,738	3,374
W_{net} [kW]	**2186**	1969	1935	1877	1898	1917	1824
AR [m^2/kW]	3,095	2,461	2,873	2,846	2,314	2,678	2,737
m_{HP} [kg/s]	162,5	101,3	89,69	39,01	62,12	65,25	33,1
m_{LP} [kg/s]	29,1	48,28	54,63	27,95	46,93	48,96	26,2
r_{ex}	1,954	1,814	1,718	1,655	1,794	1,851	1,793
T_{max} [°C]	97,7	102,8	100,3	97,85	96,74	97,17	97,03

T_{out} [°C]	54,64	61,81	63,09	65,34	67,4	66,11	67,65
φ	0,6715	0,6036	0,5916	0,5701	0,5505	0,5628	0,5482
η_{th}	0,0738	0,0740	0,0742	0,0747	0,0782	0,0772	0,0755
η_{sys}	**0,0496**	0,0447	0,0439	0,0426	0,0430	0,0435	0,0414

In Figure 33 the *T-s* diagrams are shown.

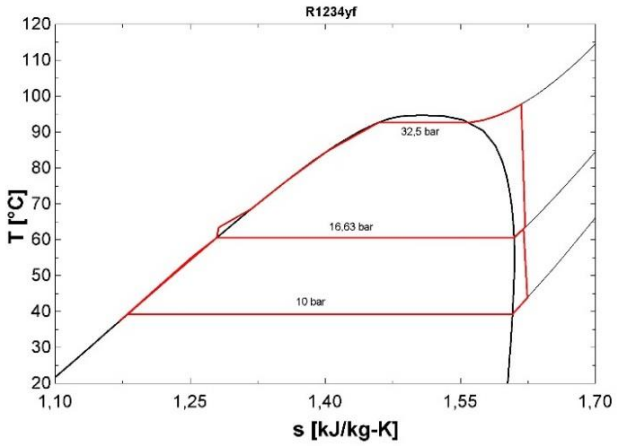

a) R1234yf

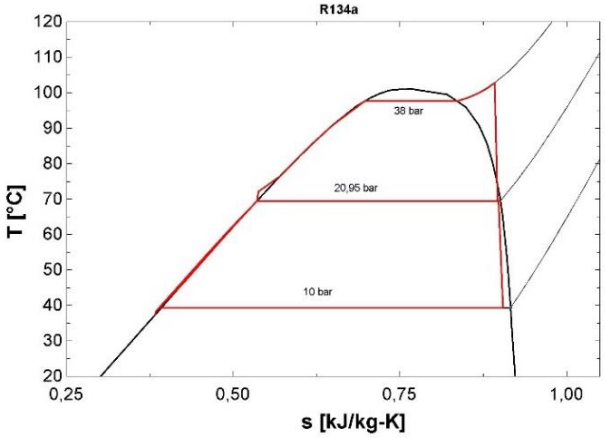

b) R134a

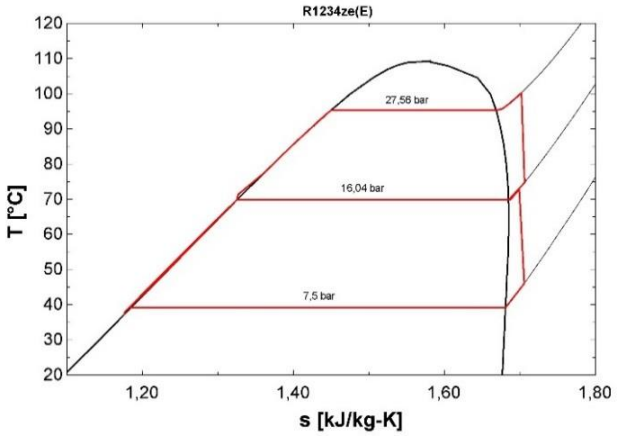

c) R1234ze(E)

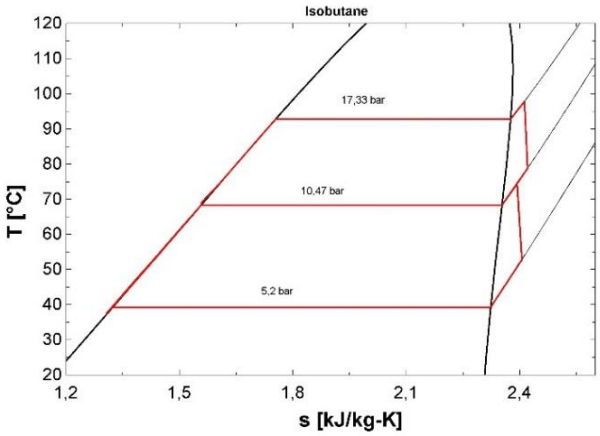

d) Isobutane

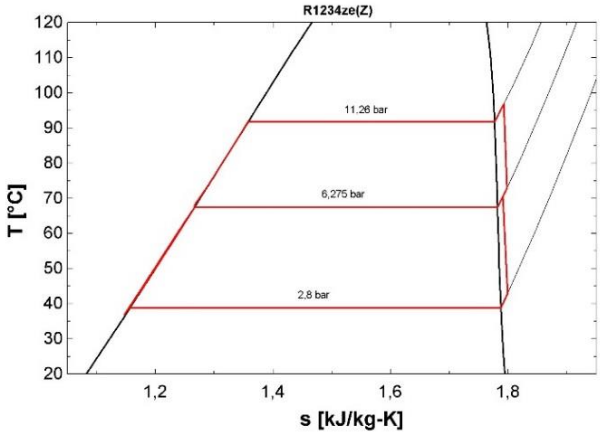

e) R1234ze(Z)

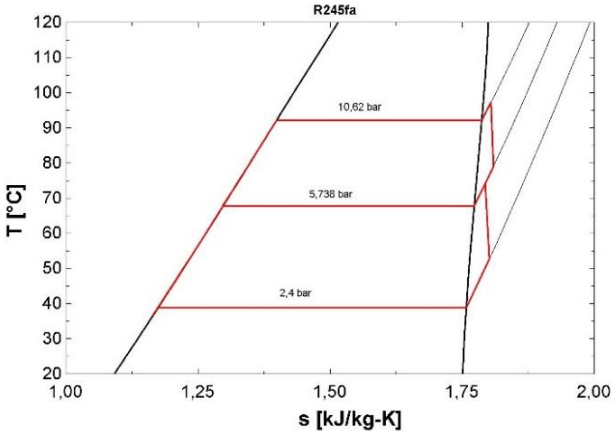

f) R245fa

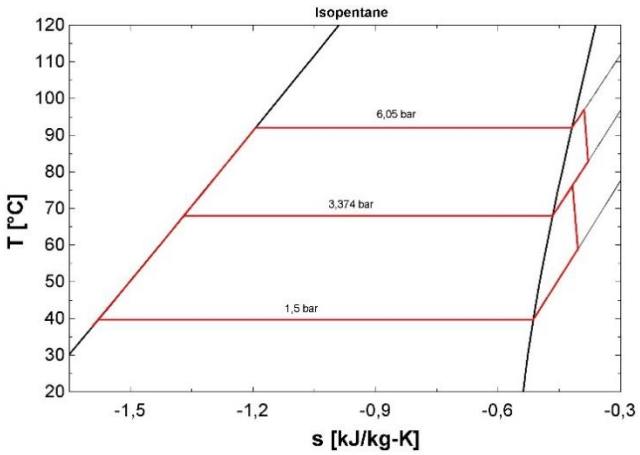

g) Isopentane

Figure 33. T-s diagrams with $T_{in,HS}$=125°C for dual pressure ORC.

In Figure 34a the good temperature profile match realized by R1234yf can be seen. Splitting the mass flow rate in two levels enables the approach of the curves especially in the HP preheating.
The improvement is more evident for R134a and R1234ze(E) (Figure 34b-c), whose φ increased by about 20%.

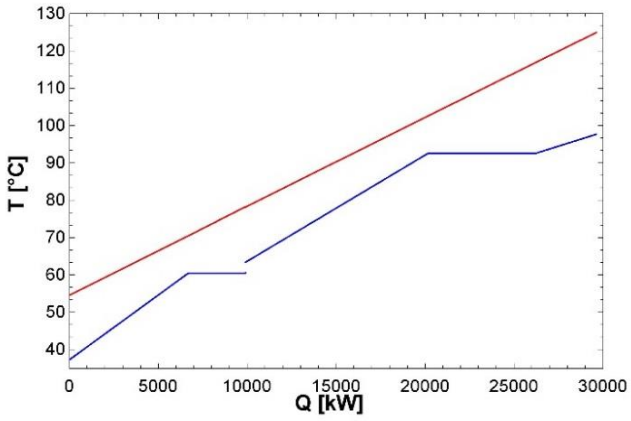

a) R1234yf

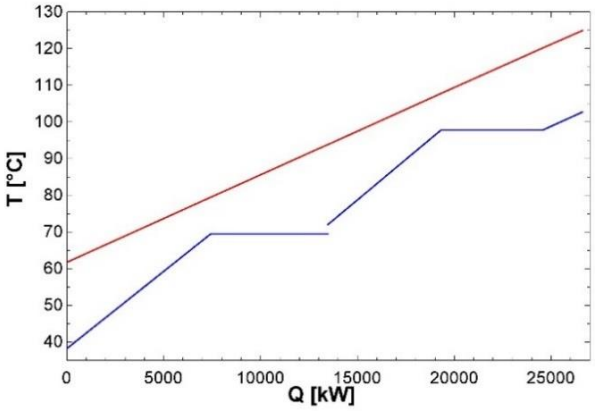

b) R134a

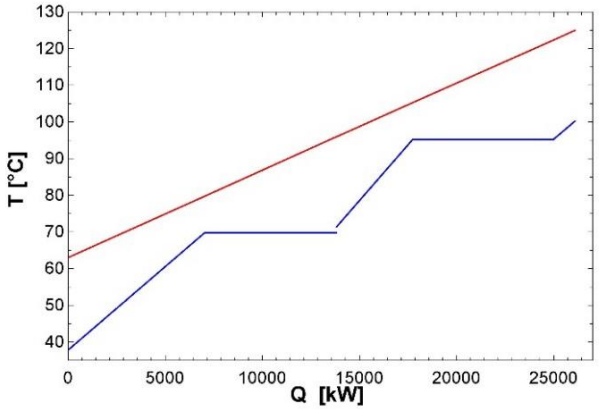

c) R1234ze(E)

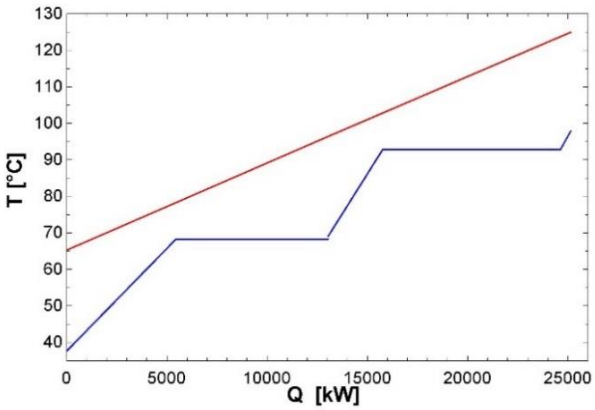

d) Isobutane

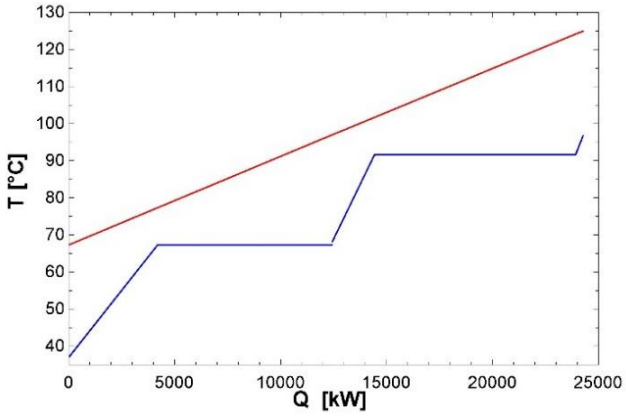

e) R1234ze(Z)

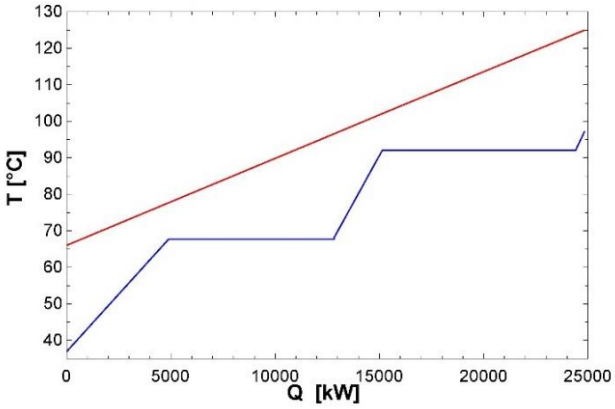

f) R245fa

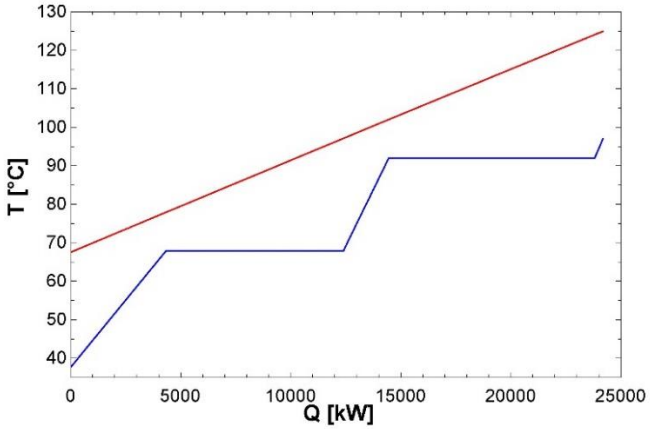

g) Isopentane

Figure 34. T-Q diagrams with $T_{in,HS}$=125°C for dual pressure ORC.

In Figure 35 the trend of Wnet versus p_HP and p_LP is plotted. With the exception of R1234yf and R134a, the diagrams are similar to those obtained with Tin,HS=100°C and the same consideration can be done.

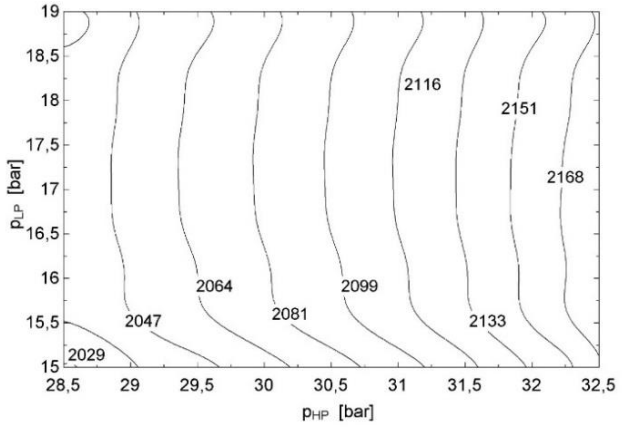

a) R1234yf

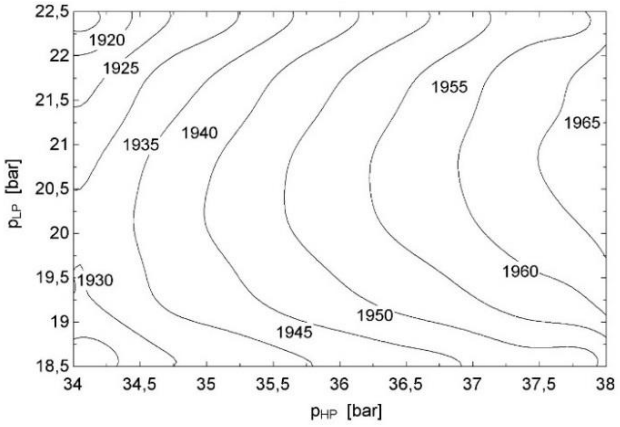

b) R134a

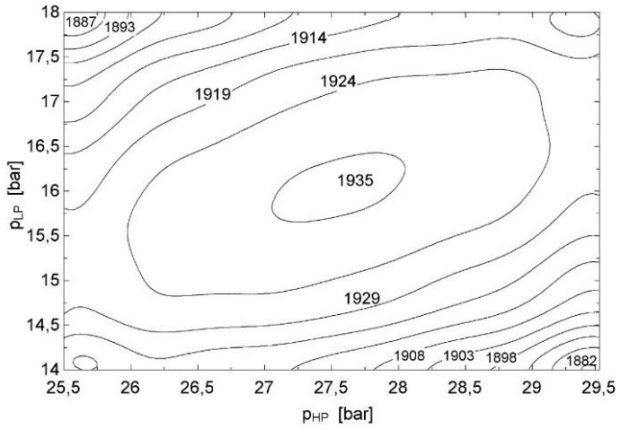

c) R1234ze(E)

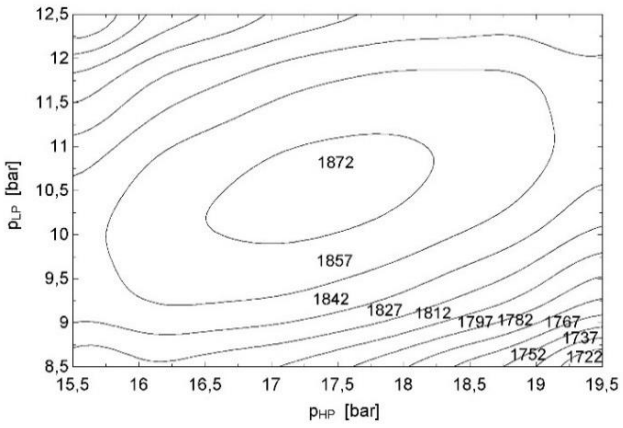

d) Isobutane

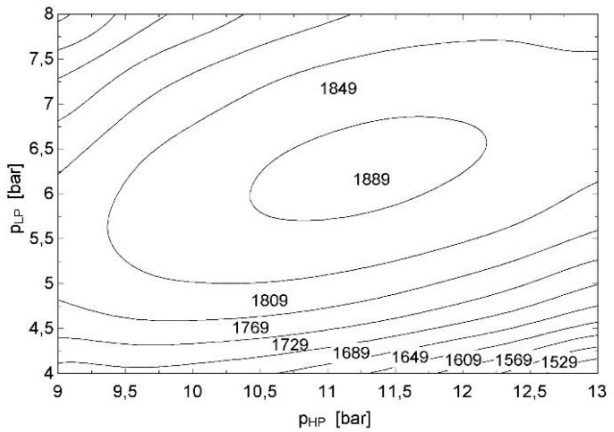

e) R1234ze(Z)

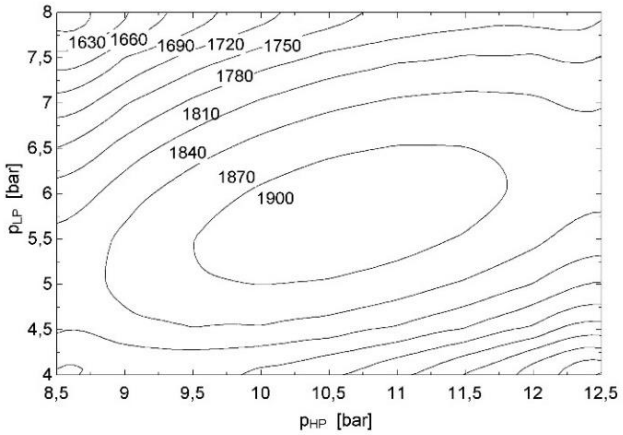

f) R245fa

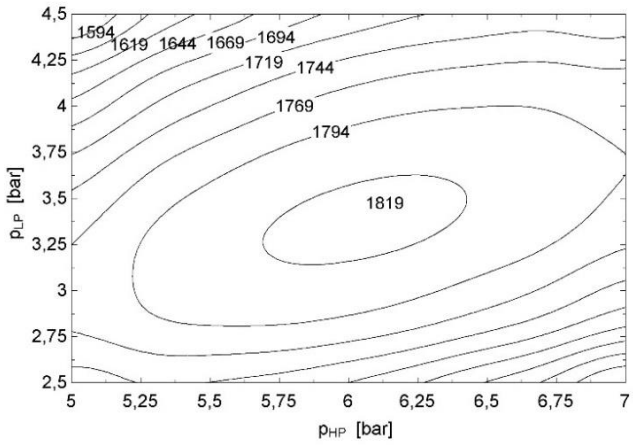

g) Isopentane

Figure 35. Variation of net power output with maximum cycle pressure and minimum cycle pressure at $T_{in,HS}$=125°C.

The influence of p_{HP}, instead, is very strong when the operation is at or near the maximum allowed pressure as for R1234yf and R134a in Figure 33a-b. In this situation, W_{net} varies a lot with p_{HP} but is flat for a wide range of p_{LP}.

- $T_{in,HS}$=150°C

At this brine inlet temperature, only five of the seven selected fluids are employed. R1234yf and R134a are excluded having a too low Tcr to operate efficiently in subcritical cycles.
Optimization results are presented in Table 15.
R1234ze(E) is the best performing fluid ,but it doesn't show any further improvement if compared to the basic ORC, having a really low $\dot{m}_{LP}$ and p_{LP} close to the condensation pressure (there is only a bar difference). As happened for R1234yf in the previous case, also with R1234ze(E) the maximum allowed pressure was already reached with the single stage ORC, but this time, the HP level does not lead to an enough higher φ to compensate the reduction of η_{th}.
Using the other fluids there is instead an increase around 20% of the performance, due especially to the increase of φ (also η_{th} slightly increases), consequently the best r_{ex} for the application of the dual stage ORC seems to be around 2.
The analysis of the results indicates that the single pressure configuration operated with R1234ze(E) is the best choice in terms of net power output.

Table 15. Optimum working point with $T_{in,HS}$=150°C for the dual stage ORC.

Fluid	**R1234ze(E)**	Isobutane	R1234ze(Z)	R245fa	Isopentane
ΔT_{SH_HP} [°C]	5	5	5	5	5
$\Delta T_{SH\ LP}$ [°C]	0,01	0,01	0,01	0,01	0,01
p_{HP} [bar]	35	25,48	16,62	16,03	8,853
p_{LP} [bar]	8,512	13,08	7.934	7,42	4,245
W_{net} [kW]	**3997**	3486	3463	3496	3314
AR [m^2/kW]	2,635	2,213	1,751	2,074	2,098
m_{HP} [kg/s]	226,9	58,9	92,96	95,83	47,33
m_{LP} [kg/s]	6,861	33,3	58,43	59,77	32,43
r_{ex}	4,112	1,948	2,095	2,16	2,086
T_{max} [°C]	112,5	118,8	115	115,9	114,8
T_{out} [°C]	48,48	64,59	68,53	66,48	68,83
φ	0,7828	0,6602	0,6299	0,6456	0,6276
η_{th}	0,0932	0,0964	0,1003	0,0988	0,0964
η_{sys}	**0,0730**	0,0636	0,0632	0,0638	0,0605

Figure 36 shows the T-s diagrams of each fluid. Figure 36a clearly proves that the optimization carried out with R1234ze(E) almost leads to a single pressure cycle.
Using the other fluids, instead (Figure 36b-e) the second stage enhances the amount of absorbed heat. This is visible also from Figure 37b-e: with two evaporations, a better match of the heating and cooling curves is realized.
In Figure 37a the T-Q diagram for R1234ze(E) is plotted. The LP evaporation zone is really short, almost leading to single pressure configuration, which already guaranteed a satisfactory approach of the two curves during the preheating.

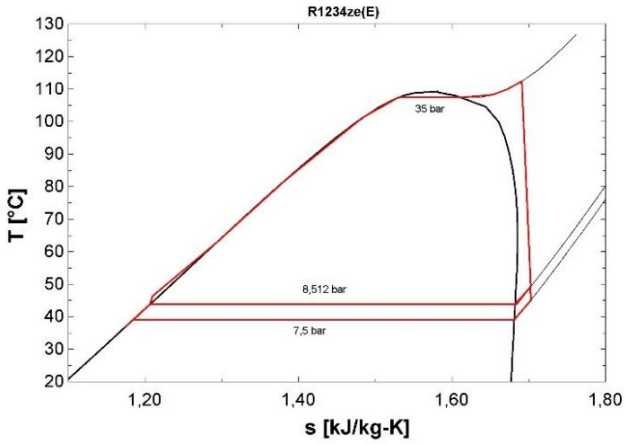

a) R1234ze(E)

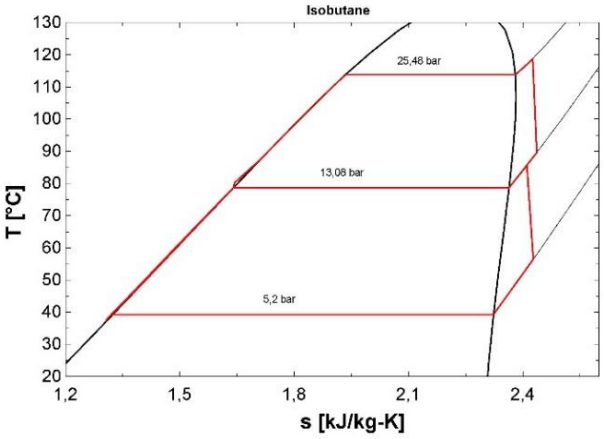

b) Isobutane

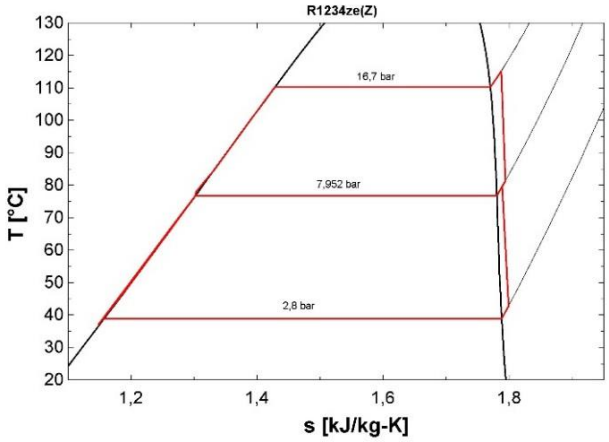

c) R1234ze(Z)

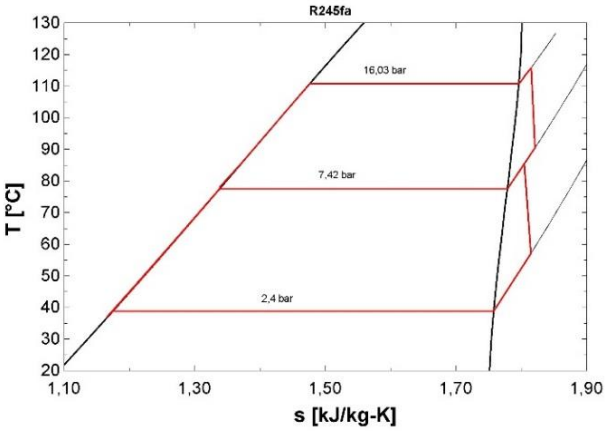

d) R245fa

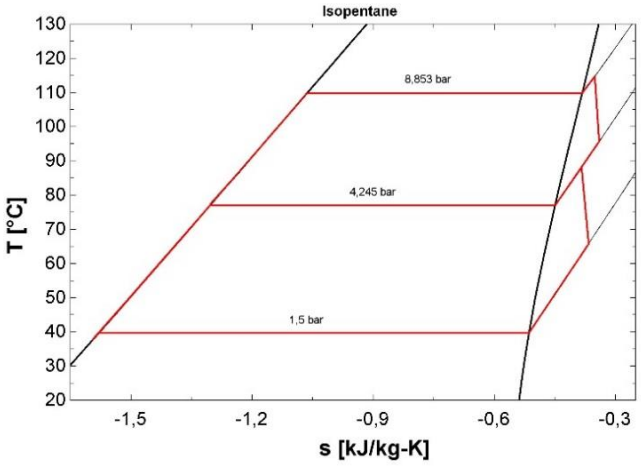

e) Isopentane

Figure 36. T-s diagrams with $T_{in,HS}$=150°C for dual pressure ORC.

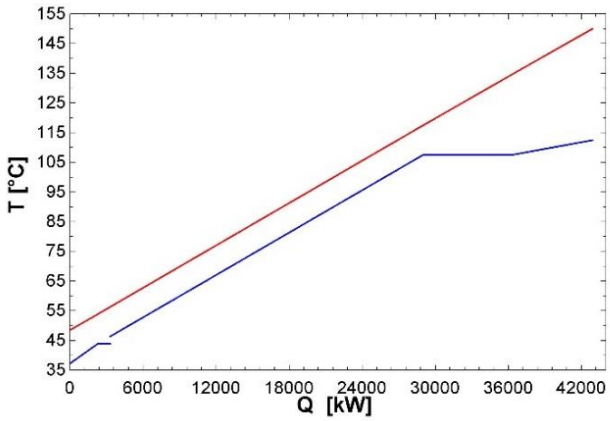

a) R1234ze(E)

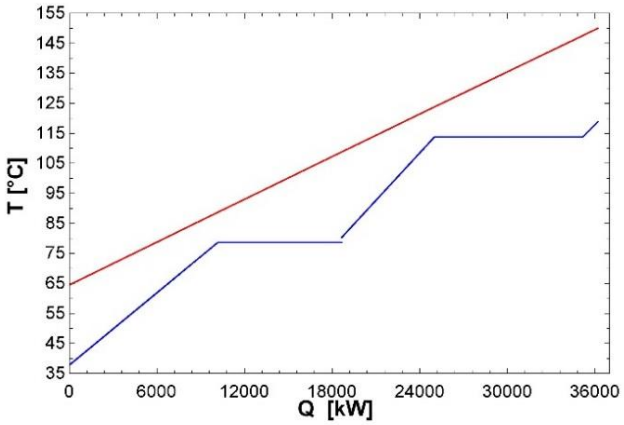

b) Isobutane

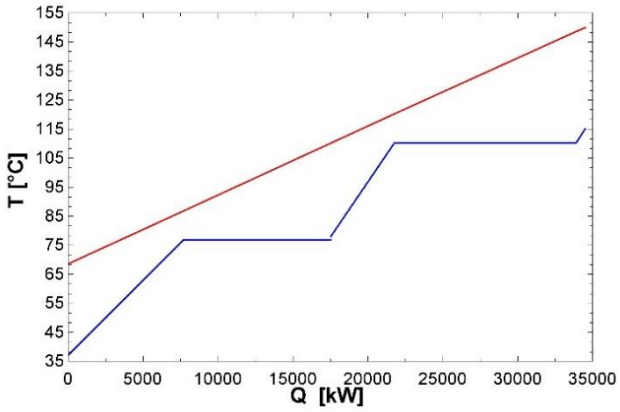

c) R1234ze(Z)

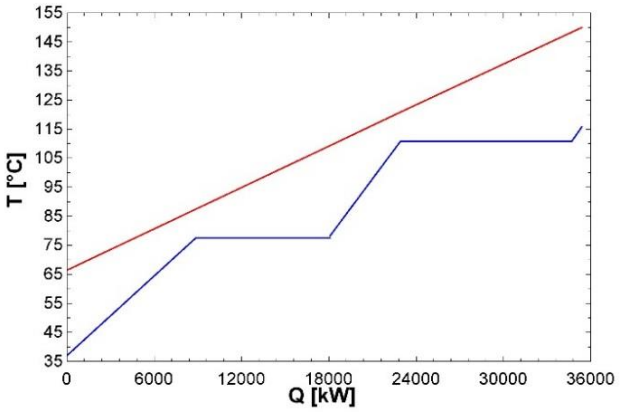

d) R245fa

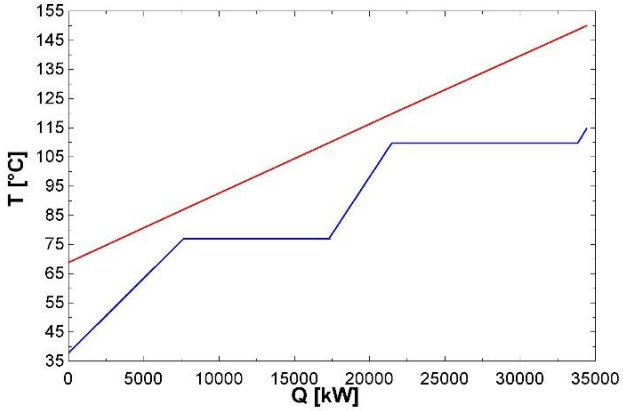

e) Isopentane

Figure 37. T-Q diagrams with $T_{in,HS}$=150°C for dual pressure ORC.

Figure 38 shows the analysis around the optimal couple p_{HP}/p_{LP}.

The effect of p_{LP} on W_{net}, when the maximum allowed pressure is reached, becomes negligible (Figure 38a) for R1234ze(E)). Whereas, when the optimum p_{HP} is far from the upper limit, the trend is the same observed at the other $T_{in,HS}$, where around the optimum working point W_{net} is more affected by p_{LP}but moving from this point also the influence of p_{HP} becomes important.

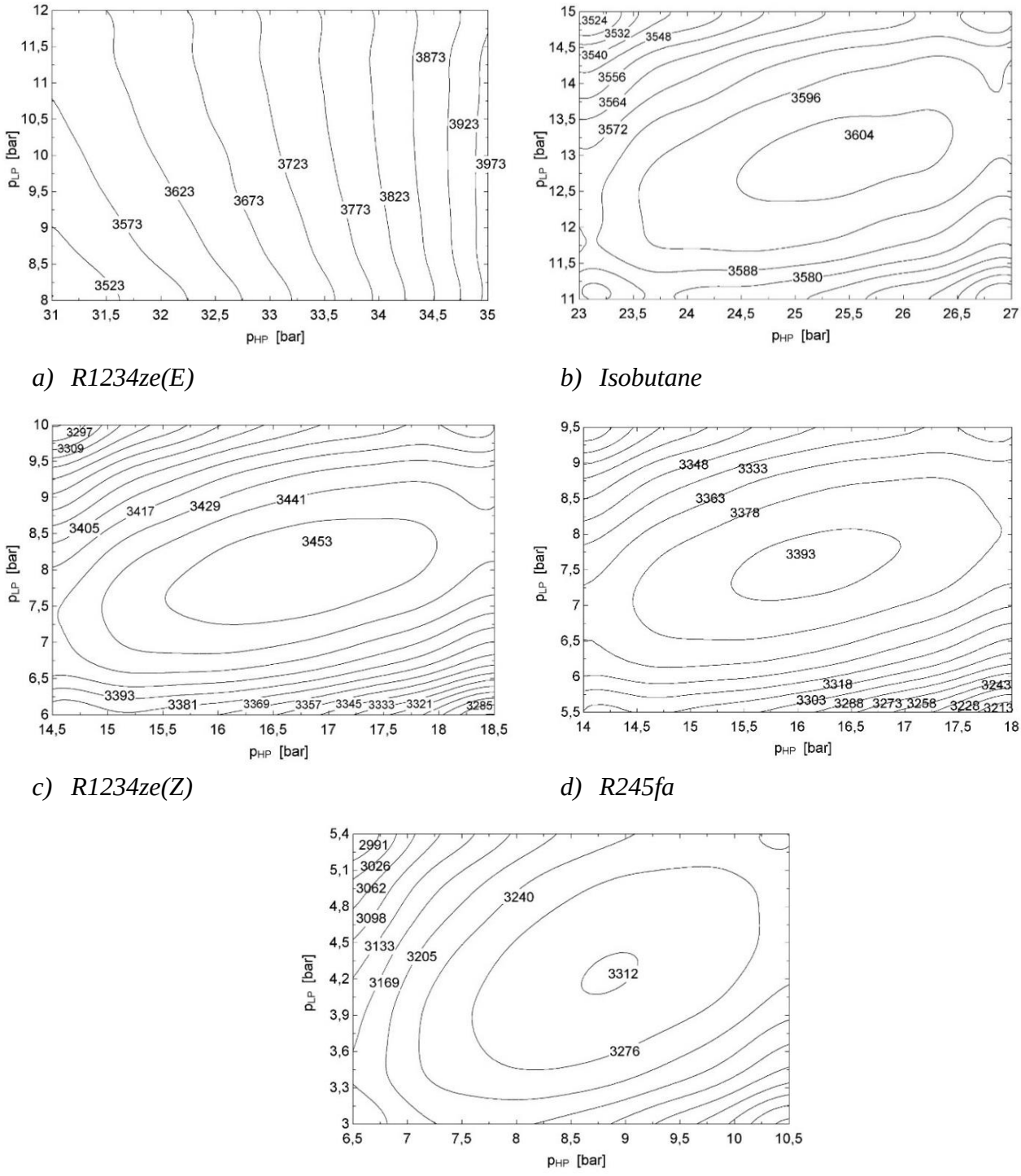

Figure 38. Variation of net power output with maximum cycle pressure and minimum cycle pressure at $T_{in,HS}$=150°C.

- $T_{in,HS}$=175°C

Isobutane, R1234ze(Z), R245fa and isopentane are employed. The excluded fluids have a too low T_{cr} and therefore cannot reach high φ with subcritical cycles.

The best performing fluid is isobutane, showing an increase in W_{net} of about 81,9% than at the previous brine inlet temperature, but there is no improvement in comparison to the basic ORC, having

reached the maximum allowed pressure, the increase of φ doesn't compensate the reduction of η_{th}. As happened for R1234ze(E) at the previous $T_{in,HS}$, $\dot{m}_{LP}$ is negligible respect to $\dot{m}_{HP}$ and p_{LP} is close to p_{cond}, so that the dual pressure configuration is almost a single pressure one.
The other fluids present instead an increase around 18% of their performance because of the improved match between the brine and working fluid temperature profiles (φ= +13% to +17%) and the little increase of η_{th} (+1,9% to +3,5%).
Table 16 shows the optimum working point for each fluid.
The optimum r_{ex} at this $T_{in,HS}$ seems to be around 2,5.

Table 16. Optimum working point with $T_{in,HS}$=175°C for the dual stage ORC.

Fluid	**Isobutane**	R1234ze(Z)	R245fa	Isopentane
ΔT_{SH_HP} [°C]	5	5	5	5
$\Delta T_{SH\ LP}$ [°C]	0,01	0,01	0,01	0,01
p_{HP} [bar]	34,94	26,79	25,25	12,77
p_{LP} [bar]	7,185	10,53	9,878	5,339
W_{net} [kW]	**6342**	5621	5652	5262
AR [m^2/kW]	2,13	1,349	1,727	1,726
m_{HP} [kg/s]	125,1	131,9	133,6	63,74
m_{LP} [kg/s]	3,929	66,77	64,56	35,96
r_{ex}	4,863	2,544	2,556	2,392
T_{max} [°C]	137,2	139,7	139,1	133,6
T_{out} [°C]	50,34	67,4	64,39	68,05
φ	0,8061	0,6989	0,7183	0,6945
η_{th}	0,1198	0,1225	0,1199	0,1154
η_{sys}	**0,0966**	0,0856	0,0861	0,0802

In Figure 39 the T-s diagram of the four selected fluids are plotted. Figure 39a refers to isobutane where between p_{LP} and p_{cond} there is less than 2 bar difference.
R1234ze(Z), R245fa and isopentane have instead two distinct stages, which allow the temperature profile to get closer, as shown in Figure 40b-d.

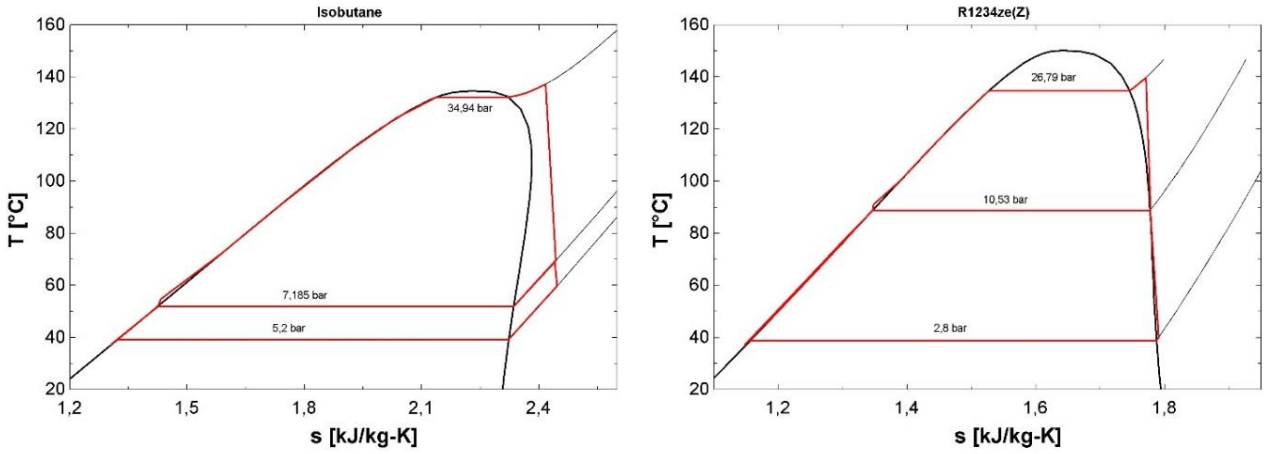

a) Isobutane *b) R1234ze(Z)*

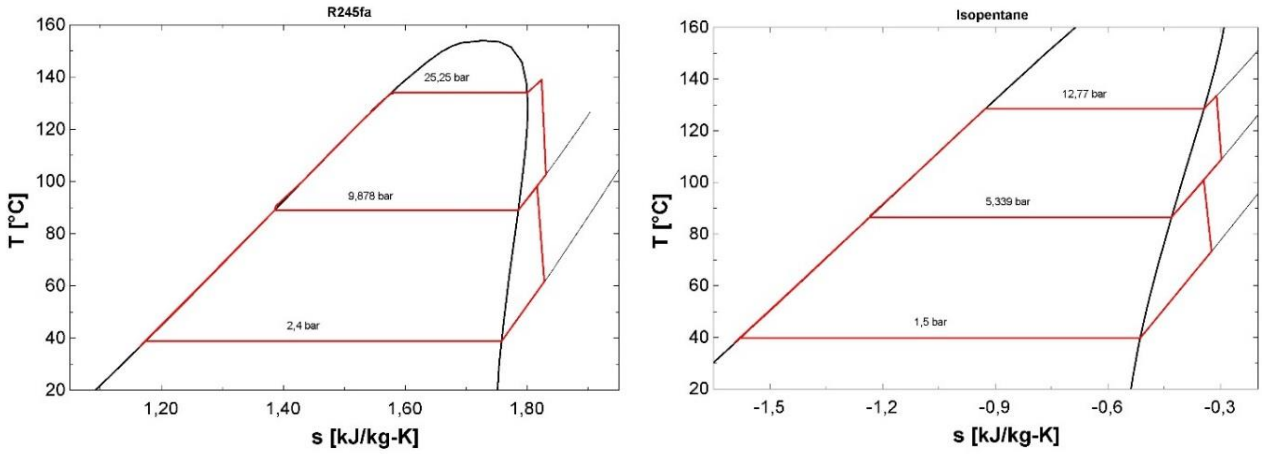

c) R245fa *d) Isopentane*

Figure 39. T-s diagrams with $T_{in,HS}$=175°C for dual pressure ORC.

Figure 40a makes clearly understand that, for isobutane, two pressure levels are useless, being the heat exchanged at LP stage negligible.

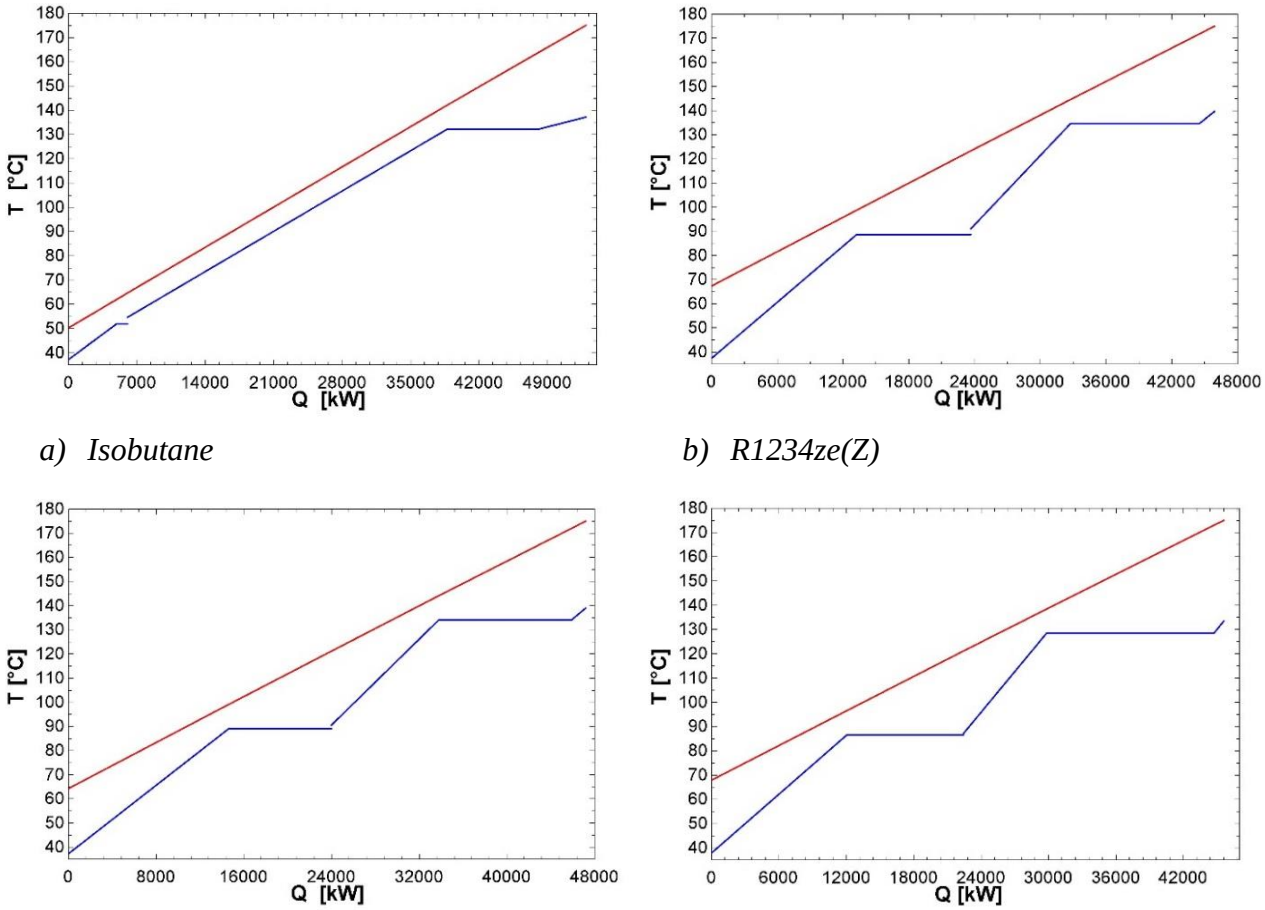

a) Isobutane *b) R1234ze(Z)*

c) R245fa *d) Isopentane*

Figure 40. T-Q diagrams with $T_{in,HS}$=175°C for dual pressure ORC.

In Figure 41 the p_{HP}-p_{LP} diagrams for each fluid are plotted. Isobutane has a different trend of W_{net} compared to the other fluids because of the limited p_{HP}, but in general W_{net} has the same behavior observed in the previous cases and the same considerations are valid.

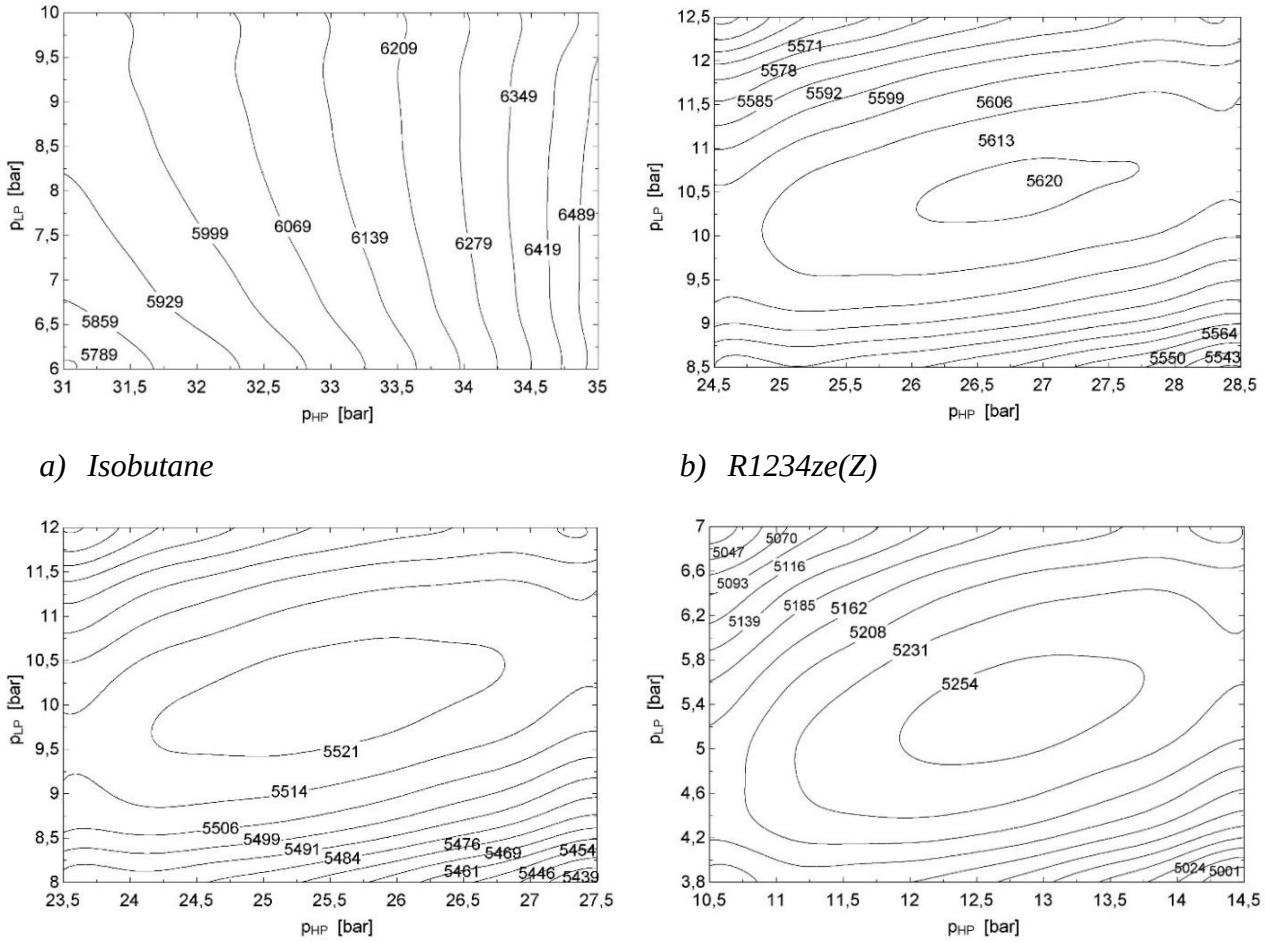

a) Isobutane *b) R1234ze(Z)*

c) R245fa *d) Isopentane*

Figure 41. Variation of net power output with maximum cycle pressure and minimum cycle pressure at $T_{in,HS}$=175°C.

From these results it can be concluded that the single pressure ORC operated with isobutane is the best choice in the search of the highest net power output.

- $T_{in,HS}$=200°C

When the brine inlet temperature is 200°C only isopentane is used, because the other fluids has a too low T_{cr} to perform well in subcritical configuration. The optimum working point is presented in Table 17.

W_{net} is increased by about 13,7% compared to the single pressure configuration, both φ and η_{th} are higher.

Figure 42 shows *T-s*, *T-Q* and p_{HP}-p_{LP} diagrams. Having two evaporation zones allows a closer approach of the cooling and heating curves (Figure 42b). The trend of W_{net} with the evaporation pressures is not different from that observed at $T_{in,HS}$=150-175°C.

Table 17. Optimum working point with $T_{in,HS}$=200°C for the dual stage ORC.

$\Delta T_{SH,HP}$	$\Delta T_{SH,HP}$	p_{HP}	p_{LP}	W_{net}	AR	m_{HP}	m_{LP}	r_{ex}	T_{max}	T_{out}	φ	η_{th}	η_{sys}
[°C]	[°C]	[bar]	[bar]	[kW]	[m^2/kW]	[kg/s]	[kg/s]		[°C]	[°C]			
5	0,01	18,55	6,669	7721	1,491	83,94	34,89	2,782	154,7	65,17	0,755	0,1333	0,1007

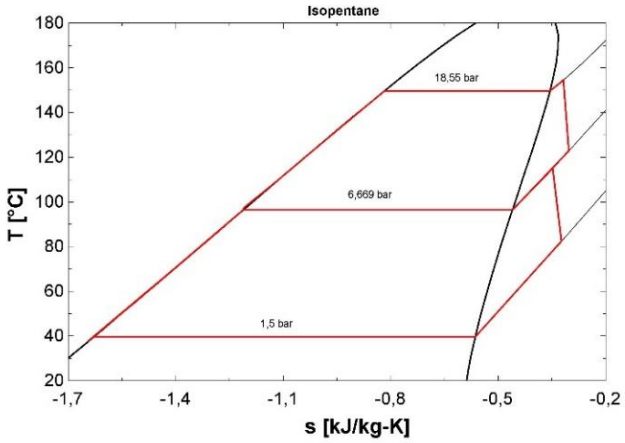

a) T-s diagram

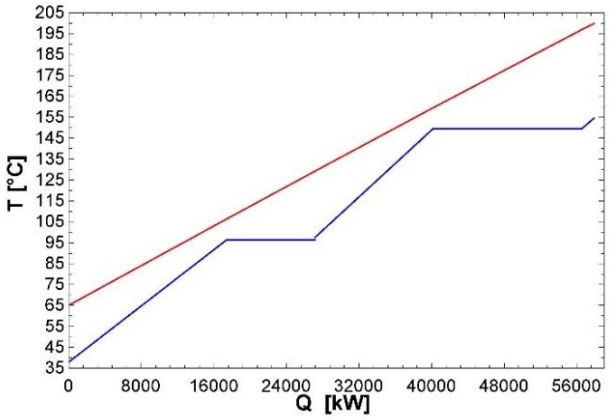

b) T-Q diagram

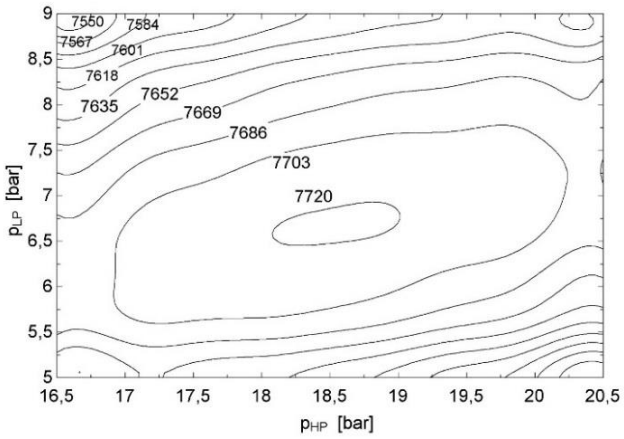

c) p_{HP}-p_{LP} diagram

Figure 42. Isopentane diagrams with $T_{in,SH}$=200°C.

Considering that, with the single pressure configuration, the maximum allowed pressure was not reached, working with two expansion stages results beneficial.

6.1.3 Comparison between single and dual pressure configuration

In this Section, the optimum working points of the best fluids of each $T_{in,HS}$ are summarized in Tables 18 to 22, giving a comparison between single and dual pressure configuration.
At $T_{in,SH}$=100°C the fluid, which gives the maximum W_{net} is R1234yf.
The dual pressure configuration allows increasing φ of 10 percentage points, but η_{th} decreases slightly. The result is, however, a higher η_{sys} and therefore a higher W_{net}.

Table 18. Comparison between single and dual pressure ORC at $T_{in,SH}$=100°C.

	W_{net} [kW]	Φ [%]	η_{th} [%]	η_{sys} [%]
Single pressure ORC	694,7	40,33	5,141	2,073
Dual pressure ORC	845,7	50,95	4,954	2,524

At $T_{in,SH}$=125°C the maximum allowed pressure is reached when using R1234yf, which is the best fluid. With the dual pressure ORC, φ remains 10 percentage points higher but the reduction of η_{th} is pronounced, so that η_{sys} increases moderately.

Table 19. Comparison between single and dual pressure ORC at $T_{in,SH}$=125°C.

	W_{net} [kW]	Φ [%]	η_{th} [%]	η_{sys} [%]
Single pressure ORC	2038	57,63	8,022	4,623
Dual pressure ORC	2186	67,15	7,381	4,956

The optimization results at $T_{in,SH}$=150°C and 175°C (with R1234ze(E) and isobutane respectively) are similar: in both cases the maximum allowed pressure was reached with the single stage configuration and the dual pressure ORC shows only a reduced improvement in the thermal match but the lower cycle efficiency penalizes the total system efficiency, so that W_{net} even decreases.

Table 20. Comparison between single and dual pressure ORC at $T_{in,SH}$=150°C.

	W_{net} [kW]	Φ [%]	η_{th} [%]	η_{sys} [%]
Single pressure ORC	4002	76,29	9,572	7,302
Dual pressure ORC	3997	78,28	9,317	7,293

Table 21. Comparison between single and dual pressure ORC at $T_{in,SH}$=175°C.

	W_{net} [kW]	Φ [%]	η_{th} [%]	η_{sys} [%]
Single pressure ORC	6349	78,98	12,25	9,671
Dual pressure ORC	6342	80,61	11,98	9,66

At $T_{in,SH}$=200°C, isopentane is used. The dual pressure configuration leads to an improvement of both φ and η_{th}, which contribute to the higher W_{net}.

Table 22. Comparison between single and dual pressure ORC at $T_{in,SH}$=200°C.

	W_{net} [kW]	Φ [%]	η_{th} [%]	η_{sys} [%]
Single pressure ORC	6828	69,0	12,90	8,902
Dual pressure ORC	7721	75,5	13,33	10,07

Regarding the opportunity to add a second pressure level and consequently an expander, optimization results show that, when the maximum allowed pressure is reached, the dual stage ORC loses its advantage in enhancing the absorbed heat through an increase of the heat recovery factor φ, because the single pressure configuration already realizes a good match of the temperature profiles. This happens when the difference between heat source inlet temperature and working fluid critical temperature is about 30°- 40°C.

6.1.4 Working selection criterion for the dual pressure ORC

Analyzing the optimization data, it can be observed that the expansion ratio between the HP and LP stages increases with the heat source inlet temperature and hence r_{ex} cannot be used as a general criterion for the selection of the working fluid when operating with the dual pressure configuration.
For this reason, also the evaporation enthalpy *r* is studied as important parameter for a preliminary selection.
r is evaluated at a reduced temperature equal to 0,9. The reduced temperature is the ratio between the working fluid temperature and its critical temperature:

$$T_r = {}^{T}/_{T_{cr}} \quad (6.1.2.1)$$

So that the evaluation temperature results from:

$$T = 0{,}9 \cdot T_{cr} \quad (6.1.2.2)$$

The resulting evaporation enthalpies are reported in Table 23.

Table 23. Evaporation enthalpies evaluated at T_r=0,9.

	r [kJ/kg]
R1234yf	114,2
R134a	134
R1234ze(E)	121,8
Isobutane	225
R1234ze(Z)	134,3
R245fa	123,3
Isopentante	212,2

Furthermore, the difference $T_{in,HS} - T_{cr}$ is considered for $T_{in,HS}$=100°C to 175°C and finally the ratio $\frac{r}{(T_{in,HS}-T_{cr})}$ is calculated. This ratio is chosen as performance predictor because it includes two important parameters: T_{in}-T_{cr}, which correlates the heat source characteristics with those of the fluid, and *r*, which is linked to the thermodynamic features of the fluid.
$\frac{r}{(T_{in,HS}-T_{cr})}$ is then correlated with the total system efficiency η_{sys}.
In Table 24 the above mentioned parameters are shown.

Table 24. T_{in}-T_{cr}, $r/(T_{in}$-$T_{cr})$ and η_{sys} for each fluid at $T_{in,HS}$=100°,125°,150°,200°C.

	$T_{in,HS}$= 100°C			$T_{in,HS}$= 125°C			$T_{in,HS}$= 150°C			$T_{in,HS}$= 175°C		
	T_{in}-T_{cr} [°C]	$r/(T_{in}$-$T_{cr})$ [kJ/kgK]	η_{sys} [%]	T_{in}-T_{cr} [°C]	$r/(T_{in}$-$T_{cr})$ [kJ/kgK]	η_{sys} [%]	T_{in}-T_{cr} [°C]	$r/(T_{in}$-$T_{cr})$ [kJ/kgK]	η_{sys} [%]	T_{in}-T_{cr} [°C]	$r/(T_{in}$-$T_{cr})$ [kJ/kgK]	η_{sys} [%]
R1234yf	5,25	21,75	2,524	30,25	3,78	4,956						
R134a	-1,05	-127,6	2,37	23,95	5,59	4,428						
R1234ze(E)	-9,35	-13,03	2,387	15,65	7,78	4,388	40,65	3,00	7,293			
Isobutane	-34,65	-6,49	2,37	-9,65	-23,32	4,256	15,35	14,66	6,361	40,35	5,58	9,66
R1234ze(Z)	-50,15	-2,68	2,429	-25,2	-5,34	4,304	-0,15	-895,3	6,319	24,85	5,40	8,562
R245fa	-54,05	-2,28	2,45	-29,1	-4,24	4,346	-4,05	-30,44	6,38	20,95	5,89	8,609
Isopentane	-87,25	-2,43	2,318	-62,3	-3,41	4,137	-37,25	-5,70	6,047	-12,25	-17,32	8,015

From Table 23-24 it can be noticed that fluids which have both

$r > 200\ kJ/kg$ (6.1.2.3)

and

$-30° < T_{in,HS} - T_{cr} < +30°C$ (6.1.2.4)

present the lowest η_{sys} or operate better in the single pressure configuration and hence should be excluded as candidate working fluid for dual pressure ORC.

This is the case of isobutane and isopentane at $T_{in,HS}$=100°C, isopentane at $T_{in,HS}$=125°-150°C and isobutane at $T_{in,HS}$=175°C.

With the remaining fluids, it is possible to analyze the trend of η_{sys} with $\frac{r}{(T_{in,HS}-T_{cr})}$ and obtain the graphic of Figure 43.

In general, fluids which a positive ratio $\frac{r}{(T_{in,HS}-T_{cr})}$ perform better, that means when $T_{in,HS}>T_{cr}$. Among them, the best are those with the lowest ratio. Also fluids with a negative ratio ($T_{in,HS}<T_{cr}$) a good performance can be achived, especially those with the highest (or less negative) ratio.

Concluding, the evaporation enthalpy alone is not sufficient as selection criterion, but its combination with the difference $T_{in,HS}$-T_{cr} seems to correlate well the optimization data.

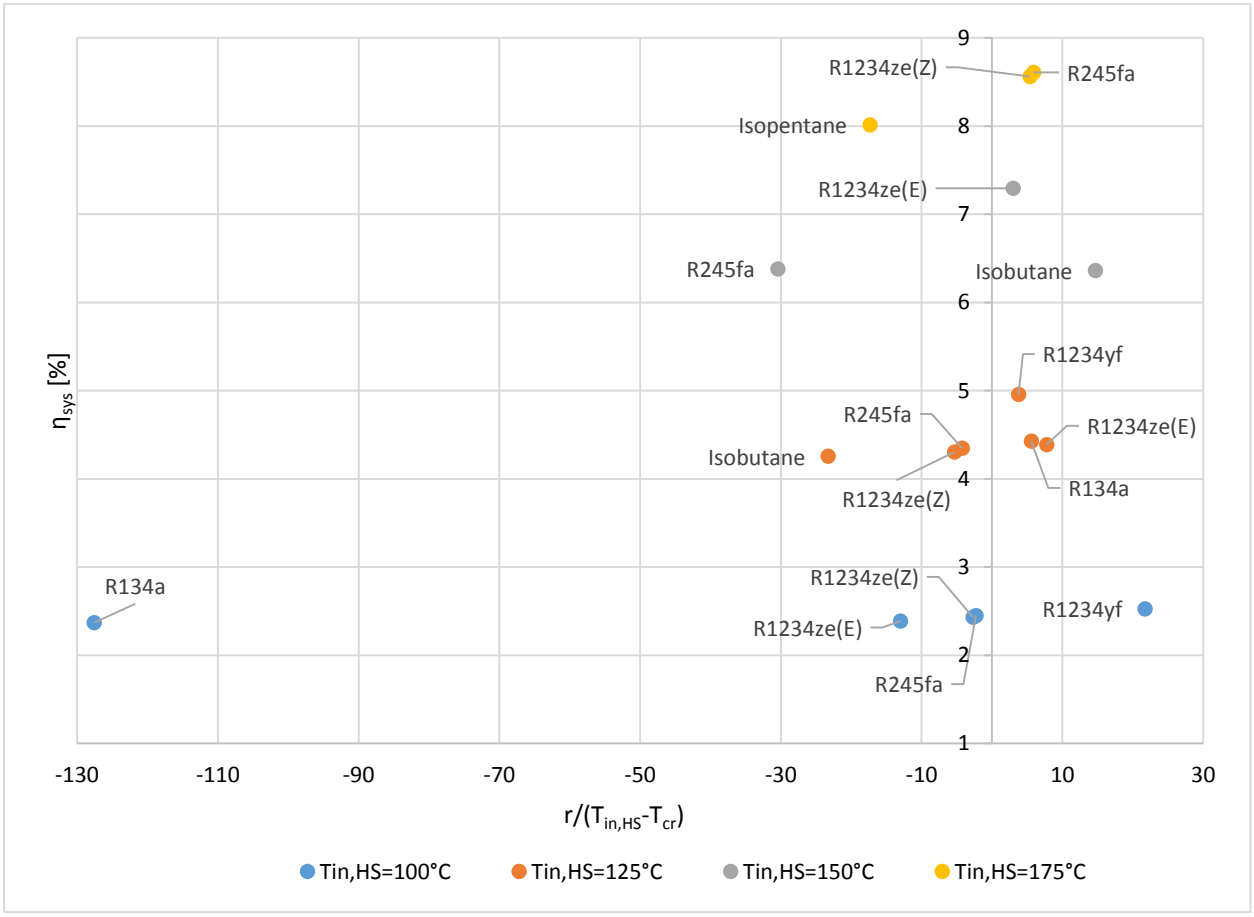

Figure 43. Trend of η_{sys} with $\frac{r}{(T_{in,HS}-T_{cr})}$ for different $T_{in,HS}$.

6.2 ECONOMIC CONSIDERATIONS

From an economic point of view it is important to consider the investment costs in the choice between single pressure and dual pressure ORC. For this purpose, results regarding the minimization of $AR = A_{tot}/W_{net}$ and the module costing technique (MCT) are here discussed.
In the literature, *AR* was chosen as optimization function for basic ORCs by Wang et al. [26] and, by Tian et al. [27] together with W_{net} and η_{th}, the same did Li et al. [16] for dual stage ORCs.
In general, the optimization of *AR* leads to very low power output, because the heat transfer area A_{tot} is drastically reduced and so is the working fluid mass flow rate which is heated up. When operating with the dual pressure configuration the optimization often brings back to a single pressure one.
Considering *AR* minimization does not give the right thermodynamic parameters for the construction of the power plant. In fact, the impact of the heat exchanger in the total purchased cost is not that relevant, as the capital cost analysis demonstrates (see Section 6.2.2). However, it is useful when there is uncertainty in the choice between two fluids that gives similar power output or when to a slight decrease in W_{net} corresponds a considerable improvement in *AR*: lower *AR* value expresses that smaller total heat transfer areas are needed and it is hence possible to partially reduce the investment costs. Furthermore, it can show, in the comparison between single and dual stage ORC, if the increase in W_{net} compensates the larger A_{tot}.
Further economic considerations, which include direct and indirect costs, are then carried out according to the model presented in Section 4.5.

6.2.1 AR minimization

The area ratio minimization ($AR = A_{tot}/W_{net}$) is here considered. The results are presented in order of increasing heat source inlet temperature giving a direct comparison between single and dual stage configuration.

- $T_{in,HS}$=100°C

Tables 25-26 show the optimum points, for the single and dual pressure ORC respectively, when the brine inlet temperature is 100°C.
The superheating is at its minimum with both configurations.
The net power output results more than halved in comparison to the optimization carried out with *max* W_{net} as objective function. This is due to the fact that the resulting heat recovery factor φ is very low. The heat source outlet temperature is only 10°-15°C lower than at the inlet, because the working fluid mass flow rate is drastically reduced.
The dual pressure configuration is reduced to a single pressure one, as shown by the expansion ratio close to the unity.
The fluid which gives the lowest *AR* is R134a with the basic ORC and R1234ze(Z) with the dual stage one.

Table 25. Optimum working point with $T_{in,HS}$=100°C for single stage ORC.

Fluid	R1234yf	R134a	R1234ze(E)
ΔT_{SH} [°C]	5	5	5
p_{max} [bar]	27,88	29,28	22,32
W_{net} [kW]	307,2	268,9	263,9
AR [m^2/kW]	3,024	2,527	2,974
T_{cond} [°C]	39,28	39,37	39,16
p_{cond} [bar]	10	10	7,5
m_{wf} [kg/s]	26,49	19,91	19,04
T_{max} [°C]	90	90	90
$T_{out,real}$ [°C]	90,09	91,34	91,66
φ	0,1245	0,1089	0,1048
η_{th}	0,0737	0,0737	0,0752
η_{sys}	0,0092	0,0080	0,0079

It is to notice that R1234yf, which gave the highest W_{net} (see Section 6.1), is one of the fluids with the highest *AR*.

Table 26. Optimum working point with $T_{in,HS}$=100°C for dual stage ORC.

Fluid	R1234yf	R134a	R1234ze(E)	Isobutane	R1234ze(Z)	R245fa	Isopentane
ΔT_{SH_HP} [°C]	5	5	5	5	5	5	5
$\Delta T_{SH\ LP}$ [°C]	0,01	0,01	0,01	0,01	0,01	0,01	0,01
p_{HP} [bar]	27,88	29,23	22,32	14,57	9,654	8,95	5.147
p_{LP} [bar]	26,14	28,76	22,31	14,46	9,648	8,947	5,145
W_{net} [kW]	463,2	309,5	264,9	305,5	251	250,7	236,9
AR [m^2/kW]	2,97	2,438	2,974	2,907	2,338	2,687	2,743
m_{HP} [kg/s]	26,49	20,2	19,04	9,767	12,76	13,65	6,989
m_{LP} [kg/s]	15,55	3,039	0,0808	0,6016	0,0330	0,0372	0,0172
r_{ex}	1,067	1,016	1	1,008	1,001	1	1
T_{max} [°C]	90	89,91	90	89,03	90	90	90
T_{out} [°C]	84,67	89,96	91,63	90,6	93,1	92,78	93,05
φ	0,1925	0,1262	0,1052	0,1181	0,08667	0,09073	0,0874
η_{th}	0,0718	0,0732	0,0752	0,0772	0,0864	0,0825	0,0809
η_{sys}	0,0138	0,0092	0,0079	0,0091	0,0075	0,0075	0,0070

- $T_{in,HS}$=125°C

At this $T_{in,HS}$, R1234yf with the single pressure configuration gives the same optimum working point obtained with W_{net} maximization. Considering, instead, R134a, with 0,56% W_{net} respect to the previous optimization, has a 9,5% lower *AR*. As Table 27 shows the power output remains high for R1234yf and R134a, but not for R1234ze(E).

In the choice between R1234yf and R134a it is necessary to evaluate if the 21% less power production is compensated by the 24% lower *AR*. Results, which will be presented in the next Section, show that the heat transfer area does not have a big influence in the total cost due to the components, so that a higher W_{net} is preferable.

Table 27. Optimum working point with $T_{in,HS}$=125°C for single stage ORC.

Fluid	R1234yf	R134a	R1234ze(E)
ΔT_{SH} [°C]	5	5	5
p_{max} [bar]	32,5	32,04	35
W_{net} [kW]	2038	1611	922,9
AR [m^2/kW]	2,694	2,039	2,140
T_{cond} [°C]	39,28	39,37	39,16
p_{cond} [bar]	10	10	7,5
m_{wf} [kg/s]	162,5	112,7	52,33
T_{max} [°C]	97,7	94,35	112,5
$T_{out,real}$ [°C]	64,66	76,2	102,2
φ	0,5763	0,4668	0,2187
η_{th}	0,0802	0,0783	0,0957
η_{sys}	0,0462	0,0365	0,0209

Considering the dual pressure configuration, all fluids, with the exception of R1234yf which has almost the same optimum parameters as with *max* W_{net}, have r_{ex} close to 1 and the loss in W_{net} is considerable.

Table 28. Optimum working point with $T_{in,HS}$=125°C for dual stage ORC.

Fluid	R1234yf	R134a	R1234ze(E)	Isobutane	R1234ze(Z)	R245fa	Isopentane
ΔT_{SH_HP} [°C]	5	5	5	5	5	5	5
$\Delta T_{SH\ LP}$ [°C]	0,01	0,01	0,01	0,01	0,01	0,01	0,01
p_{HP} [bar]	32,05	32,04	35	20,62	16,63	15,72	8.309
p_{LP} [bar]	22,13	32,02	34,69	20,61	15,68	15,72	8,307
W_{net} [kW]	2109	1612	956,6	986,4	640,1	440,9	627,1
AR [m^2/kW]	2,983	2,041	2,136	2,101	1,605	1,860	1,892
m_{HP} [kg/s]	160,2	112,7	52,33	24,86	15,41	16,43	12,75
m_{LP} [kg/s]	15,81	0,06623	2,392	0,04406	8,493	0,04892	0,017
r_{ex}	1,448	1,001	1,009	1	1,06	1	1
T_{max} [°C]	97	94,35	112,5	107,1	115	114,9	111,7
T_{out} [°C]	60,05	76,26	101,4	101,5	111,9	115,8	111,4
φ	0,6207	0,4671	0,2275	0,226	0,1257	0,0886	0,1307
η_{th}	0,0771	0,0783	0,0953	0,0990	0,1155	0,1129	0,1088
η_{sys}	0,0478	0,0366	0,0217	0,0224	0,0145	0,0100	0,0142

Between single and dual pressure ORC using R1234yf, the first is preferable, because to a little decrease in W_{net} corresponds an important improvement in *AR*.

- $T_{in,HS}$=150°C

Optimization results are presented in Table 29 for single pressure configuration.
R1234ze(E) is the only fluid which has the maximum ΔT_{SH}, and it gives 700 kW less than in the previous optimization without a significant reduction of *AR*.
R1234ze(Z) leads to the lowest *AR*, but it is not competitive because of the extremely low W_{net}, which is four times lower as in the optimization carried out with *max* W_{net} as objective function.

Table 29. Optimum working point with $T_{in,HS}$=150°C for single stage ORC.

Fluid	R1234ze(E)	Isobutane	R1234ze(Z)	R245fa	Isopentane
ΔT_{SH} [°C]	20	5	5	5	5
p_{max} [bar]	35	35	26,92	25,68	14,36
W_{net} [kW]	3327	1477	708,6	722,5	607
AR [m^2/kW]	2,232	1,641	1,170	1,478	1,449
T_{cond} [°C]	39,16	39,21	38,84	38,82	39,73
p_{cond} [bar]	7,5	5,2	2,8	2,4	1,5
$m_{\_wf}$ [kg/s]	154,6	29,22	21,77	21,77	9,095
T_{max} [°C]	127,5	137,4	140	140	140
$T_{out,real}$ [°C]	72,31	121,8	138,1	137,4	139,6
φ	0,6006	0,2201	0,0936	0,0985	0,0820
η_{th}	0,1011	0,1225	0,1382	0,1338	0,1352
η_{sys}	0,0607	0,0270	0,0129	0,0132	0,0111

In Table 30 the results for dual pressure ORC are shown. It can be noticed the optimization leads to a single stage configuration because of the really low $\dot{m}_{LP}$ using R1234ze(E) or the unitary r_{ex}.

Table 30. Optimum working point with $T_{in,HS}$=150°C for dual stage ORC.

Fluid	R1234ze(E)	Isobutane	R1234ze(Z)	R245fa	Isopentane
ΔT_{SH_HP} [°C]	5	20	5	5	13,85
$\Delta T_{SH\ LP}$ [°C]	0,01	0,01	0,01	0,01	0,01
p_{HP} [bar]	31,38	27,4	26,62	20,06	12,17
p_{LP} [bar]	19,31	27,39	25,96	20,05	12,17
W_{net} [kW]	3572	2207	955,2	1990	1404
AR [m^2/kW]	2,519	1,778	1,128	1,562	1,521
m_{HP} [kg/s]	206,5	41,98	24,13	65,95	21,93
m_{LP} [kg/s]	7,342	0,3624	5,696	0,07375	0,03339
r_{ex}	1,625	1	1,025	1	1
T_{max} [°C]	106,8	138	139,4	127	139,9
T_{out} [°C]	56,57	105	133,8	112,5	124,2
φ	0,7216	0,3512	0,1272	0,2928	0,2019
η_{th}	0,0903	0,1147	0,1371	0,124	0,1269
η_{sys}	0,0652	0,0403	0,0174	0,0363	0,0256

- $T_{in,HS}$=175°C

For what concerns *min AR*, the best fluid in the basic configuration, is R1234ze(Z), which gives though 19,9% less W_{net} respect to the optimization in Section 6.1. The other fluids (Table 31) show a similar decrease in W_{net}. As at the previous $T_{in,HS}$, the consideration, about the savings due to a reduction of the heat transfer area when it implicates a relevant decrease in W_{net}, is valid.

Table 31. Optimum working point with $T_{in,HS}$=175°C for single stage ORC.

Fluid	Isobutane	R1234ze(Z)	R245fa	Isopentane
ΔT_{SH} [°C]	20	6,5	7,43	5
p_{max} [bar]	35	32,5	34,89	22,02
W_{net} [kW]	4910	3773	3166	919,7
AR [m^2/kW]	1,630	1	1,32	1,208
T_{cond} [°C]	39,21	38,84	38,82	39,73
p_{cond} [bar]	5,2	2,8	2,4	1,5
m_{wf} [kg/s]	82,87	110,8	86,12	11,54
T_{max} [°C]	152,4	151,9	159,1	165
$T_{out,real}$ [°C]	83,62	114,2	124	161,1
φ	0,5944	0,3979	0,3350	0,0926
η_{th}	0,1258	0,1444	0,1439	0,1513
η_{sys}	0,0748	0,0575	0,0482	0,0140

With the dual pressure configuration (Table 32), only the cycle performed with isobutane does not result in a simple ORC, but the increase in W_{net} is limited.

Table 32. Optimum working point with $T_{in,HS}$=175°C for dual stage ORC.

Fluid	Isobutane	R1234ze(Z)	R245fa	Isopentane
ΔT_{SH_HP} [°C]	20	5	5	5
$\Delta T_{SH\ LP}$ [°C]	4	0,01	0,01	0,01
p_{HP} [bar]	32,33	28,29	33,93	21,65
p_{LP} [bar]	24,1	27,99	33,23	21,64
W_{net} [kW]	5130	4209	3535	1095
AR [m^2/kW]	1,783	1,049	1,339	1,210
m_{HP} [kg/s]	83,46	127	96,57	13,76
m_{LP} [kg/s]	9,12	1,339	3,262	0,06333
r_{ex}	1,341	1,011	1,021	1
T_{max} [°C]	147,6	142,7	155,2	164
T_{out} [°C]	75,47	105,2	117,7	158,4
φ	0,649	0,4589	0,3789	0,1107
η_{th}	0,1204	0,1397	0,1421	0,1508
η_{sys}	0,0781	0,0641	0,0538	0,0167

- $T_{in,HS}$=200°C

The comparison between the two configurations using isopentane is shown in Tables 33-34, the optimization with the dual pressure configuration leads to the single pressure one.
Again the reduction of *AR* has as consequence a great reduction of W_{net}.

Table 33. Optimum working point with $T_{in,HS}$=200°C for single stage ORC using isopentane.

ΔT_{SH}	p_{max}	W_{net}	AR	T_{cond}	p_{cond}	m_{wf}	T_{max}	$T_{out,real}$	φ	η_{th}	η_{sys}
[°C]	[bar]	[kW]	[m^2/kW]	[°C]	[bar]	[kg/s]	[°C]	[°C]			
5	31,89	2186	1,065	39,73	1,5	24,67	188,7	169,4	0,1763	0,1617	0,0273

Table 34. Optimum working point with T_{in_HS}=200°C for dual stage ORC using isopentane.

$\Delta T_{SH,HP}$	$\Delta T_{SH\ LP}$	p_{HP}	p_{LP}	W_{net}	AR	m_{HP}	m_{LP}	r_{ex}	T_{max}	T_{out}	φ	η_{th}	η_{sys}
[°C]	[°C]	[bar]	[bar]	[kW]	[m^2/kW]	[kg/s]	[kg/s]		[°C]	[°C]			
5	0,01	31,3	31,29	2475	1,066	27,97	0,072	1	187,4	165,5	0,2002	0,1616	0,0285

It can be concluded that the minimization of *AR* penalizes the power production in a relevant way and in next Section it will be demonstrated that it does not conduct to a significant reduction of the investment costs. This objective function can however give indications about the choice of the optimum operation parameters when to a slight decrease of W_{net} corresponds an improvement in *AR*.

6.2.2 Capital cost

In this Section the estimations of the total costs of equipment ($\sum C_P$) and the overall cost of the plant (grassroots cost C_{GR}) are presented, when the net power output is maximized.
For each heat source inlet temperature a comparison between single pressure and dual pressure configuration is shown: at $T_{in,HS}$=100°C using R1234yf, at $T_{in,HS}$=125°C using R134a, at $T_{in,HS}$=150°C using isobutane, at $T_{in,HS}$=175°C using R245fa and at $T_{in,HS}$=200°C using isopentane.
The choice of these fluids is made considering that R1234yf is the fluid which gives the maximum power output at the lowest brine inlet temperature and isopentane is the only fluid analyzed at $T_{in,HS}$=200°C. At the other $T_{in,HS}$, the most performing fluid gives limited adavantages in the dual stage configuration, so fluids which show an improvement in the performance were chosen, to see if the higher investment cost is justified. At every $T_{in,HS}$ there is no LP-superheating and consequently the LP-superheater costs are missing.
For each configuration all the necessary factors to calculate the purchased equipment cost (C_P) and the bare module cost (C_{BM}) of each component are provided, the total cost of equipment $\sum C_P$ and the percentage of this cost covered by each component and finally the overall cost of the plant C_{GR}, obtained through the total module cost (C_{TM}), which includes contingency costs and fees.
The procedure followed to evaluate the costs is explained in Section 4.5 using the module costing technique (MCT).

Table 35. Capital cost at $T_{in,HS}$=100°C for the single pressure ORC using R1234yf.

Component	n	C^0_p	Fp	F_M	F_{BM}	C_P	C_{BM}	$\%\sum C_P$
Pump	1	8030	1,266	1,5	4,45	15250	35764	0,999
Turbine	1	176976	1	4,77	11,6	844174	2052918	55,3
Evaporator	1	48417	1,064	1	3,40	51514	164433	3,38
Preheater	1	37169	1,064	1	3,40	39546	126232	2,59
Superheater	1	17982	1,064	1	3,40	19133	61071	1,25
ACC fans	12	130687	1	2,5	5	326717	653433	21,4
ACC	1	229957	1	1	2,17	229957	499007	15,1

Table 36. Capital cost at $T_{in,HS}$=100°C for the dual pressure ORC using R1234yf.

Component	n	C^0_p	Fp	F_M	F_{BM}	C_P	C_{BM}	$\%\sum C_P$
Pumps	2	9309	1,296	1,5	4,515403	18104,43	42036	0,851
HP-turbine	1	97198	1	4,77	11,6	463635,2	1127499	21,8
LP-turbine	1	161791	1	4,77	11,6	771743,2	1876776	36,2
HP-evaporator	1	46261	1,07	1	3,41	49509	157590	2,32
LP-evaporator	1	35576	1,04	1	3,36	37089	119557	1,76
HP-preheater	1	28272	1,07	1	3,41	30257	96309	1,42
LP-preheater	1	37124	1,04	1	3,36	38703	124758	1,82
Superheater	1	46326	1,07	1	3,44	49578	157811	2,33
ACC fans	15	165609	1	2,5	5	414023	828046	19,4
ACC	1	256878	1	1	2,17	256878	557426	12,1

Tables 35-36 show the results at $T_{in,HS}$=100°C using R1234yf for single pressure and dual pressure ORC respectively. It is to be noticed that with both configurations the turbine has the highest relative cost, being more than 50%, also the air cooled condenser (ACC) with the fans are expensive covering more than 30% of the total purchased cost, whereas the influence of the heat exchanger is low and that of the pumps negligible, covering less than 1% of $\sum C_P$.
The comparison of the total capital cost between the two configurations is shown in Table 37, where also the specific investment costs (*SIC*) are reported. The specific investment cost is defined as:

$$SIC = \frac{C_{GR}}{W_{net}} \left[\frac{\$}{kW}\right] \quad (6.2.2.1)$$

The expense and the specific investment cost with the dual stage ORC are, respectively, about 40% and 15,6% higher, when the power production increases by 21,7%.

Table 37. Comparison between single and dual stage configuration at $T_{in,HS}$=100°C.

	$\sum C_P$	C_{TM}	C_{GR}	SIC
Single pressure ORC	1526290	4239572	6025630	8674
Dual pressure ORC	2119671	5966623	8479845	10024

It is to notice that $\sum C_P$ is in the first case the 25,3% and in the second 25,0% of the overall plant cost, so that, even considering together the C_P of ACC and fans and the C_P of the heat exchanger, a reduction of their heat transfer area does not lead to a significant reduction of the capital cost if it implicates a relevant reduction of the net power output. The earnings derived from the energy production are, in fact, the only income of these plants.

Tables 38-39 regard the analysis carried out with R134a at $T_{in,HS}$=125°C.
Again the expander is the component with the highest relative cost, which increases with the dual pressure configuration, because two turbines, even if smaller, weigh more than one big turbine. The dual pressure ORC, therefore, entails higher costs on account of the larger heat transfer areas, but also because of the presence of two expanders. For this reason, the comparison between single and dual stage configuration based on *AR* is limiting.
The ACC equipment, instead, has a higher relative cost in the single stage configuration, whereas the percentage covered by pumps and heat exchangers is similar in both configuration and it is low.

In Table 40 $\sum C_P$, C_{TM} and C_{GR} are presented for both ORC systems. Between the two configurations there is a difference of 37,8% in C_{GR} and of 20,5% in the power production. The *SIC*s are lower than the previous case and the difference between single and dual pressure ORC is about 14%.

Table 38. Capital cost at $T_{in,HS}$=125°C for the single pressure ORC using R134a.

Component	n	C^0_p	Fp	F_M	F_{BM}	C_P	C_{BM}	$\%\sum C_P$
Pump	1	28308	1,511	1,5	4,95	64180	140146	2,84
Turbine	1	271707	1	4,77	11,6	1296041	3151799	57,3
Evaporator	1	52257	1,119	1	3,49	58454	182212	2,59
Preheater	1	57280	1,119	1	3,49	44073	199727	2,83
Superheater	1	20103	1,119	1	3,49	22487	70097	0,995
ACC fans	19	203001	1	2,5	5	507503	1015006	22,4
ACC	1	247889	1	1	2,17	247889	537920	11,0

Table 39. Capital cost at $T_{in,HS}$=125°C for the dual pressure ORC using R134a.

Component	n	C^0_p	Fp	F_M	F_{BM}	C_P	C_{BM}	$\%\sum C_P$
HP-pump	1	24817	1,665	1,5	4,515403	61990	130590	2,01
LP-pump	1	21355	1,309			41943	96985	1,36
HP-turbine	1	176541	1	4,77	11,6	842101	2047876	27,3
LP-turbine	1	253586	1	4,77	11,6	1209604	2941595	39,2
HP-evaprator	1	40327	1,157	1	3,55	46653	143177	1,51
LP-evaporator	1	42373	1,073	1	3,41	45462	144534	1,47
HP-preheater	1	50624	1,157	1	3,55	58565	179734	1,90
LP-preheater	1	56975	1,073	1	3,41	61129	194343	1,98
Superheater	1	27821	1,157	1	3,55	32185	98775	1,04
ACC fans	15	165603	1	2,5	5	414023	828046	13,4
ACC	1	271857	1	1	2,17	271857	589929	8,81

Table 40. Comparison between single and dual stage configuration at $T_{in,HS}$=125°C.

	$\sum C_P$	C_{TM}	C_{GR}	SIC
Single pressure ORC	2260628	6250351	8861831	5470
Dual pressure ORC	3085511	8612347	12215080	6235

$\sum C_P$ calculated for the single pressure ORC is the 25,5% of the overall plant cost and for the dual pressure one the 25,3%, which shows that a reduction of the components cost does not translate into an equal reduction of the general plant costs.

At $T_{in,HS}$=150°C, results are shown in Tables 41-42.
Similar considerations as in the previous case can be done when $T_{in,HS}$=150°C: the turbines have the highest relative cost, followed by the condensation equipment, which has a higher percentage than before. This happens because isobutane is a dry fluid and hence the expansion ends in the superheated

zone, whereas R134a has a slightly negative slope of the saturated vapor, so the desuperheating zone is small and, as consequence, the condensation area is reduced.
Table 43 shows the comparison between the two configurations. C_{GR} ans SIC are respectively 43% and 20% higher for the dual pressure ORC, which, on the other hand, gives 19,3% more W_{net}.
$\sum C_P$ represents for both system the 25,5% of the total capital cost.

Table 41. Capital cost at $T_{in,HS}$=150°C for the single pressure ORC using isobutane.

Component	n	C^0_p	Fp	F_M	F_{BM}	C_P	C_{BM}	$\%\sum C_P$
Pump	1	28348	1,260	1,5	4,44	53570	125896	1,87
Turbine	1	330023	1	4,77	11,6	1574209	3828264	55,0
Evaporator	1	30020	1,063	1	3,39	63784	203715	2,23
Preheater	1	67329	1,063	1	3,39	71551	228520	2,50
Superheater	1	17126		1	0,39	18200	58127	0,635
ACC fans	26	287522	1,063	2,5	5	718805	1437611	25,1
ACC	1	364294	1	1	2,17	364293	790517	12,7

Table 42. Capital cost at $T_{in,HS}$=150°C for the dual pressure ORC using isobutane.

Component	n	C^0_p	Fp	F_M	F_{BM}	C_P	C_{BM}	$\%\sum C_P$
PH-pump	1	22878	1,418	1,5	4,76	48662	108933	2,19
LP-pump	1	20749	1,077		4,07	33505	84447	0,822
HP-turbine	1	214800	1	4,77	11,6	1024597	2491683	25,1
LP-turbine	1	311128	1	4,77	11,6	1484079	3609080	36,4
HP-evaprator	1	50968	1,097	1	3,45	55897	175867	1,37
LP-evaporator	1	47729	1,030	1	3,34	49140	159371	1,21
HP-preheater	1	48597	1,097	1	3,45	53298	167688	1,31
LP-preheater	1	66210	1,030	1	3,34	68167	221080	1,67
Superheater	1	19483	1,097	1	3,45	21367	67226	0,524
ACC fans	30	335781	1	2,5	5	839454	1678907	20,6
ACC	1	397953	1	1	2,17	397953	863558	9,76

Table 43. Comparison between single and dual stage configuration at $T_{in,HS}$=150°C.

	$\sum C_P$	C_{TM}	C_{GR}	SIC
Single pressure ORC	2864411	7873726	11185507	3827
Dual pressure ORC	4076119	11261203	16003141	4591

The cases analyzed at $T_{in,HS}$=175°C and $T_{in,HS}$=200°C are similar to previous ones. Results are shown in Tables 44-49.
At $T_{in,HS}$=175°C the dual pressure configuration has a 43% higher C_{GR} but provides 16,5% more W_{net}.
The situation at $T_{in,HS}$=200°C is very similar, these percentages are respectively 42,6% and 13,7%.
$\sum C_P$ results to be about 25,5% of C_{GR} in every arrangement.
Looking at the *SIC*s, they are 22,8% and 26,2 % higher for the dual pressure ORC at $T_{in,HS}$=175°C and $T_{in,HS}$=200°C respectively.

Table 44. Capital cost at $T_{in,HS}$=175°C for the single pressure ORC using R245fa.

Component	n	C^0_p	Fp	F_M	F_{BM}	C_P	C_{BM}	$\%\sum C_P$
Pump	1	27401	1,200	1,5	4,32	49308	118354	1,43
Turbine	1	381335	1	4,77	11,6	1818970	4423490	52,8
Evaporator	1	64268	1,051	1	3,37	67544	216879	1,96
Preheater	1	87750	1,051	1	3,37	92222	296121	2,68
Superheater	1	17883	1,051	1	3,37	18794	60347	0,546
ACC fans	35	38809	1	2,5	5	972021	1944043	28,2
ACC	1	425484	1	1	2,17	425484	923300	12,4

Table 45. Capital cost at $T_{in,HS}$=175°C for the dual pressure ORC using R245fa.

Component	n	C^0_p	Fp	F_M	F_{BM}	C_P	C_{BM}	$\%\sum C_P$
PH-pump	1	25799	1,413	1,5	4,75	54676	122573	1,68
LP-pump	1	18125	1		3,92	27188	70959	0,557
HP-turbine	1	259759	1	4,77	11,6	1239047	3013196	25,4
LP-turbine	1	361219	1	4,77	11,6	1723013	4190136	35,3
HP-evaprator	1	54231	1,096	1	3,45	59412	187020	1,22
LP-evaporator	1	49391	1,013	1	3,31	50021	163543	1,03
HP-preheater	1	61447	1,096	1	3,45	67318	211907	1,38
LP-preheater	1	84058	1,013	1	3,31	85131	278332	1,74
Superheater	1	19892	1,096	1	3,45	21793	68601	0,447
ACC fans	40	437620	1	2,5	5	1094050	2188099	22,4
ACC	1	457281	1	1	2,17	457281	992300	9,37

Table 46. Comparison between single and dual stage configuration at $T_{in,HS}$=175°C.

	$\sum C_P$	C_{TM}	C_{GR}	SIC
Single pressure ORC	3444343	9419389	13388681	2759
Dual pressure ORC	4878929	13470536	19146734	3388

Table 47. Capital cost at $T_{in,HS}$=200°C for the single pressure ORC using isopentane.

Component	n	C^0_p	Fp	F_M	F_{BM}	C_P	C_{BM}	$\%\sum C_P$
Pump	1	28093	1,056	1,5	4,02	44486	113153	1,16
Turbine	1	414954	1	4,77	11,6	1979331	4813468	51,5
Evaporator	1	68700	1,026	1	3,33	70509	229026	1,83
Preheater	1	108592	1,026	1	3,33	111452	362016	2,90
Superheater	1	17726	1,026	1	3,33	18193	59093	0,473
ACC fans	41	456714	1	2,5	5	1141786	2283571	29,7
ACC	1	480597	1	1	2,17	480597	1042896	12,5

Table 48. Capital cost at $T_{in,HS}$=200°C for the dual pressure ORC using isopentane.

Component	n	C^0_p	Fp	F_M	F_{BM}	C_P	C_{BM}	$\%\sum C_P$
PH-pump	1	26549	1,246	1,5	4,41	49602	117140	0,914
LP-pump	1	16798	1		3,92	25196	65762	0,465

HP-turbine	1	300946	1	4,77	11,6	1435514	3490978	26,5
LP-turbine	1	389330	1	4,77	11,6	1857105	4516229	34,2
HP-evaprator	1	60059	1,060	1	3,39	63654	203561	1,17
LP-evaporator	1	50049	1,001	1	3,29	50088	164725	0,923
HP-preheater	1	73033	1,060	1	3,39	77405	247536	1,43
LP-preheater	1	95124	1,001	1	3,29	95197	313079	1,76
Superheater	1	18974	1,060	1	3,39	20110	64311	0,371
ACC fans	45	496990	1	2,5	5	1242475	2484950	22,9
ACC	1	5506193	1	1	2,17	506193	1098438	9,33

Table 49. Comparison between single and dual stage configuration at $T_{in,HS}$=200°C.

	$\sum C_P$	C_{TM}	C_{GR}	SIC
Single pressure ORC	3846354	10505802	14942085	2188
Dual pressure ORC	5417513	14987119	21314385	2761

6.2.3 Discussion and critical remarks

Considering the single pressure configuration, the overall plant cost increases by 47% when $T_{in,HS}$ changes from 100°C to 125°C, by 26% from 125°C to 150°C, by 19,7% from 150°C to 175°C and by 11,6% from 175°C to 200°C. The specific investment costs (*SIC*), instead, decreases by 37% from 100°C to 125°C, by 30% from 125°C to 150°C, by 28% from 150°C to 175°C and by 20,7% from 175°C to 200°C.

Similarly for the dual pressure ORC: C_{GR} increases by 44% moving from $T_{in,HS}$=100°C to 125°C, by 31% from 125°C to 150°C, by 19,6% from 150°C to 175°C and by 11,3% from 175°C to 200°C. The SIC decreases, instead, by 37,8% from 100°C to 125°C, by 26,4% from 125°C to 150°C, by 26,2% from 150°C to 175°C and by 18,5% from 175°C to 200°C.

Even if the same fluid was not employed at every $T_{in,HS}$, these data give indications about the importance of scale effect: the impact of the size/capacity parameters of the equipment has a lower effect on the total investment cost at the increasing of the plant size.

This validate the conclusion that *AR* minimization, which usually results in a low nominal power output, gives only reduced savings on the overall plant cost and would penalize the income, because the site would not be fully exploited.

Furthermore, it is shown that the capital cost increases of about 40% passing from a single to a dual stage configuration. This is due to the doubling of the heat exchangers and of the turbine, which has the highest relative costs as it was found also by Cayer et al. [29].

It is then to be evaluated if the higher power production can compensate the increased capital cost.

6.3 RESULTS FOR THE ORC FED BY MULTIPLE HEAT SOURCES

When the hot streams are multiple, the working fluid selection criteria fall, because the heat recovered by the working fluid markedly depends a lot by the HCC form. The HCC form affects also the choice between single and dual pressure configuration, with the latter that can realize a higher improvement in the temperature profiles matching when the HCC becomes more irregular.
The available hot streams and the resulting HCC are showed in Section 5. The optimizations carried out with isobutane, R1234ze(Z), R245fa and isopentane are here presented together with a performance comparison between simple and dual pressure ORCs.
The optimum working point for each fluid is showed in Table 50 for the basic configuration and in Table 51 for the dual stage one. Both configurations are able to recovery the entire amount of heat available as showed by the unitary value of φ.

Table 50. Optimum working points with single pressure ORC.

Fluid	Isobutane	**R1234ze(Z)**	R245fa	Isopentane
ΔT_{SH} [°C]	5	5	5	5
p_{max} [bar]	24,56	15,61	15,34	8,31
W_{net} [kW]	1749	**1835**	1804	1758
m_{wf} [kg/s]	39,66	69,11	68,33	35,77
T_{cond} [°C]	39,21	38,84	38,82	39,73
φ	1	1	1	1
η_{th}	0,1082	0,1136	0,1117	0,1088
η_{sys}	0,1082	**0,1136**	0,1117	0,1088

Table 51. Optimum working points with Dual pressure ORC.

Fluid	Isobutane	**R1234ze(Z)**	R245fa	Isopentane
$\Delta T_{SH,HP}$ [°C]	16	12	5	5
$\Delta T_{SH,LP}$ [°C]	0,01	0,01	0,01	0,01
p_{HP} [bar]	28	19,32	18,67	10
p_{LP} [bar]	24,14	15,56	15,36	7.508
m_{HP}/m_{LP}	0,5774	0,5725	0,6006	0,642
m_{HP} [kg/s]	22,05	38,97	41,02	22,86
m_{LP} [kg/s]	16,14	29,1	27,28	12,75
W_{net} [kW]	1811	**1948**	1894	1834
φ	1	1	1	1
η_{th}	0,1121	0,1206	0,1173	0,1135
η_{sys}	0,1121	**0,1206**	0,1173	0,1135

In Figure 44 the *T-H* diagrams are plotted, the HCC is represented in red and the CCC in blue.
With two evaporations is possible to realize a better approach of the CCC and HCC, this allows enhancing the cycle mean temperature and hence increasing the thermal efficiency, as showed by the values of η_{th} in Tables 50-51.

As consequence, the total system efficiency results higher with the dual pressure configuration and W_{net} increases of 3,54% using isobutane, of 6,16% with R1234ze(Z), 4,99% with R245fa and 4,32% using isopentane.

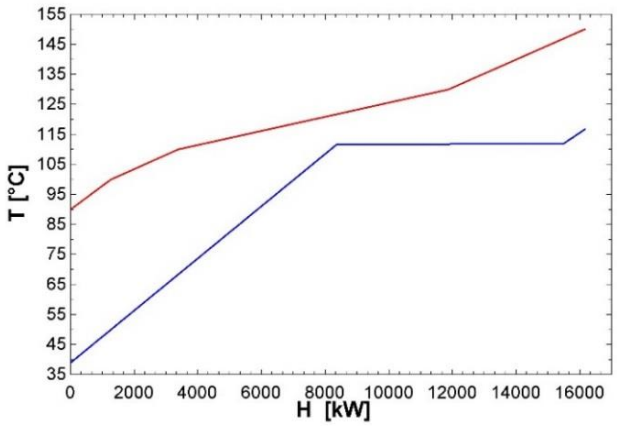

a) Isobutane, single pressure ORC

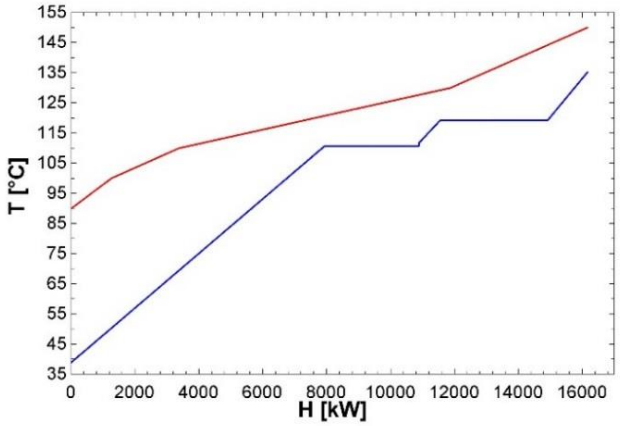

b) Isobutane, dual pressure ORC

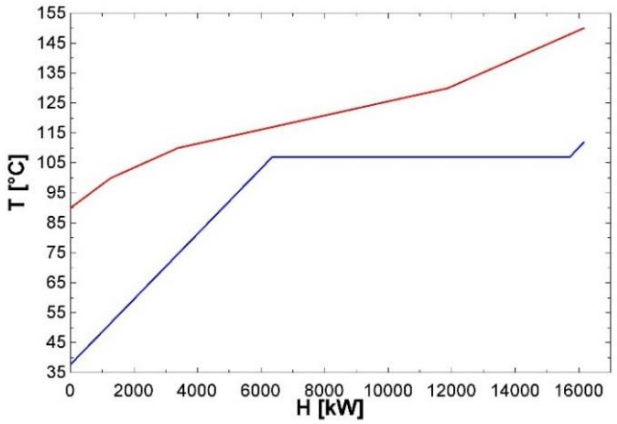

c) R1234ze(Z), single pressure ORC

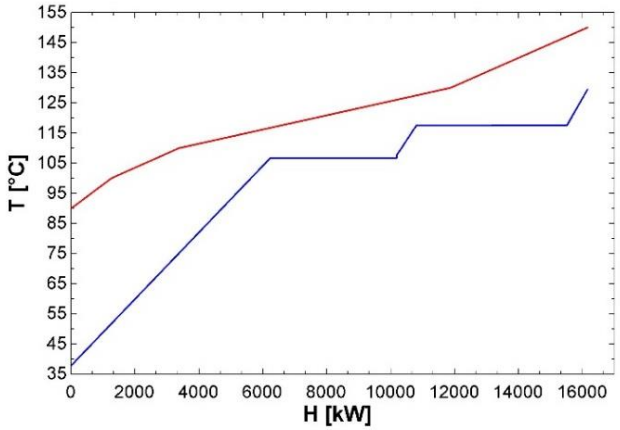

d) R1234ze(Z), dual pressure ORC

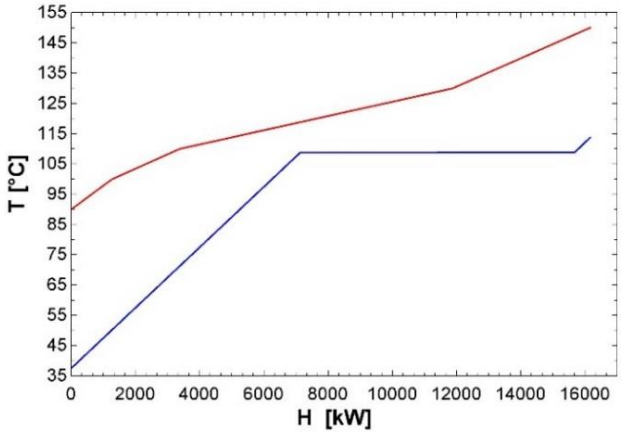

e) R245fa, single pressure ORC

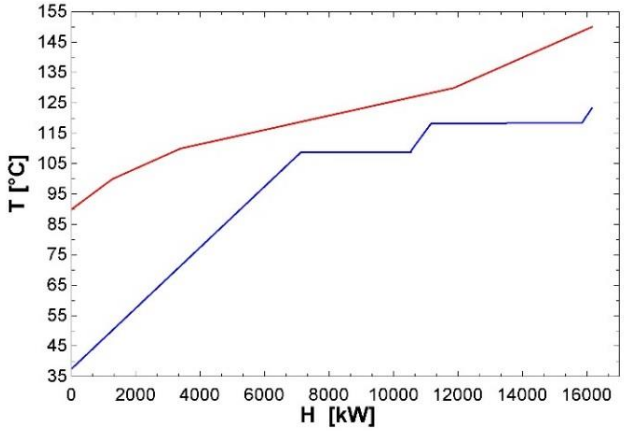

f) R245fa, dual pressure ORC

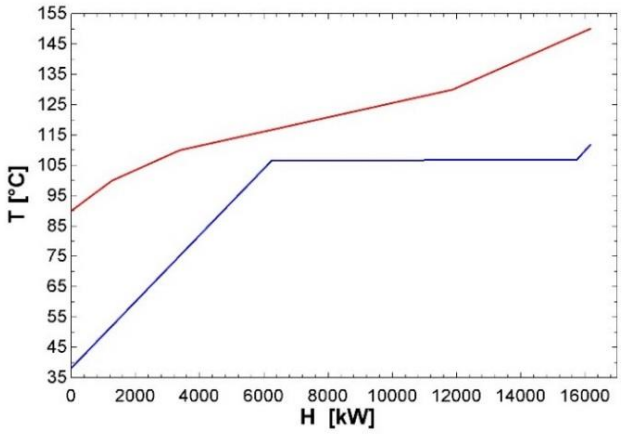

g) Isopentane, single pressure ORC

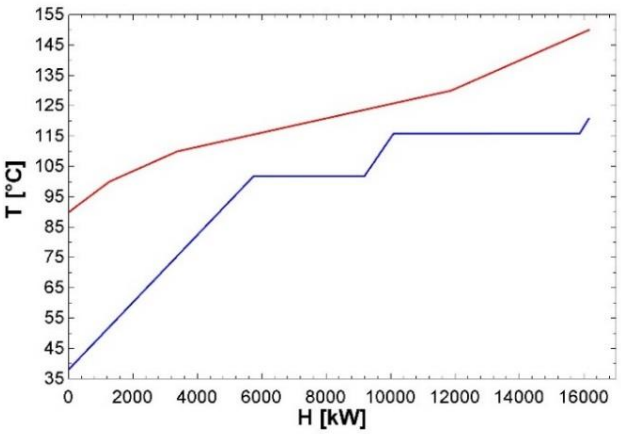

h) Isopentane, dual pressure ORC

Figure 44. T-H diagram: comparison between single and dual pressure ORC.

The fluid with the highest improvement, moving from the single to the dual stage configuration, is also the fluid which gives the maximum power output (with both configurations): R1234ze(Z).
This is due to the higher η_{th} in comparison to the other fluids.
In Figure 45 the GCCs are plotted: on the left side for the single pressure ORC and on the right side for the dual pressure one.

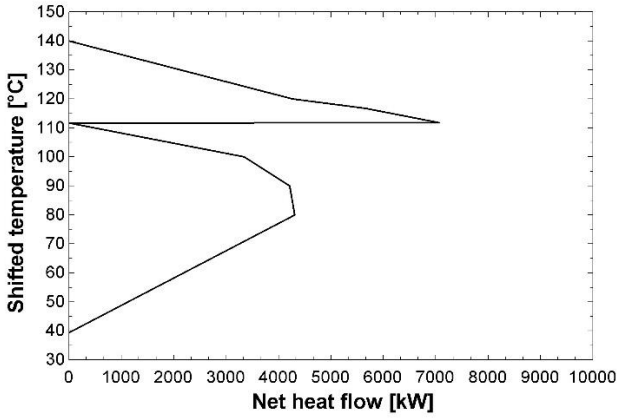

a) Isobutane, single pressure ORC

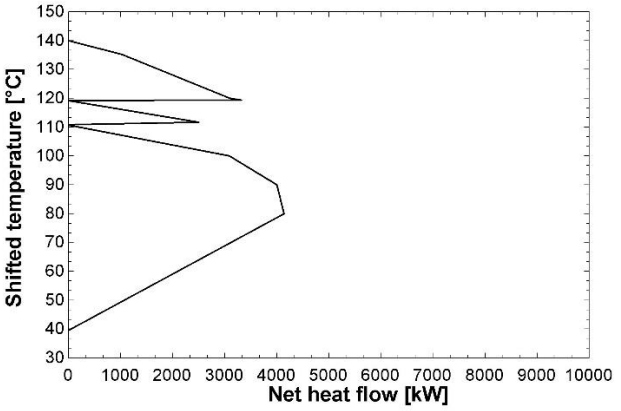

b) Isobutane, dual pressure ORC

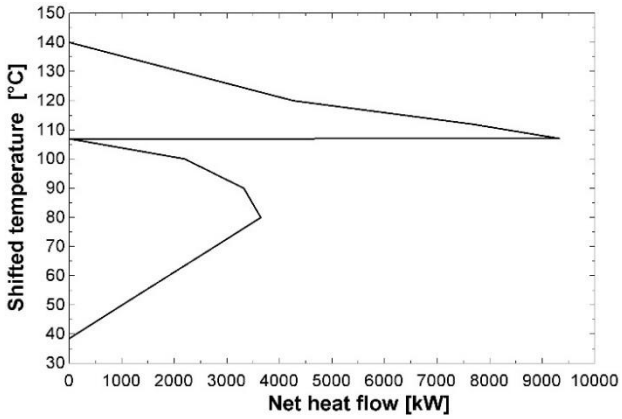

c) R1234ze(Z), single pressure ORC

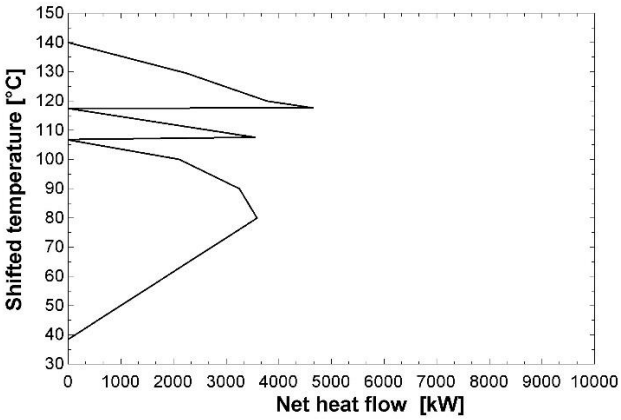

d) R1234ze(Z), dual pressure ORC

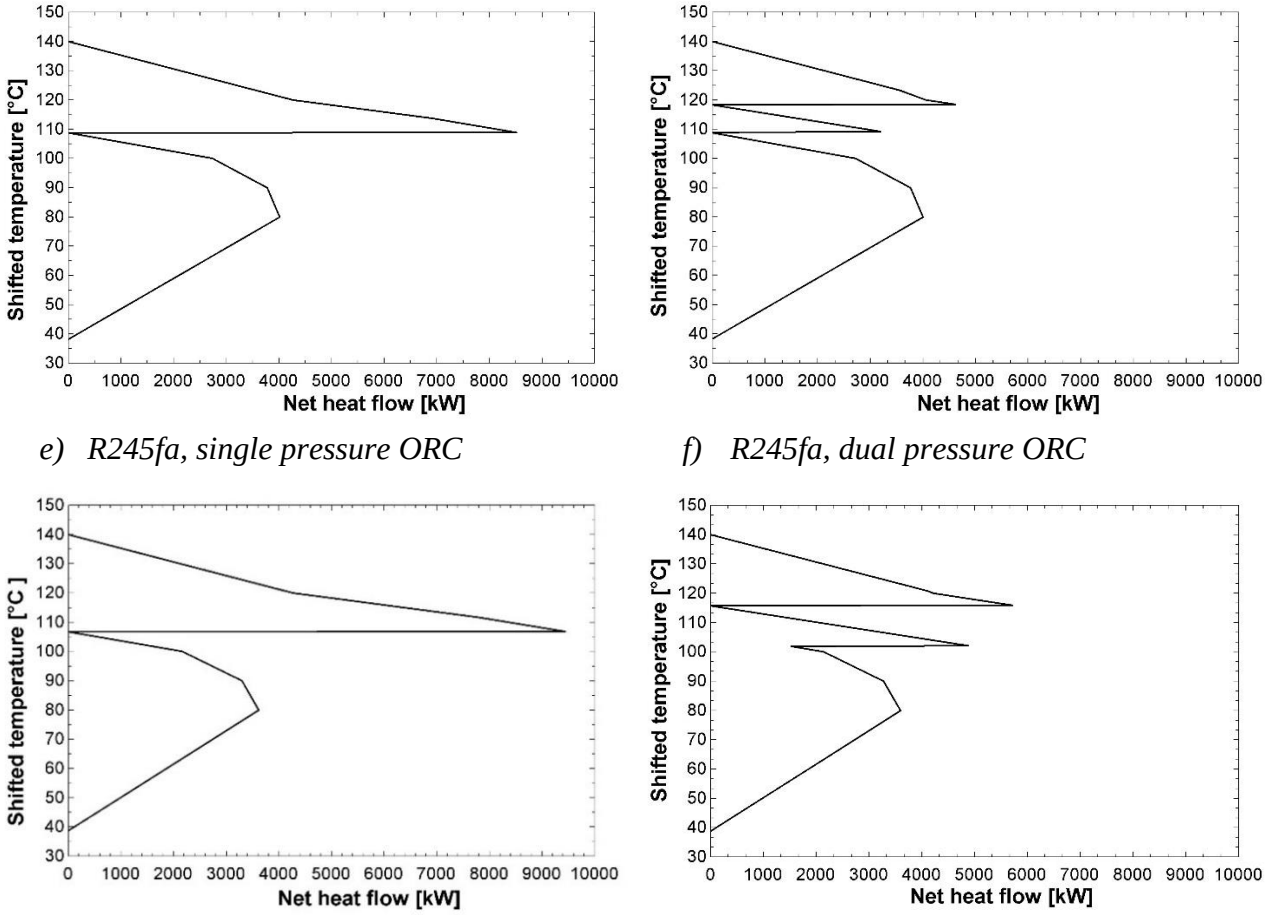

e) R245fa, single pressure ORC *f) R245fa, dual pressure ORC*

g) Isopentane, single pressure ORC *h) Isopentane, dual pressure ORC*

Figure 45. GCC: comparison between single and dual pressure ORC.

The GCC is directly obtained from the Problem Table representing for every temperature interval the heat deficit or the heat surplus. The points, which touch the y-axis, are the pinch points. With the dual pressure ORC, ΔT_{min} is reached at the beginning of both LP and HP evaporation with the exception of isopentane, when only the HP stage touches the axis.
Comparing the pictures on the left with those on the right it can be observed that the introduction of the second evaporation allowed compacting the GCC to the left at the highest temperatures, which means a reduction of the irreversibilties in the heat transfer process.

It can be concluded that, with multiple heat sources, the dual pressure configuration performs better than the single stage ORC. In the present case, both configurations could guarantee the total exploitation of the available heat (φ=1), but when the complexity of the HCC increases, the single pressure ORC can have difficulties to recover the entire amount of available heat, whereas the dual pressure ORC, in addition to a higher η_{th}, can gives also a higher φ, because of the improved match between HCC and CCC.

7. DISCUSSION AND CRITICAL REMARKS

The maximum W_{net} is the result of a compromise between high thermal efficiency (η_{th}) and high heat recovery factor (φ) as Figure 46 demonstrates for the single pressure configuration and Figure 47 for the dual pressure configuration.

With the single stage ORC, φ tends to decrease at increasing evaporation pressures whereas η_{th} shows an opposite trend (as in Fig. 46a for R1234yf). Only when the optimum p_{max} reaches the maximum value, both φ and η_{th} increase with p_{max} (as in Fig 46b for R1234ze(E)). The product between φ and η_{th} gives the total system efficiency η_{sys}, which is plotted in Figures 46c-d for R1234yf and R1234ze(E) respectively.

Using R1234yf the optimum pressure is p_{max}=19,3 bar whereas using R1234ze(E) it is 35 bar.

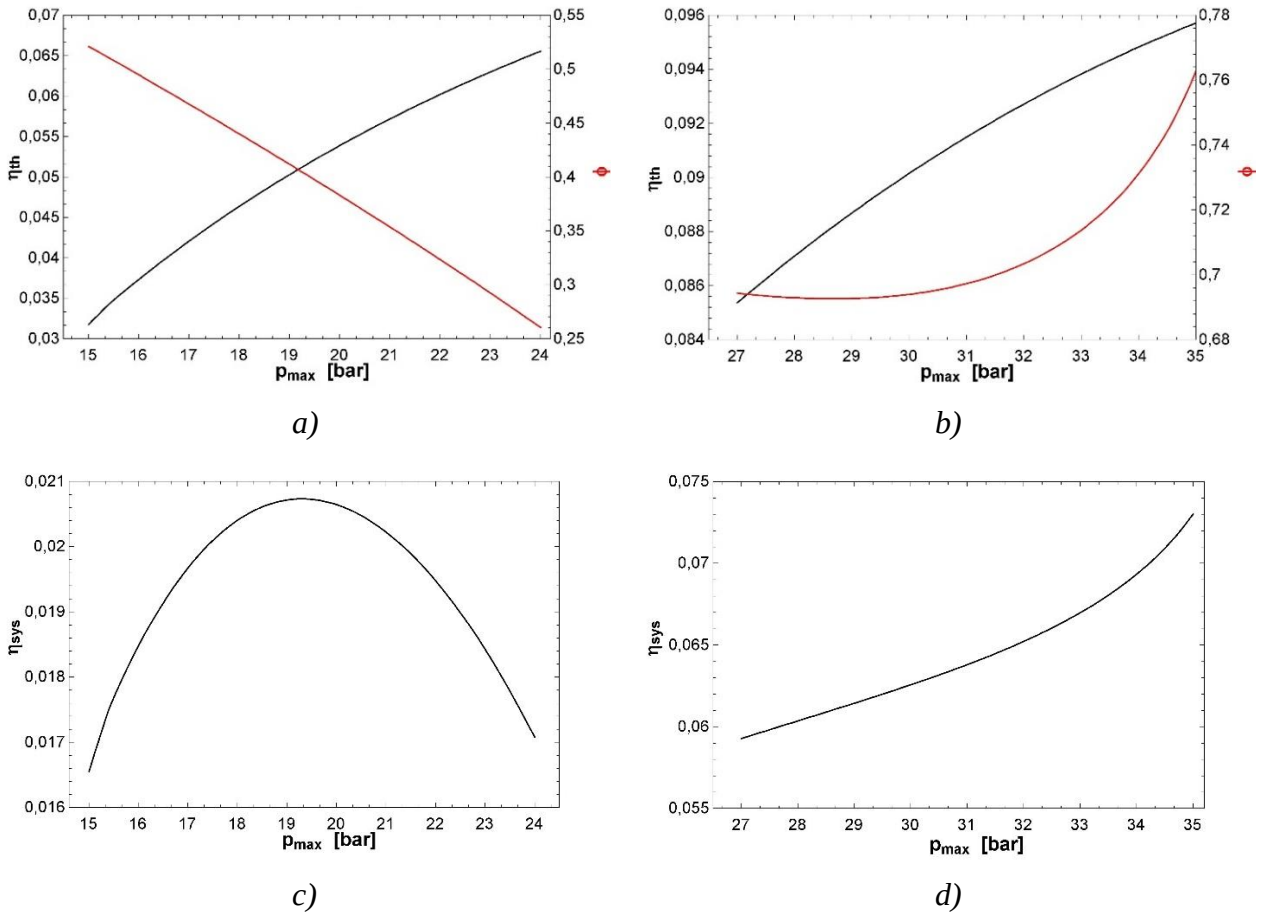

Figure 46. η_{th} (in black) and φ (in red) trend for a single pressure ORC using: a) R1234yf at $T_{in,HS}$=100°C and b) R1234ze(E) at $T_{in,HS}$=150°C c) η_{sys} for R1234yf at $T_{in,HS}$=100°C, d) η_{sys} for R1234ze(E) at $T_{in,HS}$=150°.

With the dual pressure ORC, η_{th} increases with both p_{HP} and p_{LP} when p_{HP} is far from the maximum allowed pressure (Figure 47a). Instead, when the limit is reached, the influence of p_{HP} is stonger (Figure 47c), whereas φ varies only with p_{LP} in both cases (Figures 47 b-d).

Using R1234yf the optimum pressures are: p_{HP}=20,45 bar and p_{LP}=10,42, whereas using R1234ze(E) p_{HP}=35 bar and p_{LP}=8,5 bar.

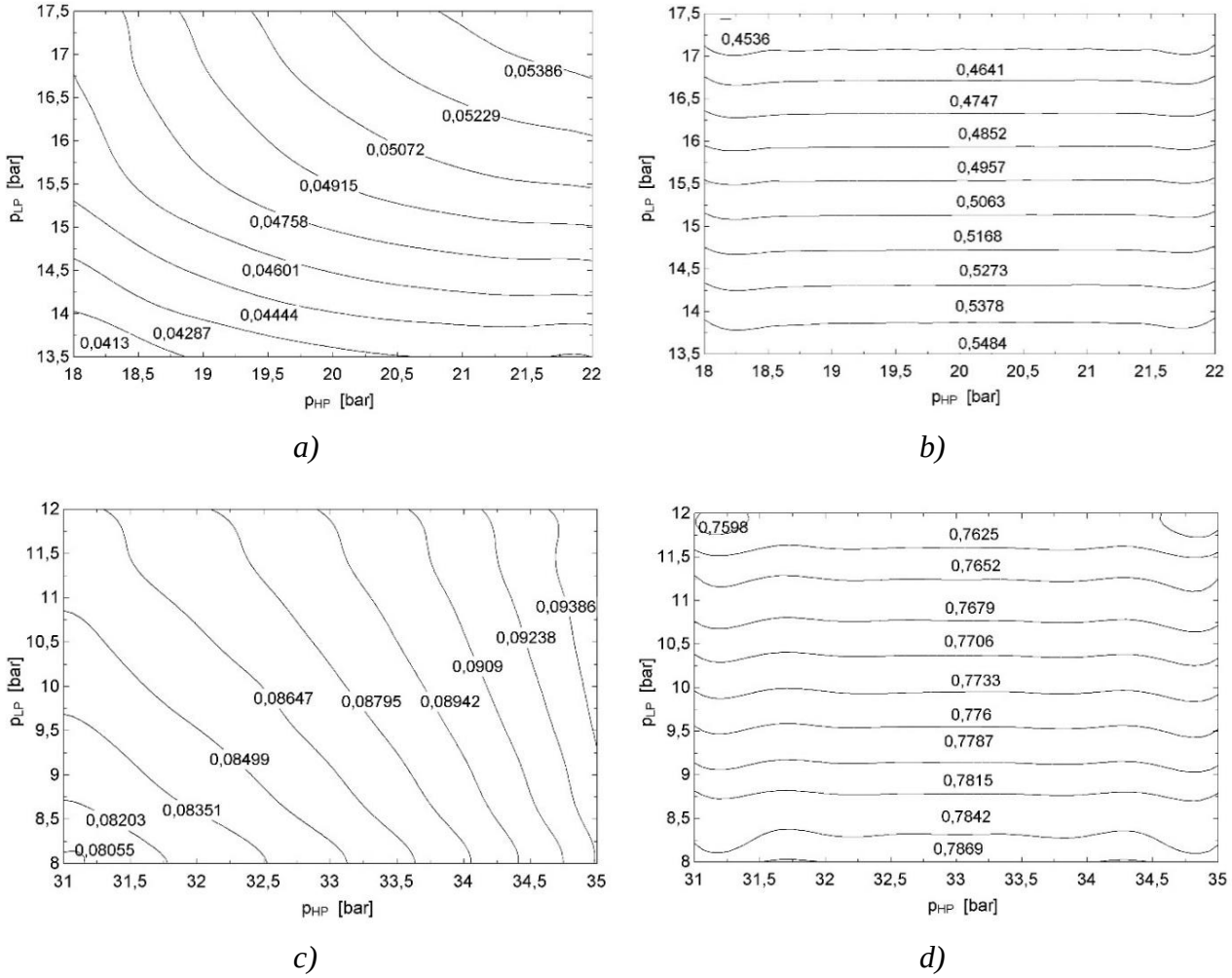

Figure 47. a) η_{th} trend using R1234yf at $T_{in,HS}$=100°C, b) φ trend using R1234yf, c) η_{th} trend using R1234ze(E) at $T_{in,HS}$=150°C, d) φ trend using R1234ze(E) at $T_{in,HS}$=150°C.

As shown in Figures 49 to 52, the dual pressure configuration brings to improvements of about 20% in all cases except for those in which the single stage ORC is working at the optimum conditions, that is when the heat source inlet temperature is approximately 30° to 40°C higher than the working fluid critical temperature [9]. Only in these conditions, the single pressure configuration is able to achieve the maximum allowed pressure while simultaneously exploiting well the heat source. When the difference between brine temperature and working fluid critical temperature becomes smaller or negative, the optimum evaporation pressure of the single stage ORC is reduced to keep the mass flow rate high and the dual pressure configuration becomes advantageous for the possibility of generating power also at a higher pressure level in the high pressure stage.

At 125°C having a dual pressure configuration still conducts to an increase in W_{net}, because there is a better matching between hot and cold curves and in turn a higher φ. At 150°C and 175°C also the better matching between heat source and working fluid fails, being the curves almost parallel (Figure

48) and, as the mass flow rate circulating in the low pressure stage becomes negligible, the dual pressure ORC becomes effectively a single pressure ORC.

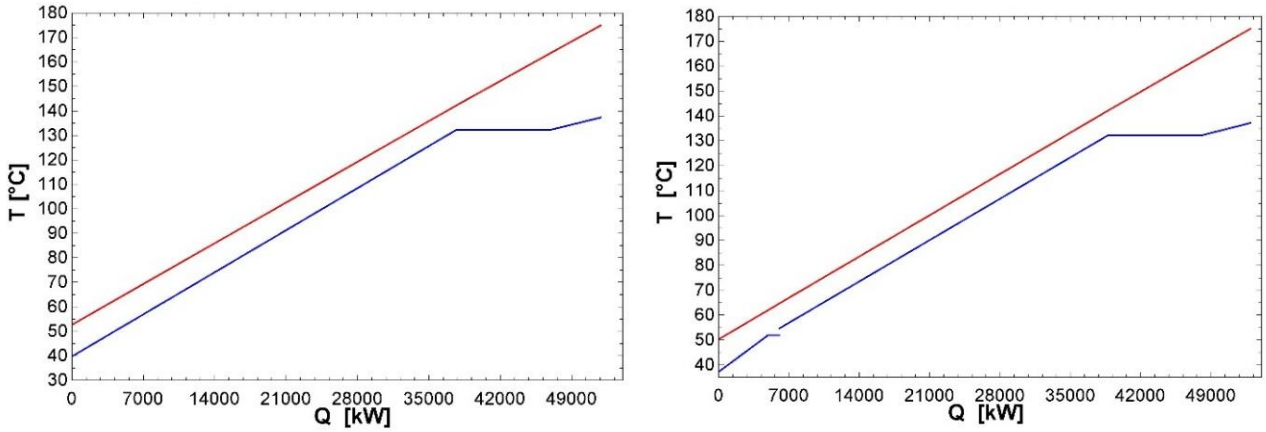

a) *b)*

Figure 48. Comparison between single stage a) and dual stages ORC b) when p_{max} is at the maximal allowed value in case of isobutane at $T_{in,HS}$=175°C.

It could be expected that the dual stage configuration could lead to an increase of W_{net} also at 150°C and 175°C when the basic ORC is operated at its optimum conditions. It is shown that there is an improvement using fluids with a higher critical temperature, nearer to the heat source inlet temperature, but none of them exceeds the performance of the best single pressure ORC at least using the fluids considered here.

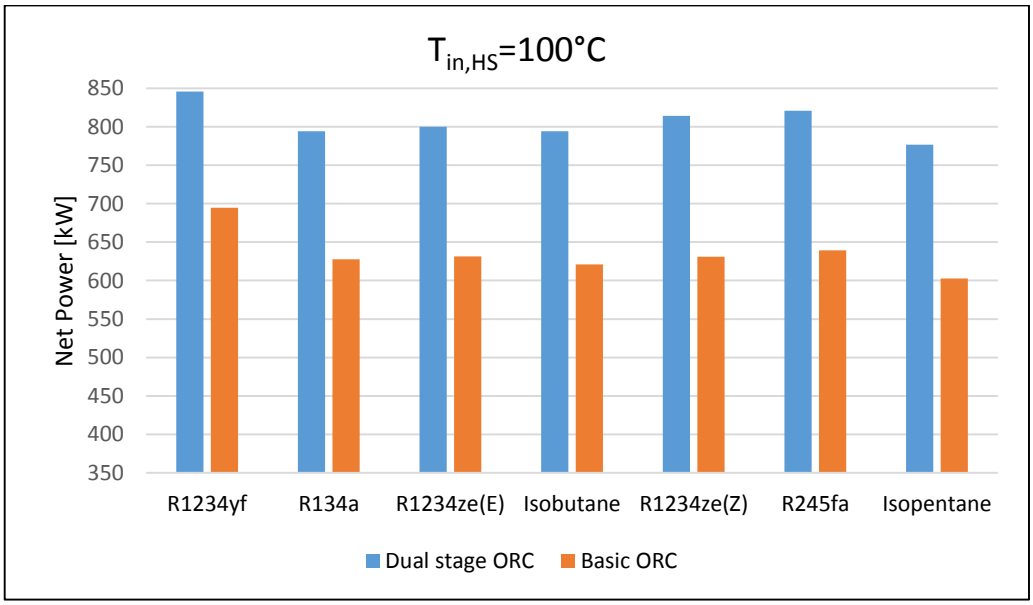

Figure 49. Comparison between basic and dual stage ORC with $T_{in,HS}$=100°C.

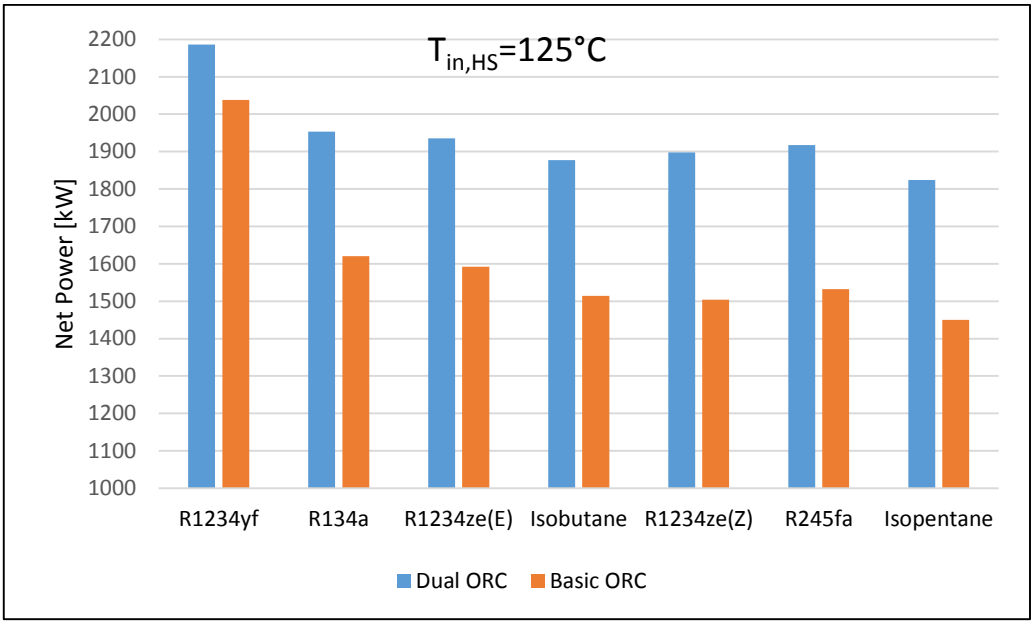

Figure 50. Comparison between basic and dual stage ORC with $T_{in,HS}$=125°C.

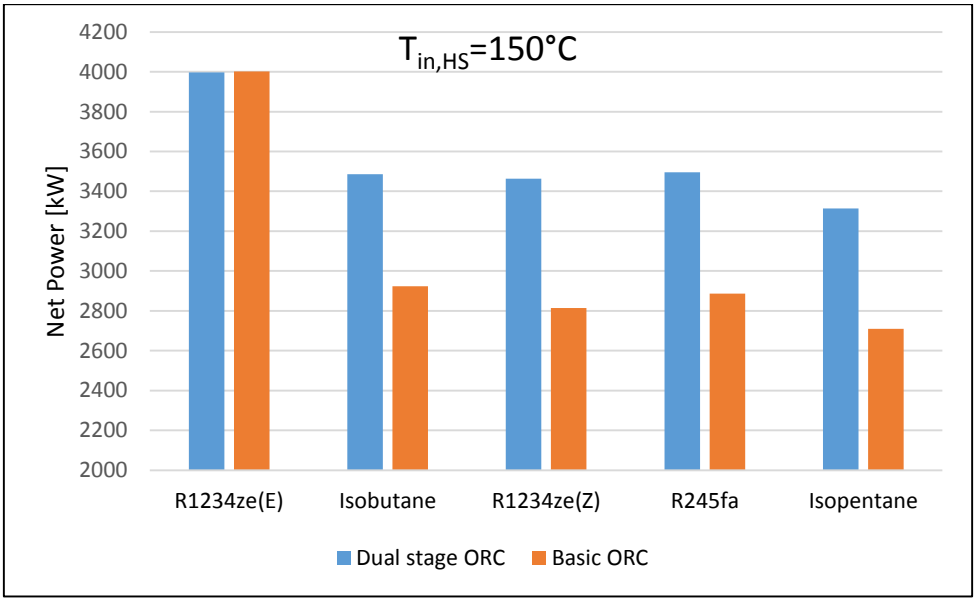

Figure 51. Comparison between basic and dual stage ORC with $T_{in,HS}$=150°C.

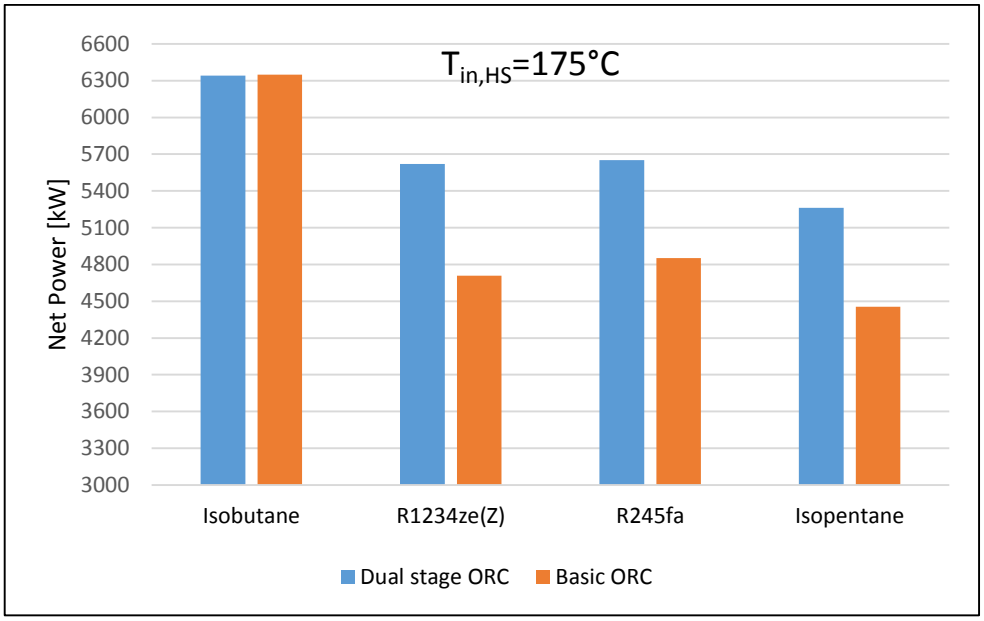

Figure 52. Comparison between basic and dual stage ORC with $T_{in,HS}$=175°C.

The situation changes when the heat source is the composition of different streams and thus the HCC is complex. In this case, the dual pressure configuration can adapt better the CCC to the HCC. With two evaporations, in fact, it is possible to move the "flat" stages with more flexibility, guaranteeing a better match of the curves.

In the analysis presented in Section 6.3, the HCC has, after all, still a quite regular profile. Both ORC system could recover the entire amount of available heat and the advantage of the dual pressure configuration was limited at a higher thermal efficiency. The benefits, however, are expected to increase with the complexity of the HCC.

In Figure 53 the difference in net power output between the two configurations is shown.

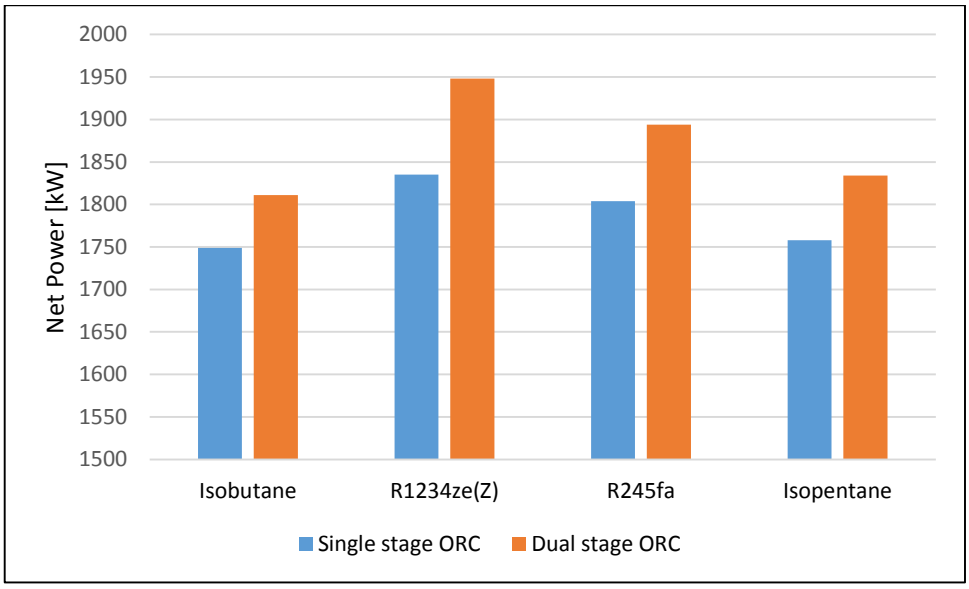

Figure 53. Comparison between single and dual stage ORC with multiple heat sources.

From this picture it can be seen, that R1234ze(Z) is the most performing working fluid with both configurations and hence the selection criteria presented for heat sources at constant heat capacity are not more valid. The performance markedly depends on the HCC profile and on the thermodynamic characteristics of each fluid.

8. CONCLUSIONS

In this work single and dual pressure ORCs are compared in the utilization of heat sources at constant heat capacity and at variable heat capacity. The performance is evaluated considering the net power output (W_{net}) and the ratio between the total heat transfer area and W_{net} (AR).

It is demonstrated that AR minimization does not lead to a considerable reduction of the capital costs, because the overall plant costs are not directly proportional to the total heat transfer area, but depend on a composition of different costs: purchased costs of equipment (with expanders having the highest relative costs), direct and indirect costs (labour and material needed for the installation, transportation costs, the engineering, etc.), contingency costs, fees, costs for site development and auxiliary facilities.

W_{net} maximization instead gives the optimum thermodynamic parameters to get the maximum profit from the ORC system operation.
For each type of heat source considered, the configuration, the fluid and the parameters that maximize the net power output are found.

Considering heat sources made of a unique geothermal flow, when $T_{in,HS}$=100°C the best fluid is R1234yf for both single and dual pressure configuration. The dual pressure configuration is advantageous because it leads to a 21% higher power output.
At $T_{in,HS}$=125°C the improvement in the performance using a dual pressure configuration with R1234yf is limited, because the maximum allowed subcritical pressure is already reached with the single pressure configuration, the dual pressure one can still improve the heat exchange approaching the cooling and the heating curve.
At $T_{in,HS}$=150°C the most performing fluid is R1234ze(E), but there is no improvement changing from single to dual pressure configuration. A similar result is found at $T_{in,HS}$=175°C with isobutane. At these temperature the maximum allowed subcritical pressure is reached and the single pressure configuration gives a higher η_{th} and only a slightly lower φ. In these situations the basic configuration can realize an optimum match between the thermal profiles.
At $T_{in,HS}$=200°C only isopentane is used. The maximum cycle pressure is far from the fluid critical temperature and the dual pressure configuration improves both φ and η_{th}, so that W_{net} results about 14% higher.
Summarizing the dual stage ORC improves the match between the geothermal water cooling curve and the working fluid heating/boiling curve. Therefore, the average temperature difference between the two fluids and in turn the irreversibilities are reduced, as shown by the increase of φ. This advantage is lost when the evaporation pressure is close to the critical pressure, because of the good match between the two curves that is also realized by the single pressure ORC. This happens when $T_{in,HS} - T_{cr} \cong 35°C$, as indicated in the literature.

Considering the heat source composed by multiple low temperature streams, the dual pressure ORC always achieves higher W_{net}, because the irreversibilities in the heat exchange are reduced, which results in a higher η_{th}. In the case analyzed, both configuration can recover the entire amount of heat (φ=1). It is expected that, with more complex HCC, the advantages of the dual stage cycle can increase, realizing a closer approach between HCC and CCC respect to the simple cycle.

To preliminary select the fluids, that show the higher increase in W_{net} passing from the single to the dual stage ORC, the mere consideration of the difference $T_{in,HS}$-T_{cr} is not sufficient as selection criteria and also the vaporization enthalpy has to be taken into account. From the results obtained, it can be concluded that the working fluids, which have:

$r > 200\ kJ/kg$

and

$-30° < T_{in,HS} - T_{cr} < +30°C$

have to be excluded.

So the ratio $\frac{r}{(T_{in,HS}-T_{cr})}$ has been proposed as indicator in the selection of the most suitable fluids for dual stage ORCs. Fluids which possess a small positive ratio seem to be advantaged.

When it is not possible to choose fluids having $T_{in,HS} - T_{cr}$>0, the fluids with the less negative ratio $\frac{r}{(T_{in,HS}-T_{cr})}$ perform better.

When the heat source is the composition of multiple streams, there is no general selection criterion, because the choice of the working fluid stongly depends on the HCC profile. In this case the dual pressure configuration leads always to a higher W_{net}.

Regarding the hydrofluoroolefins, results have shown that R1234yf, R1234ze(E) and R1234ze(Z) can replace R134a and R245fa because of the optimum environmental features and the high power generated, which is in line with the findings of Liu et al. [25].

Furthermore, the superheating is never advantageous (except for R134a and R1234ze(E) at the lowest heat source inlet temperature of 100°C in the dual pressure configuration). This is because of the additional cooling load at the condenser deriving from higher degrees of superheating at turbine outlet for dry or isentropic fluids, as also shown by Bao and Zhao [3] and Hung et al. [30].

APPENDIX A

In this section, the entire single pressure model built in EES environment is presented. In the following example R1234yf was used with 100°C brine inlet temperature, but the mathematical model is valid for all other fluids employed in this work. For a different heat source inlet temperature is sufficient to change the input variable T_in.

```
"Single pressure ORC with R1234yf"

"Input variables:"

"Brine conditions"
T_in=100
p_geo=5
m_geo=100
"The specific heat is evaluated at the mean temperature between T_in and T_out”
Tm=(T_in+T_out)/2
cp_geo=Cp(Water;T=Tm;x=0)

"Environmental conditions"
p_atm=1
T_amb=20

"decision variables: maximum cycle pressure, superheating degree;
 Independent variables: condensation pressure, temperature difference at the pinch and approach point,
components isentropic efficiencies"
{p_max=32,4}
p_cond=10
T_cond=T_sat(R1234yf;P=p_cond)
T_sat=T_sat(R1234yf;P=p_max)
Tpp=10 "ΔT pinch point"
Tap=10 " ΔT approach point"
{DeltaT_SH=5}
T_max=T_sat+DeltaT_SH
T_max_lim=T_in-Tap

"pump and turbine isentropic efficiencies"
eta_p=0,7
eta_t=0,85

"the optimization variables (p_max and DeltaT_SH) are commented in brackets"

"unknown: working fluids mass flow rate, net power"

"State 1: conditions at condenser outlet”
"a subcooling degree of 2°C is considered"
DeltaT_SR=2
T[1]=T_cond-DeltaT_SR
p[1]=p_cond
h[1]=Enthalpy(R1234yf;T=T[1];P=p_cond)
s[1]=Entropy(R1234yf;T=T[1];P=p_cond)
x[1]=Quality(R1234yf;T=T[1];h=h[1])

"State 2: feed pump"
h_id[2]=Enthalpy(R1234yf;s=s[1];P=p_max)
h[2]=h[1]+(h_id[2]-h[1])/eta_p
s[2]=Entropy(R1234yf;h=h[2];P=p_max)
```

```
x[2]=quality(R1234yf;P=p_max;h=h[2])
T[2]=Temperature(R1234yf;P=p_max;h=h[2])
p[2]=p_max

" State 3: preheating"
T_ev=T_sat(R1234yf;P=p_max)
T[3]=T_ev
"h[3]=Enthalpy(R1234yf;x=0;T=T[3])"
h[3]=Enthalpy(R1234yf;x=0;P=p_max)
x[3]=quality(R1234yf;T=T[3];h=h[3])
s[3]=Entropy(R1234yf;h=h[3];P=p_max)
p[3]=p_max

" State 4: evaporator outlet "
T[4]=T_sat
p[4]=p_max
h[4]=Enthalpy(R1234yf;T=T[4];x=1)
s[4]=Entropy(R1234yf;T=T[4];x=1)
x[4]=Quality(R1234yf;T=T[4];h=h[4])

" State 5: turbine inlet"
h[5]=Enthalpy(R1234yf;T=T_max;P=p_max)
s[5]=Entropy(R1234yf;T=T_max;P=p_max)
"s[5]=Entropy(R1234yf;T=T_max;h=h[5])"
T[5]=T_max
x[5]=quality(R1234yf;T=T[5];P=p_max)
p[5]=p_max

" State 6: turbine outlet"
"s_id[6]=s[3]"
h_id[6]=Enthalpy(R1234yf;s=s[5];P=p_cond)
h[6]=h[5]-eta_t*(h[5]-h_id[6])
T[6]=Temperature(R1234yf;P=p_cond;h=h[6])
x[6]=quality(R1234yf;h=h[6];P=p_cond)
s[6]=entropy(R1234yf;T=T[6];P=p_cond)
p[6]=p_cond

"Energy balance: heat transfer at evaporator + SH"
"m_geo*cp_geo*(T_in-Ta)=m_wf*(h[5]-h[3])"
Ta_lim=T_ev+Tpp
Ta=Ta_lim
Tm1=(Ta+T_in)/2
cp_geo1=Cp(Water;T=Tm1;P=p_geo)
m_wf=m_geo*cp_geo1*(T_in-Ta)/(h[5]-h[3])

“Energy balance: heat exchange at the preheater"
"m_geo*cp_geo*(Ta-T_out_real)=m_wf*(h[3]-h[2])"
cp_geo2=Cp(Water;T=72,5;P=p_geo) "first cp is calculated at T=Tm, after the first run cp is calculated at the mean temperature between Ta and T_out_real"
T_out_real=Ta-(m_wf*(h[3]-h[2])/(m_geo*cp_geo2))

"Air outlet temperature: setting of 5 K at the pinch point"
DeltaT_cond=5
T_air_out=T_cond-DeltaT_cond
T_air_m=(T_amb+T_air_out)/2
cp_air=Cp(Air_ha;T=T_air_m;P=p_atm)
m_air=m_wf*(h[6]-h[1])/(cp_air*(T_air_out-T_amb))

"Power absorbed at the condenser"
Qcond=m_wf*(h[6]-h[1])
"Qcond2=m_air*cp_air*(T_air_out-T_amb)"
```

```
f_c=0,01
Wcond=f_c*Qcond
Wcond2=0,15*m_air

"Energy balance"
Wt=m_wf*(h[5]-h[6])
Wp=m_wf*(h[2]-h[1])
Wnet=Wt-Wp-Wcond

T_control=T_out_real-T[2]

"Pressure ratio"
p_cr=P_crit(R1234yf)
p_rid=p_max/p_cr
r_ex=p_max/p_cond

"Heat available from the heat source"
"Qav=m_geo*cp_geo*(T_in-T_out)"
h_in=Enthalpy(Water;T=T_in;P=p_geo)
h_out=Enthalpy(Water;T=T_amb;P=p_geo)
Qav=m_geo*(h_in-h_out)

"Heat absorbed by the working fluid"
Qin=m_wf*(h[5]-h[2])

"Thermal efficiency"
eta_th=Wnet/Qin
"Heat recovery factor"
fi=Qin/Qav
"Total heat-recovery efficiency: eta_rec=fi*eta_th"
eta_rec=Wnet/Qav

"Graphical array"

s_plot[1]=s[1]
p_plot[1]=p[1]
T_plot[1]=T[1]
h_plot[1]=h[1]

s_plot[2]=s[2]
p_plot[2]=p[2]
T_plot[2]=T[2]
h_plot[2]=h[2]

T_plot[3]=Temperature(R1234yf;P=p_plot[3];x=0)
s_plot[3]=Entropy(R1234yf;P=p_plot[3];x=0)
h_plot[3]=Enthalpy(R1234yf;P=p_plot[3];x=0)
p_plot[3]=p_cond+(p_max-p_cond)*0,25

T_plot[4]=Temperature(R1234yf;P=p_plot[4];x=0)
s_plot[4]=Entropy(R1234yf;P=p_plot[4];x=0)
h_plot[4]=Enthalpy(R1234yf;P=p_plot[4];x=0)
p_plot[4]=p_cond+(p_max-p_cond)*0,5

T_plot[5]=Temperature(R1234yf;P=p_plot[5];x=0)
s_plot[5]=Entropy(R1234yf;P=p_plot[5];x=0)
h_plot[5]=Enthalpy(R1234yf;P=p_plot[5];x=0)
p_plot[5]=p_cond+(p_max-p_cond)*0,75

s_plot[6]=s[3]
p_plot[6]=p_max
```

```
T_plot[6]=T[3]
h_plot[6]=h[3]

T_plot[7]=T_sat
p_plot[7]=p_max
h_plot[7]=Enthalpy(R1234yf;T=T_plot[7];x=1)
s_plot[7]=Entropy(R1234yf;T=T_plot[7];x=1)

T_plot[8]=T_sat+(T_max-T_sat)*0,25
p_plot[8]=p_max
h_plot[8]=Enthalpy(R1234yf;T=T_plot[8];P=p_plot[8])
s_plot[8]=Entropy(R1234yf;h=h_plot[8];P=p_plot[8])

T_plot[9]=T_sat+(T_max-T_sat)*0,5
p_plot[9]=p_max
h_plot[9]=Enthalpy(R1234yf;T=T_plot[9];P=p_plot[9])
s_plot[9]=Entropy(R1234yf;h=h_plot[9];P=p_plot[9])

T_plot[10]=T_sat+(T_max-T_sat)*0,75
p_plot[10]=p_max
h_plot[10]=Enthalpy(R1234yf;T=T_plot[10];P=p_plot[10])
s_plot[10]=Entropy(R1234yf;h=h_plot[10];P=p_plot[10])

s_plot[11]=s[5]
p_plot[11]=p[5]
T_plot[11]=T[5]
h_plot[11]=h[5]

s_plot[12]=s[6]
p_plot[12]=p[6]
T_plot[12]=T[6]
h_plot[12]=h[6]

p_plot[13]=p_cond
T_plot[13]=T_cond
h_plot[13]=Enthalpy(R1234yf;x=1;P=p_plot[13])
s_plot[13]=Entropy(R1234yf;x=1;P=p_plot[13])

p_plot[14]=p_cond
T_plot[14]=T_cond
h_plot[14]=Enthalpy(R1234yf;x=0;P=p_plot[14])
s_plot[14]=Entropy(R1234yf;x=0;P=p_plot[14])

"Heat transfer area estimation"

"Superheater"
cp_geo_SH=Cp(Water;T=T_in;P=p_geo)
T_geo1=T_in-(m_wf*(h[5]-h_plot[7])/(m_geo*cp_geo_SH))
DeltaTml_SH=((T_geo1-T_plot[7])-(T_in-T[5]))/(ln((T_geo1-T_plot[7])/(T_in-T[5])))
Q_SH=m_wf*(h[5]-h_plot[7])
"Q_SH2=m_geo*cp_geo_SH*(T_in-T_geo1)"
U_SH=0,6
A_SH=Q_SH/(U_SH*DeltaTml_SH)
AU_SH=Q_SH/(DeltaTml_SH)

"Evaporator"
T_geo2=(T_geo1+Ta)/2
cp_geo_EV=Cp(Water;T=T_geo2;P=p_geo)
DeltaTml_EV=((T_geo1-T_sat)-(Ta-T_sat))/(ln((T_geo1-T_sat)/(Ta-T_sat)))
Q_EV=m_wf*(h_plot[7]-h_plot[6])
"Q_EV2=m_geo*cp_geo_EV*(T_geo1-Ta)"
```

```
U_EV=1
A_EV=Q_EV/(U_EV*DeltaTml_EV)
AU_EV=Q_EV/(DeltaTml_EV)

"Preheater"
T_geo3=(T_out_real+Ta)/2
cp_geo_PH=Cp(Water;T=T_geo3;P=p_geo)
DeltaTml_PH=((Ta-T_sat)-(T_out_real-T[2]))/(ln((Ta-T_sat)/(T_out_real-T[2])))
Q_PH=m_wf*(h_plot[6]-h[2])
"Q_PH2=m_geo*cp_geo_PH*(Ta-T_out_real)"
U_PH=0,75
A_PH=Q_PH/(U_PH*DeltaTml_PH)
AU_PH=Q_PH/(DeltaTml_PH)

"Condenser"

"1- Desuperheating"
cp_air_DS=Cp(Air_ha;T=T_air_out;P=p_atm)
T_air_DS=T_air_out-(m_wf*(h[6]-h_plot[13])/(m_air*cp_air_DS))
Q_DS=m_wf*(h[6]-h_plot[13])
"Q_DS2=m_air*cp_air_DS*(T_air_out-T_air_DS)"
DeltaTml_DS=((T[6]-T_air_out)-(T_plot[13]-T_air_DS))/(ln((T[6]-T_air_out)/(T_plot[13]-T_air_DS)))
AU_DS=Q_DS/DeltaTml_DS
U_DS=0,1
A_DS=Q_DS/(DeltaTml_DS*U_DS)

"2- Condensation"
T_cp=(T_air_DS+T_amb)/2
cp_air_cond=Cp(Air_ha;T=T_cp;P=p_atm)
T_air_SR=T_air_DS-(m_wf*(h_plot[13]-h_plot[14])/(m_air*cp_air_cond))
Q_cond=m_wf*(h_plot[13]-h_plot[14])
"Q_cond2=m_air*cp_air_cond*(T_air_DS-T_air_SR)"
DeltaTml_cond=((T_plot[14]-T_air_SR)-(T_plot[13]-T_air_DS))/(ln((T_plot[14]-T_air_SR)/(T_plot[13]-
T_air_DS)))
AU_cond=Q_cond/DeltaTml_cond
U_cond=0,85
A_cond=Q_cond/(DeltaTml_cond*U_cond)

"3- Subcooling"
cp_air_SR=Cp(Air_ha;T=T_amb;P=p_atm)
Q_SR=m_wf*(h_plot[14]-h[1])
"Q_SR2=m_air*cp_air_SR*(T_air_SR-T_amb)"
DeltaTml_SR=((T[1]-T_amb)-(T_plot[14]-T_air_SR))/(ln((T[1]-T_amb)/(T_plot[14]-T_air_SR)))
AU_SR=Q_SR/DeltaTml_SR
U_SR=0,85
A_SR=Q_SR/(DeltaTml_SR*U_SR)

A_tot=A_SH+A_EV+A_PH+A_DS+A_cond+A_SR

"Second optimization function (to be minimized)"
F_ob=A_tot/Wnet

"Plot T-Q"
Q[1]=0
Q[2]=Q_PH
Q[3]=Q[2]+Q_EV
Q[4]=Q[3]+Q_SH
T_geo[1]=T_out_real
T_geo[2]=Ta
T_geo[3]=T_geo1
T_geo[4]=T_in
```

T_wf[1]=T[2]
T_wf[2]=T_plot[6]
T_wf[3]=T_plot[7]
T_wf[4]=T[5]

Q_c[1]=0
Q_c[2]=Q_SR
Q_c[3]=Q_SR+Q_cond
Q_c[4]=Q_DS+Q_cond+Q_SR
T_c_wf[1]=T[1]
T_c_wf[2]=T_cond
T_c_wf[3]=T_cond
T_c_wf[4]=T[6]
T_c_air[1]=T_amb
T_c_air[2]=T_air_SR
T_c_air[3]=T_air_DS
T_c_air[4]=T_air_out

APPENDIX B

The complete dual pressure ORC model is reported below. The cycle refers to the "series configuration". In the example R1234ze(Z) was used with 100°C brine inlet temperature, but the model is valid for all other fluids employed in this work. For a different heat source inlet temperature is sufficient to change the input variable T_in.

"Dual pressure ORC with R1234ze(Z) in the series configuration"

"Input variables:"

"Brine conditions"
T_in=100
p_geo=5
m_geo=100

"Environmental conditions"
p_atm=1
T_amb=20

"decision variables: evaporation pressures, superheating degrees;
Independent variables: condensation pressure, temperature difference at the pinch and approach point, components isentropic efficiencies"

{p_HP=34
p_LP=4,3}
p_cond=2,8 "
T_cond=T_sat(R1234ze(Z);P=p_cond)
T_sat_HP=T_sat(R1234ze(Z);P=p_HP)
T_sat_LP=T_sat(R1234ze(Z);P=p_LP)
{DeltaT_SH_HP=5
DeltaT_SH_LP=0,01}
T_max=T_sat_HP+DeltaT_SH_HP
T_max_lim=T_in-Tap
Tpp=10 "Temperature difference at pinch point"
Tpp_LP=10
Tap=10 " Temperature difference at approach point"

"Pump and turbine isentropic efficiencies"
eta_p=0,7
eta_t=0,85

"Optimization variables (p_HP and p_LP, DeltaT_SH_HP, DeltaT_SH_LP) are commented in brackets"

"Unknown: HP and LP mass flow rate, power output"

"State 1: condenser outlet"
"Assumption: 1 is 2 K subcooled"
p[1]=p_cond
T[1]=T_cond-2 h[1]=Enthalpy(R1234ze(Z);T=T[1];P=p[1])
s[1]=Entropy(R1234ze(Z);T=T[1];P=p[1])
x[1]=Quality(R1234ze(Z);T=T[1];h=h[1])

"State 2: LP pump"
p[2]=p_LP
hid[2]=Enthalpy(R1234ze(Z);s=s[1];P=p_LP)
h[2]=h[1]+(hid[2]-h[1])/eta_p

```
s[2]=Entropy(R1234ze(Z);h=h[2];P=p[2])
x[2]=quality(R1234ze(Z);P=p[2];h=h[2])
T[2]=Temperature(R1234ze(Z);P=p[2];h=h[2])

"State 3: LP preheating, assuming 3 at the liquid saturated condition"
T[3]=T_sat_LP
p[3]=p_LP
h[3]=Enthalpy(R1234ze(Z);x=0;P=p_LP)
"h[3]=Enthalpy(R1234ze(Z);x=0;T=T[3]) "
x[3]=quality(R1234ze(Z);T=T[3];h=h[3])
s[3]=Entropy(R1234ze(Z);h=h[3];P=p[3])

"State 4: HP pump"
p[4]=p_HP
hid[4]=Enthalpy(R1234ze(Z);s=s[3];P=p_HP)
h[4]=h[3]+(hid[4]-h[3])/eta_p
s[4]=Entropy(R1234ze(Z);h=h[4];P=p_HP)
x[4]=quality(R1234ze(Z);P=p_HP;h=h[4])
T[4]=Temperature(R1234ze(Z);P=p_HP;h=h[4])

"State 5: HP turbine inlet"
p[5]=p_HP
h[5]=Enthalpy(R1234ze(Z);T=T_max;P=p_HP)
s[5]=Entropy(R1234ze(Z);T=T_max;P=p_HP)
"s[5]=Entropy(R1234ze(Z);T=T_max;h=h[5])"
T[5]=T_max
x[5]=quality(R1234ze(Z);T=T[5];P=p_HP)
h_sat[5]=Enthalpy(R1234ze(Z);T=T_sat_HP;x=0)
"h_sat[5]=Enthalpy(R1234ze(Z);P=p_HP;x=0)"

"State 6: HP turbine outlet"
p[6]=p_LP
hid[6]=enthalpy(R1234ze(Z);P=p_LP; s=s[5])
h[6]=h[5]-eta_t*(h[5]-hid[6])
T[6]=temperature(R1234ze(Z);P=p_LP; h=h[6])
s[6]=entropy(R1234ze(Z);P=p[6]; h=h[6])
x[6]=quality(R1234ze(Z);P=p[6]; h=h[6])

"State 7: LP evaporator outlet"
p[7]=p_LP
T[7]=T_sat_LP+DeltaT_SH_LP
h[7]=Enthalpy(R1234ze(Z);T=T[7];P=p_LP)
s[7]=Entropy(R1234ze(Z);T=T[7];P=p_LP)
"s[7]=Entropy(R1234ze(Z);T=T[7];h=h[7])"
x[7]=quality(R1234ze(Z);T=T[7];P=p_LP)
h_sat[7]=Enthalpy(R1234ze(Z);T=T_sat_LP;x=1)

"Energy balances"

"1- Balance at the HP evaporator"
"m_geo*cp_geo1*(T_in-Ta)=m_HP*(h[5]-h_sat[5])"
Ta=T_sat_HP+Tpp "fixing of the pinch point"
Tm1=(T_in+Ta)/2 "cp is evaluated at the brine mean temperature in the evaporator"
cp_geo1=Cp(Water;T=Tm1;P=p_geo)
m_HP=m_geo*cp_geo1*(T_in-Ta)/(h[5]-h_sat[5])

"2- Balance at the HP preheater"
"m_geo*cp_geo2*(Ta-Tb)=m_HP*(h_sat[5]-h[4])"
cp_geo2=Cp(Water;T=133;P=p_geo) "first cp was calculated at T=Ta, after the fist run cp was evaluated at
the mean temperature between Ta and Tb"
Tb=Ta-(m_HP*(h_sat[5]-h[4])/(m_geo*cp_geo2))
```

```
T_lim=Tb-T[7] "the pich point could be at the end of SH LP"
T_lim2=Tb-T[4] "the pinch point could be at the beginning of di EV HP"

"3- Balance at LP evaporator"
"m_geo*cp_geo3*(Tb-Tc)=m_LP*(h[7]-h[3])"
Tc=T_sat_LP+Tpp_LP
Tm3=(Tb+Tc)/2 "mean temperature for the evaluation of cp"
cp_geo3=Cp(Water;T=Tm3;P=p_geo)
m_LP=m_geo*cp_geo3*(Tb-Tc)/(h[7]-h[3])

"Mass balance"
m_wf=m_HP+m_LP

"4- Balance at the LP preheater"
"m_geo*cp_geo4*(Tc-T_out)=m_wf*(h[3]-h[2])"
"Tm4=(T_out+Tc)/2"
Tm4=Tc
cp_geo4=Cp(Water;T=Tc;P=p_geo)
Td=Tc-(m_wf*(h[3]-h[2])/(m_geo*cp_geo4))
"Temperature control at the preheater inlet, it has to be higher than Tpp"
T_control=Td-T[2]

"State 8: LP turbine inlet, resulting from the mixing between 6 and 7"
"Energy balance: m_wf*h[8]=m_HP*h[6]+m_LP*h[7]"
h[8]=(m_HP*h[6]+m_LP*h[7])/m_wf
p[8]=p_LP
T[8]=Temperature(R1234ze(Z);P=p_LP;h=h[8])
{s[8]=Entropy(R1234ze(Z);T=T[8];P=p_LP)}
s[8]=Entropy(R1234ze(Z);T=T[8];h=h[8])
x[8]=quality(R1234ze(Z);h=h[8];P=p_LP)

"State 9: LP turbine outlet"
p[9]=p_cond
hid[9]=enthalpy(R1234ze(Z);P=p_cond; s=s[8])
h[9]=h[8]-eta_t*(h[8]-hid[9])
T[9]=temperature(R1234ze(Z);P=p_cond; h=h[9])
s[9]=entropy(R1234ze(Z);P=p[9]; h=h[9])
x[9]=quality(R1234ze(Z);P=p[9]; h=h[9])

"Balance at the condenser, supposing an air cooling"
T_air_out=T_cond-5
T_air_m=(T_amb+T_air_out)/2
cp_air=Cp(Air_ha;T=T_air_m;P=p_atm)
m_air=m_wf*(h[9]-h[1])/(cp_air*(T_air_out-T_amb))

"Power absorbed at the condenser: 1kWel every100kWt removed"
f_c=0,01
Qcond=m_wf*(h[9]-h[1])
Wcond=f_c*Qcond
Wcond2=0,15*m_air

"Pump work"
Wp_LP=m_wf*(h[2]-h[1])
Wp_HP=m_HP*(h[4]-h[3])
Wp=m_wf*(h[2]-h[1])+m_HP*(h[4]-h[3])

"Turbine work"
Wt_HP=m_HP*(h[5]-h[6])
Wt_LP=m_wf*(h[8]-h[9])
Wt=m_HP*(h[5]-h[6])+m_wf*(h[8]-h[9])
```

"Net Power"
Wnet=Wt-Wp-Wcond

"Pressure ratio"
p_cr=P_crit(R1234ze(Z))
p_rid=p_HP/p_cr
r_exHP=p_HP/p_LP
r_exLP=p_LP/p_cond

"Efficiencies"

"Heat available from the heat source"
Tm=(T_in+T_out)/2
cp_geo=Cp(Water;T=Tm;P=p_geo)
"Qav2=m_geo*cp_geo*(T_in-T_out)"
h_in=Enthalpy(Water;T=T_in;P=p_geo)
h_out=Enthalpy(Water;T=T_amb;P=p_geo)
Qav=m_geo*(h_in-h_out)

"Heat absorbed by the working fluid"
Qin=m_wf*(h[3]-h[2])+m_LP*(h[7]-h[3])+m_HP*(h[5]-h[4])

"Thermal efficiency"
eta_th=Wnet/Qin
"Heat recovery factor"
fi=Qin/Qav
"Total heat recovery efficiency: eta_rec=fi*eta_th "
eta_rec=Wnet/Qav

"Graphical array"

s_plot[1]=s[1]
p_plot[1]=p[1]
T_plot[1]=T[1]
h_plot[1]=h[1]

s_plot[2]=s[2]
p_plot[2]=p[2]
T_plot[2]=T[2]
h_plot[2]=h[2]

T_plot[3]=T_cond+(T_sat_LP-T_cond)*0,25
s_plot[3]=Entropy(R1234ze(Z);T=T_plot[3];x=0)
h_plot[3]=Enthalpy(R1234ze(Z);T=T_plot[3];x=0)
p_plot[3]=Pressure(R1234ze(Z);T=T_plot[3];x=0)

T_plot[4]=T_cond+(T_sat_LP-T_cond)*0,5
s_plot[4]=Entropy(R1234ze(Z);T=T_plot[4];x=0)
h_plot[4]=Enthalpy(R1234ze(Z);T=T_plot[4];x=0)
p_plot[4]=Pressure(R1234ze(Z);T=T_plot[4];x=0)

T_plot[5]=T_cond+(T_sat_LP-T_cond)*0,75
s_plot[5]=Entropy(R1234ze(Z);T=T_plot[5];x=0)
h_plot[5]=Enthalpy(R1234ze(Z);T=T_plot[5];x=0)
p_plot[5]=Pressure(R1234ze(Z);T=T_plot[5];x=0)

s_plot[6]=s[3]
p_plot[6]=p[3]
T_plot[6]=T[3]
h_plot[6]=h[3]

```
s_plot[7]=s[4]
p_plot[7]=p[4]
T_plot[7]=T[4]
h_plot[7]=h[4]

T_plot[8]=T_sat_LP+(T_sat_HP-T_sat_LP)*0,25
s_plot[8]=Entropy(R1234ze(Z);T=T_plot[8];x=0)
h_plot[8]=Enthalpy(R1234ze(Z);T=T_plot[8];x=0)
p_plot[8]=Pressure(R1234ze(Z);T=T_plot[8];x=0)

T_plot[9]=T_sat_LP+(T_sat_HP-T_sat_LP)*0,5
s_plot[9]=Entropy(R1234ze(Z);T=T_plot[9];x=0)
h_plot[9]=Enthalpy(R1234ze(Z);T=T_plot[9];x=0)
p_plot[9]=Pressure(R1234ze(Z);T=T_plot[9];x=0)

T_plot[10]=T_sat_LP+(T_sat_HP-T_sat_LP)*0,75
s_plot[10]=Entropy(R1234ze(Z);T=T_plot[10];x=0)
h_plot[10]=Enthalpy(R1234ze(Z);T=T_plot[10];x=0)
p_plot[10]=Pressure(R1234ze(Z);T=T_plot[10];x=0)

p_plot[11]=p_HP
T_plot[11]=T_sat_HP
s_plot[11]=Entropy(R1234ze(Z);T=T_plot[11];x=0)
h_plot[11]=Enthalpy(R1234ze(Z);T=T_plot[11];x=0)

p_plot[12]=p_HP
T_plot[12]=T_sat_HP
s_plot[12]=Entropy(R1234ze(Z);T=T_plot[12];x=1)
h_plot[12]=Enthalpy(R1234ze(Z);T=T_plot[12];x=1)

p_plot[13]=p_HP
h_plot[13]=h_plot[12]+(h[5]-h_plot[12])*0,25
T_plot[13]=Temperature(R1234ze(Z);P=p_HP;h=h_plot[13])
s_plot[13]=Entropy(R1234ze(Z);h=h_plot[13];P=p_HP)

p_plot[14]=p_HP
h_plot[14]=h_plot[12]+(h[5]-h_plot[12])*0,5
T_plot[14]=Temperature(R1234ze(Z);P=p_HP;h=h_plot[14])
s_plot[14]=Entropy(R1234ze(Z);h=h_plot[14];P=p_HP)

p_plot[15]=p_HP
h_plot[15]=h_plot[12]+(h[5]-h_plot[12])*0,75
T_plot[15]=Temperature(R1234ze(Z);P=p_HP;h=h_plot[15])
s_plot[15]=Entropy(R1234ze(Z);h=h_plot[15];P=p_HP)

s_plot[16]=s[5]
p_plot[16]=p[5]
T_plot[16]=T[5]
h_plot[16]=h[5]

s_plot[17]=s[6]
p_plot[17]=p[6]
T_plot[17]=T[6]
h_plot[17]=h[6]

p_plot[18]=p_LP
T_plot[18]=T_sat_LP
h_plot[18]=h_sat[7]
s_plot[18]=Entropy(R1234ze(Z);h=h_plot[18];P=p_LP)

s_plot[19]=s[7]
```

```
p_plot[19]=p[7]
T_plot[19]=T[7]
h_plot[19]=h[7]

s_plot[20]=s[8]
p_plot[20]=p[8]
T_plot[20]=T[8]
h_plot[20]=h[8]

s_plot[21]=s[9]
p_plot[21]=p[9]
T_plot[21]=T[9]
h_plot[21]=h[9]

p_plot[22]=p_cond
h_plot[22]=Enthalpy(R1234ze(Z);x=1;P=p_cond)
T_plot[22]=Temperature(R1234ze(Z);P=p_cond;h=h_plot[22])
s_plot[22]=Entropy(R1234ze(Z);h=h_plot[22];P=p_cond)

p_plot[23]=p_cond
h_plot[23]=Enthalpy(R1234ze(Z);x=0;P=p_cond)
T_plot[23]=Temperature(R1234ze(Z);P=p_cond;h=h_plot[23])
s_plot[23]=Entropy(R1234ze(Z);h=h_plot[23];P=p_cond)


"Evaluation of the heat transfer area"

"HP superheater"
cp_geo_SH_HP=Cp(Water;T=T_in;P=p_geo)
T_geo1=T_in-(m_HP*(h[5]-h_plot[12])/(m_geo*cp_geo_SH_HP))
DeltaTml_SH_HP=((T_geo1-T_plot[12])-(T_in-T[5]))/(ln((T_geo1-T_plot[12])/(T_in-T[5])))
Q_SH_HP=m_HP*(h[5]-h_plot[12])
"Q_SH_HP2=m_geo*cp_geo_SH_HP*(T_in-T_geo1)"
U_SH_HP=0,6
A_SH_HP=Q_SH_HP/(U_SH_HP*DeltaTml_SH_HP)
AU_SH_HP=Q_SH_HP/(DeltaTml_SH_HP)

"HP evaporator"
T_geo2=(T_geo1+Ta)/2
cp_geo_EV_HP=Cp(Water;T=T_geo2;P=p_geo)
DeltaTml_EV_HP=((T_geo1-T_sat_HP)-(Ta-T_sat_HP))/(ln((T_geo1-T_sat_HP)/(Ta-T_sat_HP)))
Q_EV_HP=m_HP*(h_plot[12]-h_plot[11])
Q_EV_HP2=m_geo*cp_geo_EV_HP*(T_geo1-Ta)
U_EV_HP=1
A_EV_HP=Q_EV_HP/(U_EV_HP*DeltaTml_EV_HP)
AU_EV_HP=Q_EV_HP/(DeltaTml_EV_HP)

"HP preheater"
T_geo3=(Tb+Ta)/2
cp_geo_PH_HP=Cp(Water;T=T_geo3;P=p_geo)
DeltaTml_PH_HP=((Ta-T_sat_HP)-(Tb-T[4]))/(ln((Ta-T_sat_HP)/(Tb-T[4])))
Q_PH_HP=m_HP*(h_plot[11]-h[4])
"Q_PH_HP2=m_geo*cp_geo_PH_HP*(Ta-Tb)"
U_PH_HP=0,75
A_PH_HP=Q_PH_HP/(U_PH_HP*DeltaTml_PH_HP)
AU_PH_HP=Q_PH_HP/(DeltaTml_PH_HP)

"LP superheater"
cp_geo_SH_LP=Cp(Water;T=Tb;P=p_geo)
T_geo4=Tb-(m_LP*(h[7]-h_plot[18])/(m_geo*cp_geo_SH_LP))
DeltaTml_SH_LP=((T_geo4-T_plot[18])-(Tb-T[7]))/(ln((T_geo4-T_plot[18])/(Tb-T[7])))
```

```
Q_SH_LP=m_LP*(h[7]-h_plot[18])
"Q_SH_LP2=m_geo*cp_geo_SH_LP*(Tb-T_geo4)"
U_SH_LP=0,6
A_SH_LP=Q_SH_LP/(U_SH_LP*DeltaTml_SH_LP)
AU_SH_LP=Q_SH_LP/(DeltaTml_SH_LP)

"LP evaporator"
T_geo5=(T_geo4+Tc)/2
cp_geo_EV_LP=Cp(Water;T=T_geo5;P=p_geo)
DeltaTml_EV_LP=((T_geo4-T_sat_LP)-(Tc-T_sat_LP))/(ln((T_geo4-T_sat_LP)/(Tc-T_sat_LP)))
Q_EV_LP=m_LP*(h_plot[18]-h_plot[6])
Q_EV_LP2=m_geo*cp_geo_EV_LP*(T_geo4-Tc)
U_EV_LP=1
A_EV_LP=Q_EV_LP/(U_EV_LP*DeltaTml_EV_LP)
AU_EV_LP=Q_EV_LP/(DeltaTml_EV_LP)

"LP preheater"
T_geo6=(Tc+Td)/2
cp_geo_PH_LP=Cp(Water;T=T_geo6;P=p_geo)
DeltaTml_PH_LP=((Tc-T[3])-(Td-T[2]))/(ln((Tc-T[3])/(Td-T[2])))
Q_PH_LP=m_wf*(h[3]-h[2])
"Q_PH_LP2=m_geo*cp_geo_PH_LP*(Tc-Td)"
U_PH_LP=0,75
A_PH_LP=Q_PH_LP/(U_PH_LP*DeltaTml_PH_LP)
AU_PH_LP=Q_PH_LP/(DeltaTml_PH_LP)

"Condenser"

"1- Desuperheating"
cp_air_DS=Cp(Air_ha;T=T_air_out;P=p_atm)
T_air_DS=T_air_out-(m_wf*(h[9]-h_plot[22])/(m_air*cp_air_DS))
Q_DS=m_wf*(h[9]-h_plot[22])
"Q_DS2=m_air*cp_air_DS*(T_air_out-T_air_DS)"
DeltaTml_DS=((T[9]-T_air_out)-(T_plot[22]-T_air_DS))/(ln((T[9]-T_air_out)/(T_plot[22]-T_air_DS)))
AU_DS=Q_DS/DeltaTml_DS
U_DS=0,1
A_DS=Q_DS/(DeltaTml_DS*U_DS)

"2- Condensation"
T_cp=(T_air_DS+T_amb)/2
cp_air_cond=Cp(Air_ha;T=T_cp;P=p_atm)
T_air_SR=T_air_DS-(m_wf*(h_plot[22]-h_plot[23])/(m_air*cp_air_cond))
Q_cond=m_wf*(h_plot[22]-h_plot[23])
"Q_cond2=m_air*cp_air_cond*(T_air_DS-T_air_SR)"
DeltaTml_cond=((T_plot[23]-T_air_SR)-(T_plot[22]-T_air_DS))/(ln((T_plot[23]-T_air_SR)/(T_plot[22]-
T_air_DS)))
AU_cond=Q_cond/DeltaTml_cond
U_cond=0,85
A_cond=Q_cond/(DeltaTml_cond*U_cond)

"3- Subcooling"
cp_air_SR=Cp(Air_ha;T=T_amb;P=p_atm)
Q_SR=m_wf*(h_plot[23]-h[1])
"Q_SR2=m_air*cp_air_SR*(T_air_SR-T_amb)"
DeltaTml_SR=((T[1]-T_amb)-(T_plot[23]-T_air_SR))/(ln((T[1]-T_amb)/(T_plot[23]-T_air_SR)))
AU_SR=Q_SR/DeltaTml_SR
U_SR=0,85
A_SR=Q_SR/(DeltaTml_SR*U_SR)

A_tot=A_SH_HP+A_EV_HP+A_PH_HP+A_SH_LP+A_EV_LP+A_PH_LP+A_cond+A_SR+A_DS
```

"Second optimization function to be minimized"
F_ob=A_tot/Wnet

"T-Q diagram"
Q_geo[1]=0
Q_geo[2]=Q_PH_LP
Q_geo[3]=Q_geo[2]+Q_EV_LP
Q_geo[4]=Q_geo[3]+Q_SH_LP
Q_geo[5]=Q_geo[4]+Q_PH_HP
Q_geo[6]=Q_geo[5]+Q_EV_HP
Q_geo[7]=Q_geo[6]+Q_SH_HP
T_geo[1]=Td
T_geo[2]=Tc
T_geo[3]=T_geo4
T_geo[4]=Tb
T_geo[5]=Ta
T_geo[6]=T_geo1
T_geo[7]=T_in

T_HP[1]=T[4]
T_HP[2]=T_plot[11]
T_HP[3]=T_plot[12]
T_HP[4]=T[5]
Q_HP[1]=Q_geo[4]
Q_HP[2]=Q_geo[5]
Q_HP[3]=Q_geo[6]
Q_HP[4]=Q_geo[7]

T_LP[1]=T[2]
T_LP[2]=T[3]
T_LP[3]=T_plot[18]
T_LP[4]=T[7]
Q_LP[1]=Q_geo[1]
Q_LP[2]=Q_geo[2]
Q_LP[3]=Q_geo[3]
Q_LP[4]=Q_geo[4]

APPENDIX C

When the heat source is made of three different streams, the following single pressure model, built in EES environment according to the pinch analysis, is used. In the example here presented, R245fa is used, but the mathematical model is valid for all other fluids employed with the composite heat source.

```
PROCEDURE TEMP (T_hot[1];T_hot[2];T_cold[4]:T_in_pt1;T_out_pt1;T_in_pt2;T_out_pt2;T_in_pt3)
IF T_hot[2]>T_cold[4] THEN
T_in_pt1=T_hot[1]
T_out_pt1=T_hot[2]
T_in_pt2=T_hot[2]
T_out_pt2=T_cold[4]
T_in_pt3=T_cold[4]

ELSE
T_in_pt1=T_hot[1]
T_out_pt1=T_cold[4]
T_in_pt2=T_cold[4]
T_out_pt2=T_hot[2]
T_in_pt3=T_hot[2]
ENDIF
END

"Composite heat source"
p_geo=10
m_geo1=50
m_geo2=30
m_geo3=20
T_in1=150
T_in2=130
T_in3=130
T_out1=110
T_out2=90
T_out3=100

“Setting of DeltaTmin”
DeltaTmin=10

"Building of HCC"
T_in[1]=T_in1-DeltaTmin
T_out[1]=T_in2-DeltaTmin
T_in[2]=T_out[1]
T_out[2]=T_out1-DeltaTmin
T_in[3]=T_out[2]
T_out[3]=T_out3-DeltaTmin
T_in[4]=T_out[3]
T_out[4]=T_out2-DeltaTmin
m_geo[1]=m_geo1
m_geo[2]=m_geo1+m_geo2+m_geo3
m_geo[3]=m_geo2+m_geo3
m_geo[4]=m_geo2
T_m1=(T_in1+T_in2)/2
cp1=Cp(Water;T=T_m1;P=p_geo)
T_m2=(T_in2+T_out1)/2
cp2=Cp(Water;T=T_m2;P=p_geo)
T_m3=(T_out1+T_out3)/2
```

```
cp3=Cp(Water;T=T_m3;P=p_geo)
T_m4=(T_out3+T_out2)/2
cp4=Cp(Water;T=T_m4;P=p_geo)
C[1]=m_geo[1]*cp1
C[2]=m_geo[2]*cp2
C[3]=m_geo[3]*cp3
C[4]=m_geo[4]*cp4
Q[1]=C[1]*(T_in[1]-T_out[1])
Q[2]=C[2]*(T_in[2]-T_out[2])
Q[3]=C[3]*(T_in[3]-T_out[3])
Q[4]=C[4]*(T_in[4]-T_out[4])
H_geo[4]=Q[4]
H_geo[3]=Q[3]+Q[4]
H_geo[2]=Q[2]+Q[3]+Q[4]
H_geo[1]=Q[1]+Q[2]+Q[3]+Q[4]
Q_geo_tot=Q[1]+Q[2]+Q[3]+Q[4]

"Plot"
H_plot[5]=0
H_plot[4]=H_geo[4]
H_plot[3]=H_geo[3]
H_plot[2]=H_geo[2]
H_plot[1]=H_geo[1]
T_hot[1]=T_in[1] + DeltaTmin
T_hot[2]=T_in[2] + DeltaTmin
T_hot[3]=T_in[3] + DeltaTmin
T_hot[4]=T_in[4] + DeltaTmin
T_hot[5]=T_out[4] + DeltaTmin

"Simple ORC thermodynamic cycle;
fixed variables: pump and turbine efficiencies, condensation pressure
decision variable: evaporation pressure, superheating degree"
eta_p=0,7
eta_t=0,85
{p_max=15,07}
p_cond=2,4
T_cond=T_sat(R245fa;P=p_cond)
T_sat=T_sat(R245fa;P=p_max)
{DeltaT_SH=5}
T_max=T_sat+DeltaT_SH
T_max_lim=T_in1-DeltaTmin

"State 1: condenser outlet”
T[1]=T_cond-2
p[1]=p_cond
h[1]=Enthalpy(R245fa;T=T[1];P=p[1])
s[1]=Entropy(R245fa;T=T[1];P=p_cond)
x[1]=Quality(R245fa;T=T[1];h=h[1])

"State 2: feed pump"
h_id2=Enthalpy(R245fa;s=s[1];P=p_max)
h[2]=h[1]+(h_id2-h[1])/eta_p
s[2]=Entropy(R245fa;h=h[2];P=p_max)
x[2]=quality(R245fa;P=p_max;h=h[2])
T[2]=Temperature(R245fa;P=p_max;h=h[2])
p[2]=p_max

"State 3: preheating"
T_ev=T_sat(R245fa;P=p_max)
T[3]=T_ev
"h[3]=Enthalpy(R245fa;x=0;T=T[3])"
```

```
h[3]=Enthalpy(R245fa;x=0;P=p_max)
x[3]=quality(R245fa;T=T[3];h=h[3])
s[3]=Entropy(R245fa;h=h[3];P=p_max)
p[3]=p_max

"State 4: evaporator outlet"
T[4]=T_sat
p[4]=p_max
h[4]=Enthalpy(R245fa;T=T[4];x=1)
s[4]=Entropy(R245fa;T=T[4];x=1)
x[4]=1

"State 5: turbine inlet"
h[5]=Enthalpy(R245fa;T=T_max;P=p_max)
s[5]=Entropy(R245fa;T=T_max;P=p_max)
"s[5]=Entropy(R245fa;T=T_max;h=h[5])"
T[5]=T_max
x[5]=quality(R245fa;T=T[5];P=p_max)
p[5]=p_max

"State 6: turbine outlet"
"s_id[6]=s[5]"
h_id6=Enthalpy(R245fa;s=s[5];P=p_cond)
h[6]=h[5]-eta_t*(h[5]-h_id6)
T[6]=Temperature(R245fa;P=p_cond;h=h[6])
x[6]=quality(R245fa;h=h[6];P=p_cond)
s[6]=entropy(R245fa;T=T[6];P=p_cond)
p[6]=p_cond

"Specific work"
Ws_t=(h[5]-h[6])
Ws_p=(h[2]-h[1])
Ws_net=Ws_t-Ws_p

"There is a limit to the working fluid mass flow rate, given by the available heat, m_wf is optimized within this
limit”
m_wf_lim=H_geo[1]/(h[5]-h[2])
{m_wf=m_wf_lim}

"Bulding of CCC"
Tin_wf[1]=T[2]
Tout_wf[1]=T[3]
Tin_wf[2]=Tout_wf[1]
Tout_wf[2]=Tin_wf[2]+0,1
Tin_wf[3]=Tout_wf[2]
Tout_wf[3]=T[5]

Q_wf[1]=m_wf*(h[3]-h[2])
Q_wf[2]=m_wf*(h[4]-h[3])
Q_wf[3]=m_wf*(h[5]-h[4])
Q_wf_tot=Q_wf[1]+Q_wf[2]+Q_wf[3]

"Plot"
H_wf[1]=0
H_wf[2]=Q_wf[1]
H_wf[3]=Q_wf[1]+Q_wf[2]
H_wf[4]=Q_wf[1]+Q_wf[2]+Q_wf[3]
T_cold[1]=Tin_wf[1]
T_cold[2]=Tout_wf[1]
T_cold[3]=Tout_wf[2]
T_cold[4]=Tout_wf[3]
```

"Condensator power"
Qcond=m_wf*(h[6]-h[1])
f_c=0,01
Wcond=f_c*Qcond

"Enegy balances"
Wt=m_wf*(h[5]-h[6])
Wp=m_wf*(h[2]-h[1])
Wnet=Wt-Wp-Wcond

"Heat available from the heat source"
Qav=H_geo[1]
"Heat absorbed by the working fluid"
Qin=m_wf*(h[5]-h[2])

"Thermal efficiency"
eta_th=Wnet/Qin
"Heat recovery factor"
fi=Qin/Qav
"Total heat recovery efficiency: eta_rsys=fi*eta_th (è il parametro da massimizzare)"
eta_sys=Wnet/Qav

CALL TEMP (T_hot[1];T_hot[2];T_cold[4]:T_in_pt1;T_out_pt1;T_in_pt2;T_out_pt2;T_in_pt3)

{T_hot[1]=145
T_cold[4]=118,7
T_hot[2]=125}

"Building of the Problem Table"
T_in_pt[1]=T_in_pt1
T_out_pt[1]=T_out_pt1
T_in_pt[2]=T_in_pt2
T_out_pt[2]=T_out_pt2
T_in_pt[3]=T_in_pt3
T_out_pt[3]=T_cold[3]
T_in_pt[4]=T_cold[3]
T_out_pt[4]=T_cold[2]
T_in_pt[5]=T_cold[2]
T_out_pt[5]=T_hot[3]
T_in_pt[6]=T_hot[3]
T_out_pt[6]=T_hot[4]
T_in_pt[7]=T_hot[4]
T_out_pt[7]=T_hot[5]
T_in_pt[8]=T_hot[5]
T_out_pt[8]=T_cold[1]

"Building of the Grand Composite Curve"
h_geo_pt[1]=Enthalpy(Water;T=T_in_pt[1];P=p_geo)
h_geo_pt[2]=Enthalpy(Water;T=T_out_pt[1];P=p_geo)
h_geo_pt[3]=Enthalpy(Water;T=T_out_pt[2];P=p_geo)
h_geo_pt[4]=Enthalpy(Water;T=T_out_pt[3];P=p_geo)
h_geo_pt[5]=Enthalpy(Water;T=T_out_pt[4];P=p_geo)
h_geo_pt[6]=Enthalpy(Water;T=T_out_pt[5];P=p_geo)
h_geo_pt[7]=Enthalpy(Water;T=T_out_pt[6];P=p_geo)
h_geo_pt[8]=Enthalpy(Water;T=T_out_pt[7];P=p_geo)

h_wf_pt[1]=Enthalpy(R245fa;T=T_in_pt[3];P=p_max)
h_wf_pt[2]=Enthalpy(R245fa;T=T_out_pt[3];P=p_max)
h_wf_pt[3]=Enthalpy(R245fa;T=T_in_pt[6];P=p_max)
h_wf_pt[4]=Enthalpy(R245fa;T=T_out_pt[6];P=p_max)

```
h_wf_pt[5]=Enthalpy(R245fa;T=T_out_pt[7];P=p_max)
h_wf_pt[6]=Enthalpy(R245fa;T=T_out_pt[8];P=p_max)

H_pt[1]=m_geo[1]*(h_geo_pt[1]-h_geo_pt[2])
H_pt[2]=m_geo[2]*(h_geo_pt[2]-h_geo_pt[3])
H_pt[3]=m_geo[2]*(h_geo_pt[3]-h_geo_pt[4])-m_wf*(h_wf_pt[1]-h_wf_pt[2])
H_pt[4]=m_geo[2]*(h_geo_pt[4]-h_geo_pt[5])-m_wf*(h[4]-h[3])
H_pt[5]=m_geo[2]*(h_geo_pt[5]-h_geo_pt[6])-m_wf*(h[3]-h_wf_pt[3])
H_pt[6]=m_geo[3]*(h_geo_pt[6]-h_geo_pt[7])-m_wf*(h_wf_pt[3]-h_wf_pt[4])
H_pt[7]=m_geo[4]*(h_geo_pt[7]-h_geo_pt[8])-m_wf*(h_wf_pt[4]-h_wf_pt[5])
H_pt[8]=-m_wf*(h_wf_pt[5]-h_wf_pt[6])

"Cumulative heat load"
Q_pt[1]=H_pt[1]
Q_pt[2]=Q_pt[1]+H_pt[2]
Q_pt[3]=Q_pt[2]+H_pt[3]
Q_pt[4]=Q_pt[3]+H_pt[4]
Q_pt[5]=Q_pt[4]+H_pt[5]
Q_pt[6]=Q_pt[5]+H_pt[6]
Q_pt[7]=Q_pt[6]+H_pt[7]
Q_pt[8]=Q_pt[7]+H_pt[8]

"GCC drawing"
T_GCC[1]=T_in_pt[1]
T_GCC[2]=T_in_pt[2]
T_GCC[3]=T_in_pt[3]
T_GCC[4]=T_in_pt[4]
T_GCC[5]=T_in_pt[5]
T_GCC[6]=T_in_pt[6]
T_GCC[7]=T_in_pt[7]
T_GCC[8]=T_in_pt[8]
T_GCC[9]=T_out_pt[8]
Q_GCC[1]=0
Q_GCC[2]=Q_pt[1]
Q_GCC[3]=Q_pt[2]
Q_GCC[4]=Q_pt[3]
Q_GCC[5]=Q_pt[4]
Q_GCC[6]=Q_pt[5]
Q_GCC[7]=Q_pt[6]
Q_GCC[8]=Q_pt[7]
Q_GCC[9]=Q_pt[8]
```

APPENDIX D

The following model refers to the multiple heat source. It is written in EES environment applying the pinch analysis procedure for the optimization of a dual stage ORC using R1234ze(Z). The model is valid also for the other fluids, it is sufficient to substitute the fluid's name.

```
"Dual pressure ORC with R1234ze(Z)"

{PROCEDURE TEMP (T_w[2];T_w[3];m_geo[1];m_geo[2];h_w[1];h_w[2];h[7];h[5]:mHP)
IF T_w[3]<T_w[2] THEN
mHP=(m_geo[1]*(h_w[1]-h_w[2])+m_geo[2]*(h_w[2]-h_w[3]))/(h[7]-h[5])
ELSE
mHP=(m_geo[1]*(h_w[1]-h_w[3]))/(h[7]-h[5])
ENDIF
END}

"Heat source with variable heat capacities"
p_geo=10
m_geo1=50
m_geo2=30
m_geo3=20
T_in1=150
T_in2=130
T_in3=130
T_out1=110
T_out2=90
T_out3=100

“Setting of DeltaTmin”
DeltaTmin=10

h_w[1]=Enthalpy(Water;T=T_in1;P=p_geo)
h_w[2]=Enthalpy(Water;T=T_in2;P=p_geo)
h_w[4]=Enthalpy(Water;T=T_out1;P=p_geo)
h_w[5]=Enthalpy(Water;T=T_out3;P=p_geo)
h_w[6]=Enthalpy(Water;T=T_out2;P=p_geo)
T_w[1]=T_in1
T_w[2]=T_in2
T_w[4]=T_out1
T_w[5]=T_out3
T_w[6]=T_out2

"Building of HCC"
T_in[1]=T_in1-DeltaTmin
T_out[1]=T_in2-DeltaTmin
T_in[2]=T_out[1]
T_out[2]=T_out1-DeltaTmin
T_in[3]=T_out[2]
T_out[3]=T_out3-DeltaTmin
T_in[4]=T_out[3]
T_out[4]=T_out2-DeltaTmin
m_geo[1]=m_geo1
m_geo[2]=m_geo1+m_geo2+m_geo3
m_geo[3]=m_geo2+m_geo3
m_geo[4]=m_geo2
T_m1=(T_in1+T_in2)/2
cp1=Cp(Water;T=T_m1;P=p_geo)
T_m2=(T_in2+T_out1)/2
```

```
cp2=Cp(Water;T=T_m2;P=p_geo)
T_m3=(T_out1+T_out3)/2
cp3=Cp(Water;T=T_m3;P=p_geo)
T_m4=(T_out3+T_out2)/2
cp4=Cp(Water;T=T_m4;P=p_geo)
C1=m_geo[1]*cp1
C2=m_geo[2]*cp2
C3=m_geo[3]*cp3
C4=m_geo[4]*cp4
Q[1]=m_geo[1]*(h_w[1]-h_w[2])
Q[2]=m_geo[2]*(h_w[2]-h_w[4])
Q[3]=m_geo[3]*(h_w[4]-h_w[5])
Q[4]=m_geo[4]*(h_w[5]-h_w[6])
H_geo[4]=Q[4]
H_geo[3]=Q[3]+Q[4]
H_geo[2]=Q[2]+Q[3]+Q[4]
H_geo[1]=Q[1]+Q[2]+Q[3]+Q[4]
Q_geo_tot=Q[1]+Q[2]+Q[3]+Q[4]

"Plot"
H_plot[5]=0
H_plot[4]=H_geo[4]
H_plot[3]=H_geo[3]
H_plot[2]=H_geo[2]
H_plot[1]=H_geo[1]
T_hot[1]=T_in[1]
T_hot[2]=T_in[2]
T_hot[3]=T_in[3]
T_hot[4]=T_in[4]
T_hot[5]=T_out[4]

"Building of the thermodynamic cycle with two pressure levels; fixed variables: pump and turbine efficiencies,
condensation T and p, pinch point and approach point temperature differences”
eta_p=0,7
eta_t=0,85

"Decision variables: evaporation pressure p_HP, p_LP, superheating degrees, m_HP/m_wf”
{p_HP=19,32
p_LP=15,56}
p_cond=2,8
T_cond=T_sat(R1234ze(Z);P=p_cond)
T_sat_HP=T_sat(R1234ze(Z);P=p_HP)
T_sat_LP=T_sat(R1234ze(Z);P=p_LP)
{DeltaT_SH_HP=5
DeltaT_SH_LP=0,01}
T_max=T_sat_HP+DeltaT_SH_HP
T_max_lim=T_in1-Tap
Tpp=10 " Delta T pinch point"
Tpp_LP=10
Tap=10 "Delta T approach point"

"Variable to be optimized: Wnet"
"Unknowns: HP and LP mass flow rates, net power output"

"Building of the thermodynamic cycle"

"State 1: condenser outlet"
"1 is in the subcooled conditions"
p[1]=p_cond
T[1]=T_cond-2 "subcooling 2°C"
h[1]=Enthalpy(R1234ze(Z);T=T[1];P=p[1])
```

```
s[1]=Entropy(R1234ze(Z);T=T[1];P=p[1])
x[1]=Quality(R1234ze(Z);T=T[1];h=h[1])

"State 2: LP pump outlet"
p[2]=p_LP
hid2=Enthalpy(R1234ze(Z);s=s[1];P=p_LP)
h[2]=h[1]+(hid2-h[1])/eta_p
s[2]=Entropy(R1234ze(Z);h=h[2];P=p[2])
x[2]=quality(R1234ze(Z);P=p[2];h=h[2])
T[2]=Temperature(R1234ze(Z);P=p[2];h=h[2])

"State 3: LP preheating, assuming 3 in the saturated liquid condition"
T[3]=T_sat_LP
p[3]=p_LP
h[3]=Enthalpy(R1234ze(Z);x=0;P=p_LP)
"h[3]=Enthalpy(R1234ze(Z);x=0;T=T[3]) "
x[3]=quality(R1234ze(Z);T=T[3];h=h[3])
s[3]=Entropy(R1234ze(Z);h=h[3];P=p[3])

"State 4: HP pump outlet"
p[4]=p_HP
hid4=Enthalpy(R1234ze(Z);s=s[3];P=p_HP)
h[4]=h[3]+(hid4-h[3])/eta_p
s[4]=Entropy(R1234ze(Z);h=h[4];P=p_HP)
x[4]=quality(R1234ze(Z);P=p_HP;h=h[4])
T[4]=Temperature(R1234ze(Z);P=p_HP;h=h[4])

"State 5: HP evaporator inlet"
p[5]=p_HP
T[5]=T_sat_HP
s[5]=Entropy(R1234ze(Z);T=T[5];x=0)
h[5]=Enthalpy(R1234ze(Z);T=T[5];x=0)
x[5]=Quality(R1234ze(Z);T=T[5];h=h[5])

"State 6: HP evaporator outlet"
p[6]=p_HP
T[6]=T_sat_HP
s[6]=Entropy(R1234ze(Z);T=T[6];x=1)
h[6]=Enthalpy(R1234ze(Z);T=T[6];x=1)
x[6]=Quality(R1234ze(Z);T=T[6];h=h[6])

"State 7: HP turbine inlet"
p[7]=p_HP
h[7]=Enthalpy(R1234ze(Z);T=T_max;P=p_HP)
s[7]=Entropy(R1234ze(Z);T=T_max;P=p_HP)
"s[7]=Entropy(R1234ze(Z);T=T_max;h=h[7])"
T[7]=T_max
x[7]=quality(R1234ze(Z);T=T[7];P=p_HP)

"State 8: HP turbine outlet"
p[8]=p_LP
hid8=enthalpy(R1234ze(Z);P=p_LP; s=s[7])
h[8]=h[7]-eta_t*(h[7]-hid8)
T[8]=temperature(R1234ze(Z);P=p_LP; h=h[8])
s[8]=entropy(R1234ze(Z);P=p[8]; h=h[8])
x[8]=quality(R1234ze(Z);P=p[8]; h=h[8])

"State 9: LP evaporator+SH  outlet"
p[9]=p_LP
T[9]=T_sat_LP+DeltaT_SH_LP
h[9]=Enthalpy(R1234ze(Z);T=T[9];P=p_LP)
```

s[9]=Entropy(R1234ze(Z);T=T[9];P=p_LP)
"s[9]=Entropy(R1234ze(Z);T=T[9];h=h[9])"
x[9]=quality(R1234ze(Z);T=T[9];P=p_LP)

"State 10: LP turbine inlet, given by the mixing of 8 and 9"
"Energy balance: m_wf*h[10]=m_HP*h[8]+m_LP*h[9]"
h[10]=(m_HP*h[8]+m_LP*h[9])/m_wf
p[10]=p_LP
T[10]=Temperature(R1234ze(Z);P=p_LP;h=h[10])
{s[10]=Entropy(R1234ze(Z);T=T[10];P=p_LP)}
s[10]=Entropy(R1234ze(Z);T=T[10];h=h[10])
x[10]=quality(R1234ze(Z);T=T[10];P=p_LP)

"State 11: LP turbine outlet"
p[11]=p_cond
hid11=enthalpy(R1234ze(Z);P=p_cond; s=s[10])
h[11]=h[10]-eta_t*(h[10]-hid11)
T[11]=temperature(R1234ze(Z);P=p_cond; h=h[11])
s[11]=entropy(R1234ze(Z);P=p[11]; h=h[11])
x[11]=quality(R1234ze(Z);P=p[11]; h=h[11])

"HP evaporator energy balance to find m_HP. I assume the pinch point location, after the first optimization run I verify the exact pinch point position point"
"m_geo[1]*(h_w[1]-h_w[2])+m_geo[2]*(h_w[2]-h_w[3])=m_HP*(h[7]-h[5])"
T_w[3]=T_sat_HP+Tpp "fisso il pinch point"
h_w[3]=Enthalpy(Water;T=T_w[3];P=p_geo)

"if cycle to calculate m_wf_HP: if T_w[3]<T_w[2] the following statement occurs "
m_HP=(m_geo[1]*(h_w[1]-h_w[2])+m_geo[2]*(h_w[2]-h_w[3]))/(h[7]-h[5])
"Se T_w[3]>T_w[2] allora m_HP è:"
"m_HP=(m_geo[1]*(h_w[1]-h_w[3]))/(h[7]-h[5])"

{CALL TEMP (T_w[2];T_w[3];m_geo[1];m_geo[2];h_w[1];h_w[2];h[7];h[5]:mHP)
m_HP=mHP}

"Mass balances"
"the ratio m_HP/m_wf have to be optimize"
{rapp=0,601} "=m_HP/m_wf"
m_wf=m_HP/rapp
m_LP=m_wf-m_HP

"Condenser power: 1kWel every 100kWt removed"
f_c=0,01
Qcond=m_wf*(h[11]-h[1])
Wcond=f_c*Qcond

"Pumps power"
Wp=m_wf*(h[2]-h[1])+m_HP*(h[4]-h[3])

"Turbines power"
Wt=m_HP*(h[7]-h[8])+m_wf*(h[10]-h[11])

"Net power"
Wnet=Wt-Wp-Wcond

"Heat available from the heat source"
Qav=H_geo[1]
"Heat absorbed by the working fluid"
Qin=m_wf*(h[3]-h[2])+m_LP*(h[9]-h[3])+m_HP*(h[7]-h[4])

"Thermal efficiency"
eta_th=Wnet/Qin
"Heat recovery factor"
fi=Qin/Qav
"Total heat recovery efficiency: eta_rec=fi*eta_th”
eta_rec=Wnet/Qav

"Building of the CCC"
Tin_wf[1]=T[2]
Tout_wf[1]=T[3]
Tin_wf[2]=Tout_wf[1]
Tout_wf[2]=T[9]
Tin_wf[3]=T[4]
Tout_wf[3]=T[5]
Tin_wf[4]=T[5]
Tout_wf[4]=T[6]+0,1
Tin_wf[5]=Tout_wf[4]
Tout_wf[5]=T[7]

Q_wf[1]=m_wf*(h[3]-h[2])
Q_wf[2]=m_LP*(h[9]-h[3])
Q_wf[3]=m_HP*(h[5]-h[4])
Q_wf[4]=m_HP*(h[6]-h[5])
Q_wf[5]=m_HP*(h[7]-h[6])
Q_wf_tot=Q_wf[1]+Q_wf[2]+Q_wf[3]+Q_wf[4]+Q_wf[5]

"Plot"
H_wf[1]=0
H_wf[2]=Q_wf[1]
H_wf[3]=H_wf[2]+Q_wf[2]
H_wf[4]=H_wf[3]
H_wf[5]=H_wf[4]+Q_wf[3]
H_wf[6]=H_wf[5]+Q_wf[4]
H_wf[7]=H_wf[6]+Q_wf[5]
T_cold[1]=Tin_wf[1]
T_cold[2]=Tout_wf[1]
T_cold[3]=Tout_wf[2]
T_cold[4]=Tin_wf[3]
T_cold[5]=Tout_wf[3]
T_cold[6]=Tout_wf[4]
T_cold[7]=Tout_wf[5]

"Building of the Problem Table"
T_in_pt[1]=T_hot[1]
T_out_pt[1]=T_cold[7]
T_in_pt[2]=T_out_pt[1]
T_out_pt[2]=T_hot[2]
T_in_pt[3]=T_out_pt[2]
T_out_pt[3]=T_cold[6]
T_in_pt[4]=T_out_pt[3]
T_out_pt[4]=T_cold[5]
T_in_pt[5]=T_out_pt[4]
T_out_pt[5]=T_cold[4]
T_in_pt[6]=T_out_pt[5]
T_out_pt[6]=T_cold[3]
T_in_pt[7]=T_out_pt[6]
T_out_pt[7]=T_cold[2]
T_in_pt[8]=T_out_pt[7]
T_out_pt[8]=T_hot[3]
T_in_pt[9]=T_out_pt[8]
T_out_pt[9]=T_hot[4]

T_in_pt[10]=T_out_pt[9]
T_out_pt[10]=T_hot[5]
T_in_pt[11]=T_out_pt[10]
T_out_pt[11]=T_cold[1]

"Building of the Grand Composite curve"
h_geo_pt[1]=Enthalpy(Water;T=T_in_pt[1];P=p_geo)
h_geo_pt[2]=Enthalpy(Water;T=T_in_pt[2];P=p_geo)
h_geo_pt[3]=Enthalpy(Water;T=T_in_pt[3];P=p_geo)
h_geo_pt[4]=Enthalpy(Water;T=T_in_pt[4];P=p_geo)
h_geo_pt[5]=Enthalpy(Water;T=T_in_pt[5];P=p_geo)
h_geo_pt[6]=Enthalpy(Water;T=T_in_pt[6];P=p_geo)
h_geo_pt[7]=Enthalpy(Water;T=T_in_pt[7];P=p_geo)
h_geo_pt[8]=Enthalpy(Water;T=T_in_pt[8];P=p_geo)
h_geo_pt[9]=Enthalpy(Water;T=T_in_pt[9];P=p_geo)
h_geo_pt[10]=Enthalpy(Water;T=T_in_pt[10];P=p_geo)
h_geo_pt[11]=Enthalpy(Water;T=T_in_pt[11];P=p_geo)

h_wf_pt[1]=Enthalpy(R1234ze(Z);T=T_out_pt[1];P=p_HP)
h_wf_pt[2]=Enthalpy(R1234ze(Z);T=T_out_pt[2];P=p_HP)
h_wf_pt[3]=Enthalpy(R1234ze(Z);T=T_out_pt[3];P=p_HP)
h_wf_pt[4]=h[5]
h_wf_pt[5]=h[4]
h_wf_pt[6]=h[9]
h_wf_pt[7]=h[3]
h_wf_pt[8]=Enthalpy(R1234ze(Z);T=T_out_pt[8];P=p_LP)
h_wf_pt[9]=Enthalpy(R1234ze(Z);T=T_out_pt[9];P=p_LP)
h_wf_pt[10]=Enthalpy(R1234ze(Z);T=T_out_pt[10];P=p_LP)
h_wf_pt[11]=h[2]

H_pt[1]=m_geo[1]*(h_geo_pt[1]-h_geo_pt[2])
H_pt[2]=m_geo[1]*(h_geo_pt[2]-h_geo_pt[3])-m_HP*(h_wf_pt[1]-h_wf_pt[2])
H_pt[3]=m_geo[2]*(h_geo_pt[3]-h_geo_pt[4])-m_HP*(h_wf_pt[2]-h_wf_pt[3])
H_pt[4]=m_geo[2]*(h_geo_pt[4]-h_geo_pt[5])-m_HP*(h_wf_pt[3]-h_wf_pt[4])
H_pt[5]=m_geo[2]*(h_geo_pt[5]-h_geo_pt[6])-m_HP*(h_wf_pt[4]-h_wf_pt[5])
H_pt[6]=m_geo[2]*(h_geo_pt[6]-h_geo_pt[8])-m_LP*(h_wf_pt[6]-h_wf_pt[7])
H_pt[7]=m_geo[2]*(h_geo_pt[8]-h_geo_pt[9])-m_wf*(h_wf_pt[7]-h_wf_pt[8])
H_pt[8]=m_geo[3]*(h_geo_pt[9]-h_geo_pt[10])-m_wf*(h_wf_pt[8]-h_wf_pt[9])
H_pt[9]=m_geo[4]*(h_geo_pt[10]-h_geo_pt[11])-m_wf*(h_wf_pt[9]-h_wf_pt[10])
H_pt[10]=-m_wf*(h_wf_pt[10]-h_wf_pt[11])

"Cumulative heat load"
Q_pt[1]=H_pt[1]
Q_pt[2]=Q_pt[1]+H_pt[2]
Q_pt[3]=Q_pt[2]+H_pt[3]
Q_pt[4]=Q_pt[3]+H_pt[4]
Q_pt[5]=Q_pt[4]+H_pt[5]
Q_pt[6]=Q_pt[5]+H_pt[6]
Q_pt[7]=Q_pt[6]+H_pt[7]
Q_pt[8]=Q_pt[7]+H_pt[8]
Q_pt[9]=Q_pt[8]+H_pt[9]
Q_pt[10]=Q_pt[8]+H_pt[10]

"GCC drawing"
T_GCC[1]=T_in_pt[1]
T_GCC[2]=T_in_pt[2]
T_GCC[3]=T_in_pt[3]
T_GCC[4]=T_in_pt[4]
T_GCC[5]=T_in_pt[5]
T_GCC[6]=T_in_pt[6]
T_GCC[7]=T_in_pt[7]

T_GCC[8]=T_in_pt[9]
T_GCC[9]=T_in_pt[10]
T_GCC[10]=T_in_pt[11]
T_GCC[11]=T_out_pt[11]
Q_GCC[1]=0
Q_GCC[2]=Q_pt[1]
Q_GCC[3]=Q_pt[2]
Q_GCC[4]=Q_pt[3]
Q_GCC[5]=Q_pt[4]
Q_GCC[6]=Q_pt[5]
Q_GCC[7]=Q_pt[6]
Q_GCC[8]=Q_pt[7]
Q_GCC[9]=Q_pt[8]
Q_GCC[10]=Q_pt[9]
Q_GCC[11]=Q_pt[10]

REFERENCES

[1] http://ec.europa.eu/clima/policies/international/negotiations/paris/index_en.htm

[2] Tchanche B.F., Lambrinos Gr., Frangoudakis A., Papadakis G., Low-grade heat conversion into power using organic Rankine cycles – A review of various applications; Renewable and Sustainable Energy Reviews 2011.

[3] Bao J., Zhao L., A review of working fluid and expander selections for organic Rankine cycle; Renewable and Sustainable Energy Reviews 2012.

[4] Papadopoulos A.I., Stijepovic A., Linke P., On the systematic design and selection of optimal working fluids for Organic Rankine Cycles; Applied Thermal Engineering 2009.

[5] Quoilin S., Van Den Broek M., Declaye S., Dewallef P., Lemort V., Techno-economic survey of Organic Rankine Cycle (ORC) systems; Renewable and Sustainable Energy Reviews 2013.

[6] Vetter C., Wiemer HJ., Kuhn D., Comparison of sub- and supercritical organic Rankine cycles for power generation from low-temperature/low-enthalpy geothermal wells, considering specific net power output and efficiency; Applied Thermal Engineering 2013.

[7] Astolfi M., Romano MC., Bombarda P., Macchi E., Binary ORC (organic Rankine cycles) power plants for the exploitation of medium–low temperature geothermal sources e Part A: thermodynamic optimization; Energy 2014.

[8] Li XG., Zhao WJ., Lin DD., Qiang Z., Working fluid selection based on critical temperature and water temperature in organic Rankine cycle; Science China, Technological Science 2015.

[9] Vivian J., Manente G., Lazzaretto A., A general framework to select working fluid and configuration of ORCs for low-to-medium temperature heat sources; Applied Science 2015.

[10] Guzovic Z., Raskovic P., Blataric Z., The comparision of a basic and a dual-pressure ORC (Organic Rankine Cycle): Geothermal Power Plant Velika Ciglena case study; Energy 2013.

[11] Li T., Zhang Z., Lu J., Yang J., Hu Y., Two-stage evaporation strategy to improve system performance for organic Rankine cycle; Applied Energy 2014.

[12] Di Genova K. J., Botros B. B., Brisson J.G., Method for customizing an organic Rankine cycle to a complex heat source for efficient energy conversion, demonstrated on a Fischer Tropsch plant; Applied Energy 2012.

[13] Desai N. B., Bandyopadhyay S., Process integration of organic Rankine cycle; Energy 2009.

[14] Linde industrial gases. GWP values available at www.linde-gas.com.

[15] Honeywell official website. GWP values available at www.honeywell-refrigerants.com.

[16] Li T., Zhang Z., Lu J., Yang J., Hu Y., Two-stage evaporation strategy to improve system performance for organic Rankine cycle; Applied Energy 2014.

[17] Toffolo A., Lazzaretto A., Manente G., Paci M., A multi-criteria approach for the optimal selection of working fluid and design parameters in Organic Rankine Cycle; Applied Energy 2014.

[18] Seider WD., Seader JD., Lewin DR., Product & process design principles: synthesis, analysis and evaluation; John Wiley & Sons; 2009.

[19] Stijepovic M.Z., Papadopoulos A.I., Linke P., Grujic A.S., Seferlis P., An exergy composite curves approach for the design of optimum multi-pressure organic Rankine cycle processes; Energy 2014.

[20] Kakaç S., Liu H.; Heat Exchangers: selection, rating and thermal design; CRC Press; 2002.

[21] Soffiato M., Frangopoulos C. A., Manente G., Rech S., Lazzaretto A., Design optimization of ORC systems for waste heat recovery on board a LNG carrier; Energy Conversion and Management 2014.
[22] Kemp I. C., Pinch Analysis and Process Integration; Elsevier 2007.
[23] Toffolo A., Lazzaretto A., Manente G., M:, Paci M., A multi-criteria approach for the optimal selection of working fluid and design parameters in Organic Rankine Cycle systems; Applied Energy 2014.
[24] Heberle F., Brüggemann D., Exergy based fluid selection for a geothermal Organic Rankine Cycle for combined heat and power generation; Applied Thermal Engineering 2010.
[25] Liu W., Meinel D., Wieland C., Spliethoff H., Investigation of hydrofluoroolefins as potential working fluids in organic Rankine cycle for geothermal power generation; Energy 2013.
[26] Wang Z.Q.,. Zhou N.J, Guo J., Wang X.Y., Fluid selection and parametric optimization of organic Rankine cycle using low temperature waste heat; Energy 2012.
[27] Tian H. , Shu G., Wei H., Liang X., Liu L., Fluids and parameters optimization for the organic Rankine cycles (ORCs) used in exhaust heat recovery of Internal Combustion Engine (ICE); Energy 2012.
[28] Turton R, Bailie RC, Whiting WB, Shaeiwitz JA. Analysis, synthesis and design of chemical processes. 3rd ed. Boston: Prentice Hall; 2009.
[29] Cayer E., Galanis N, Nesreddine H., Parametric study and optimization of a transcritical power cycle using a low temperature source; Applied Energy 2009.
[30] Hung TC, Shai TY, Wang SK., A review of organic Rankine cycles (ORCs) for the recovery of low-grade waste heat; Energy 1997.

AKNOWLEDGEMENTS

I would like to thank Dr. Giovanni Manente and Prof. Andrea Lazzaretto for helping me writing this work with suggestions and corrections, my family for the constant support during these years and the friends who shared with me part of my university experience.
A special thought goes to my niece Arianna, who brought us a lot of happiness.